



Technische  
Universität  
Braunschweig

**Joaquin M. Cuomo**

Matrikelnr. 4425287

## Reduction of disturbing influences and artifacts in capacitive EEG

### Masterarbeit

*Betreuer* Prof. Dr. rer. nat. Meinhard Schilling  
Christof Wehrmann, M. Sc.

*Beginn* 8. Januar 2014

*Abschluss* 4. Juli 2014

**emg**

Institut für Elektrische Messtechnik und  
Grundlagen der Elektrotechnik



# **Declaration of authorship**

I confirm that this Master's thesis is my own work and I have documented all sources and material used.

This thesis was not previously presented to another examination board and has not been published.

Braunschweig, 4. Juli 2014



# Abstract

Electroencephalography (EEG) is an important medical resource for diagnosis, but traditional acquisition systems with resistive electrodes demand a lot of time before and after a measurement. One attempt to overcome this problem is capacitive EEG (cEEG) where non-contact capacitive electrodes are used. However, the main hold back to this system are motion artifacts caused by the movement of the electrodes. The aim of this thesis is to assess some of the most effective algorithms used in traditional EEG to denoise the measurements, giving special attention to motion artifacts and SSVEP signals.

A first step into understanding this motion artifacts was reproducing a simple oscillatory movement of the capacitor's plates. It was found out that wavelet transform seems to be a good approach to overcome motion artifacts at low frequencies, while ICA could be used effectively with different types of artifacts in combination with wavelets. Auxiliary sensors –gyroscope and accelerometer–were not useful to denoise motion artifacts but help to reduce ECG disturbances. Finally, SSVEP could be enhanced with help of ICA and a proper bipolar lead selection. Some recommendations for future works are: increase the shielding of the electrodes, correct the coordinates axis of the auxiliary sensors and use a common mode electrode. An interesting work line would be doing a deeper analytical analysis on the movement of the electrodes.



# Contents

<b>Declaration of authorship</b>	<b>III</b>
<b>Abstract</b>	<b>V</b>
<b>Contents</b>	<b>VII</b>
<b>Nomenclature</b>	<b>IX</b>
<b>List of abbreviations</b>	<b>XI</b>
<b>1. Introduction</b>	<b>1</b>
<b>2. Background information</b>	<b>3</b>
<b>3. State of art</b>	<b>9</b>
<b>4. Research methodology and materials</b>	<b>11</b>
4.1. Study of the acquisition system . . . . .	11
4.1.1. Analysis of leads . . . . .	12
4.1.2. Common mode rejection . . . . .	14
4.1.3. Crosstalk . . . . .	15
4.1.4. Noise sources . . . . .	17
4.2. Motion artifact analysis . . . . .	19
4.2.1. Analytical . . . . .	19
4.2.2. Experimental . . . . .	19
4.2.3. Evaluation . . . . .	21
4.3. Algorithms . . . . .	21
4.3.1. Wavelets . . . . .	21
4.3.2. Independent component decomposition . . . . .	23
4.3.3. Adaptive filters . . . . .	25
4.4. Denoising methods . . . . .	27
4.4.1. Auxiliary sensors: gyroscope and accelerometer . . . . .	27
4.4.2. Pre-processing . . . . .	27
4.4.3. Motion artifacts . . . . .	29
4.4.4. ECG artifacts . . . . .	31
4.4.5. SSVEP enhancement: bipolar lead and SNR . . . . .	32

<b>5. Results</b>	<b>35</b>
5.1. Study of the acquisition system . . . . .	35
5.1.1. Analysis of leads . . . . .	35
5.1.2. Common mode rejection . . . . .	37
5.1.3. Crosstalk . . . . .	39
5.1.4. Noise sources . . . . .	41
5.2. Motion artifact analysis . . . . .	42
5.2.1. Analytical . . . . .	42
5.2.2. Experimental . . . . .	44
5.2.3. Evaluation . . . . .	46
5.3. Denoising methods . . . . .	47
5.3.1. Auxiliary sensors: gyroscope and accelerometer . . . . .	47
5.3.2. Motion artifacts . . . . .	49
5.3.3. ECG artifacts . . . . .	55
5.3.4. SSVEP enhancement . . . . .	56
<b>6. Discussion</b>	<b>61</b>
<b>7. Conclusion</b>	<b>65</b>
7.1. Prospect for future researches . . . . .	65
<b>A. Appendix</b>	<b>67</b>
A.1. Noise sources . . . . .	67
A.2. Comparison of ICA, wavelets and the combination of both . . . . .	68
A.3. Wavelet example . . . . .	72
A.4. Each lead at a time . . . . .	73
A.5. Crosstalk with dummy head . . . . .	76
A.6. Crosstalk without dummy head . . . . .	79
A.7. Time span selection . . . . .	82
<b>Bibliography</b>	<b>83</b>
<b>Danksagung</b>	<b>91</b>
Table of Contents	

# Nomenclature

**7-Helmet**      Electroencephalography acquisition system with seven leads

$\rho_{ij}$            Correlation coefficient between  $i$  and  $j$

**acc**           Accelerometer

**Ag**           Chemical abbreviation for *silver*

**AgCl**          Chemical abbreviation for *Silver chloride*

**cov**           Covariance

**FastICA**       Type of ICA implementation called Fast ICA

**gyr**           Gyroscope

**KDICA**       Type of BSS technique called Kernel ICA

**QRS**           Name for three of the electrocardiogram deflections

**SOBI**           Type of BSS technique called Second Order Blind Identification

**var**           Variance



# List of abbreviations

<b>BSS</b>	Blind Source Separation
<b>cEEG</b>	Capacitive Electroencephalography
<b>CMRR</b>	Common Mode Rejection Ratio
<b>ECG</b>	Electrocardiography
<b>EEG</b>	Electroencephalography
<b>EMG</b>	Electromyography
<b>EOG</b>	Electrooculography
<b>ICA</b>	Independent Component Analysis
<b>IMU</b>	Inertial Measurement Unit
<b>PSD</b>	Power Spectral Density
<b>SNR</b>	Signal to Noise Ratio
<b>SSVEP</b>	Steady-State Visual-Evoked Potential
<b>XT</b>	Crosstalk



# 1. Introduction

## Motivation

Electroencephalography (EEG) is an important medical resource for diagnosis of different diseases, among others epilepsy, brain death, coma, brain tumors and headache. Traditional acquisition systems have resistive electrodes, which require a special gel to reduce the contact impedance with the skin, and it demands a lot of time before and after a measurement. In other applications, like emergencies where it is useful to detect seizures and other neuropathological conditions, it is not possible or really inconvenient to use these traditional systems because the time is critical. Another area of application which requires an easy-to-use system is in research field, where long term measurements are run and no skin irritation is wanted as occurs with traditional resistive electrodes.

One attempt to overcome this problem is capacitive EEG (cEEG) where non-contact capacitive electrodes are used and the time needed for preparation before and cleaning after the measurements is minimized. Despite this great advantage it is not yet possible to use it in clinical research because of the artifacts contaminating the EEG data, making the analysis of neurological signals very complicated. On the other hand, for ECG, where the signals are of one magnitude order higher and the pressure applied to the chest can be higher than on the head, there is already a commercial system [1].

## Aim of the research

The main focus of this thesis is to assess performance of already known techniques, used in traditional EEG to remove artifacts, in the new capacitive EEG system.

## Objectives

Motion artifacts occur both in traditional systems and capacitive systems, but due to the non-contact nature of electrodes in cEEG, every movement of the body during the acquisition will impact in electrode's movement, causing a disturbance in the measurements. Therefore, special attention will be given to remove motion artifacts, as their influence in

cEEG is the main hold back for this novel system.

Particularly, Steady-State Visual-Evoked Potential (SSVEP) detection will be pursued to be enhanced owing the research focus of the hosting institute [2].

## Research questions

Can differences between EEG and cEEG be quantified? All of them? How?

Why do denoising motion artifacts in cEEG present so many difficulties?

Could noise be reproduced? And denoised? How?

Will traditional denoising methods work in capacitive EEG? Do they need any adjustment?

Will auxiliary sensors—accelerometer and gyroscope—be useful to denoise motion artifacts?

## Summary of the structure of this thesis

The first step will be study the main characteristics of the acquisition system, for example gain and crosstalk of each electrode, the effectiveness of reference electrode and the inherent noise sources.

Then, a preliminary study of artifacts and disturbances is performed, which are present in a EEG measurement. Afterwards, a deeper analysis of motion artifacts will be conducted in order to reproduce them and understand how they interact with the sensed signal.

As the acquisition system has already built-in two triaxial accelerometer and gyroscope sensors, is investigated how to use them for denoising and reducing motion and other artifacts.

Afterwards, further denoising methods such as wavelets, independent component analysis (ICA) and adaptive filters will be tested in EEG measurements acquired with two different cEEG systems. First trials will be on motion artifacts, then on ECG artifact and at last on SSVEP measurements. This final experiment will be followed by the encoding of an algorithm, which chooses a bipolar lead to improve the SSVEP signals.

Finally, a discussion of results will be given followed by the main conclusion of this thesis and prospects for future research.

## 2. Background information

### **Basics of bioelectrical signals and EEG**

The discovery of electricity in living organism dates back to 1791, when Luigi Galvani (1737-1798) described electricity effects in frogs. Julius Bernstein (1839-1917) made a great number of contributions to the understanding of how the nerve membranes were polarized and depolarized during the action potential –a term coined by him. He proposed around 1870 the modern theory that the inactive nerve or muscle fiber is normally electrically polarized, with the external surface positive in relation to the internal one, and that the action potential is a self-propagated depolarization of the membrane [3].

The cell membrane consists of a physical barrier between the cell interior and its surroundings. Communication between the two spaces is possible by various mechanisms that constitute biological signals. The signals are generated by the exchange of charge, mainly ions, and excitable cells exert their functions by generating electrical signals in terms of changes in cell membrane potential [4].

The primary function of neurons is to integrate information gathered at synaptic contacts and send signals to other neurons and effectors –muscle cells and secretion organs. In human brain there are about 100 billion neurons and 100 trillion synapses, which are the connection between neurons.

The bioelectric signals require a transducer for acquisition because the electrical conduction in the biological environment is through ions, while the measurement system uses electrons conduction. In measurements on isolated cells, where microelectrodes are used as transducers, the action potential itself is the signal measured. While measurements in large cell groups –where surface electrodes are used as transducers –the electric field generated by the action potentials of many cells distributed in the vicinity of the electrodes constitutes the bioelectrical signal [5].

Electroencephalography is a graphical representation of the voltage differences between

two different cerebral locations plotted over time. The scalp measurement of neural activity is modified by electrical conductive properties of the tissues between the electrical source and the recording electrode on the scalp, also by the conductive properties of the electrode itself as well as the orientation of the cortical generator to the recording electrode.

In scalp, the most widely used placement of electrodes is the so called 10-20 system, a standardized distribution that specifies the relative distance between electrodes. The brain signals appear in a wide range of frequencies, from barely zero to over 60 Hz, and they are divided in frequency bands related to different brain states, functions or pathologies.

EEG frequency bands [6];

- Delta rhythms (0.5-3.5Hz): characteristics in deep sleep stages. Furthermore, delta oscillations with certain specific morphologies, localizations and rhythmicities are correlated with different pathologies.
- Theta rhythms (3.5-7.5Hz): enhanced during sleep and play an important role in infancy and childhood. In the awake adult, high theta activity is considered abnormal and it is related with different brain disorders.
- Alpha rhythms (7.5-12.5Hz): appear spontaneously in normal adults during wakefulness, under relaxation and mental inactivity conditions. They are clearly seen in the EEG with closed eyes and are most pronounced in occipital locations.
- Beta rhythms (12.5-30Hz): defined in central and frontal locations with less amplitude than alpha waves and are enhanced upon expectancy states, tension and demanding mental activities as calculating.
- Gamma rhythms (30-60Hz): related with linking of stimulus features into a common perceptual information.

An EEG measurement usually is done with a series of electrodes located on the scalp sensing a potential difference between its location and other position of the head where the reference electrode is located (for example on ears or forehead).

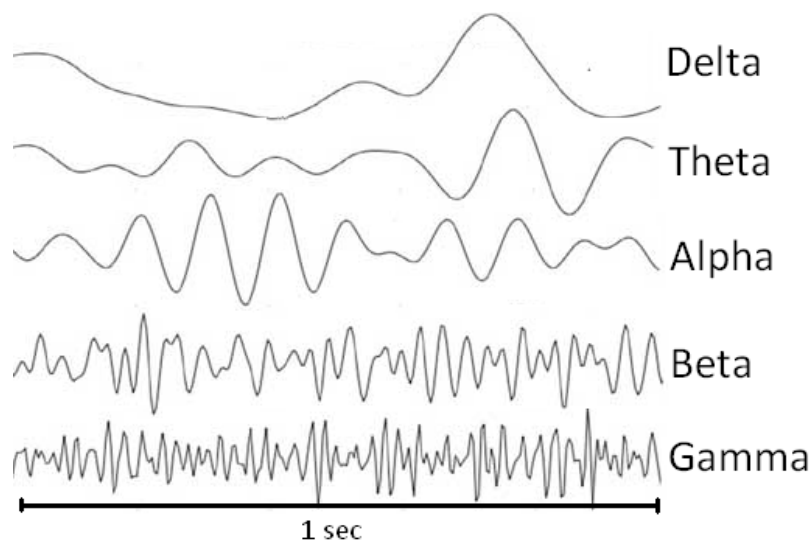


Figure 2.1.: Types of brain waves [7]

## Types of electrodes

The main technical difficulty in measuring bioelectric signals from the body lies in establishing a good and stable electrical connection with the skin. Therefore, electrodes are constantly under development [8, 9, 10, 11, 12].

### Conventional resistive contact electrodes

The silver/silver chloride ( $\text{Ag}/\text{AgCl}$ ) is the most common type of electrode. The fact of using electrolytic gel to improve contact impedance allows a little movement keeping a good contact. Despite this, the gel smearing and even absorption is a problem. For patients with sleep problems, or for any other kind of long term monitoring, the use of gel is tedious, since it has to be replaced periodically due to the signal degradation over time. Before placing a resistive electrode on a patient, the skin is usually cleaned with alcohol to remove sweat and skin oils that would otherwise prevent the adhesive paste from holding the electrode in contact with the patient skin—it also requires an after-measurement cleaning. This setup with more than 20 electrodes becomes a tedious task and a waste of time.

### Dry contact electrodes

In the group of dry contact electrodes inert metals can be found, since they are difficult to oxidize and dissolve, for example platinum or gold. They offer a faster skin implementation, but still need direct contact with the skin. In this sense, there can not be hair between

the scalp and the electrode.

### Capacitive insulating electrodes

The charge movement detected by the capacitive electrodes is produced by means of capacitance, coupled between the skin and the electrode. This capacitance is purely dependent on the area, the distance and the permitivity of the material found between the scalp and the electrode. If a tiny movement is done, the distance changes, and so the voltage does. The main problem appears when there is hair in between, which is the usual case in an EEG device. In this situation, a movement not only changes that distance, but also the movement itself generates triboelectricity, which is in fact charge movement producing undesired noise.

Using the capacitive electrodes the capacitance can be better controlled by means of a non-conductive dielectric separator than with dry insulating electrodes. On the other hand, the capacitance is greatly reduced by the dielectric, therefore an active buffering/amplification stage must be used. Otherwise, the capacitance of the cables and the interferences would prevent to detect the brain signals [9].

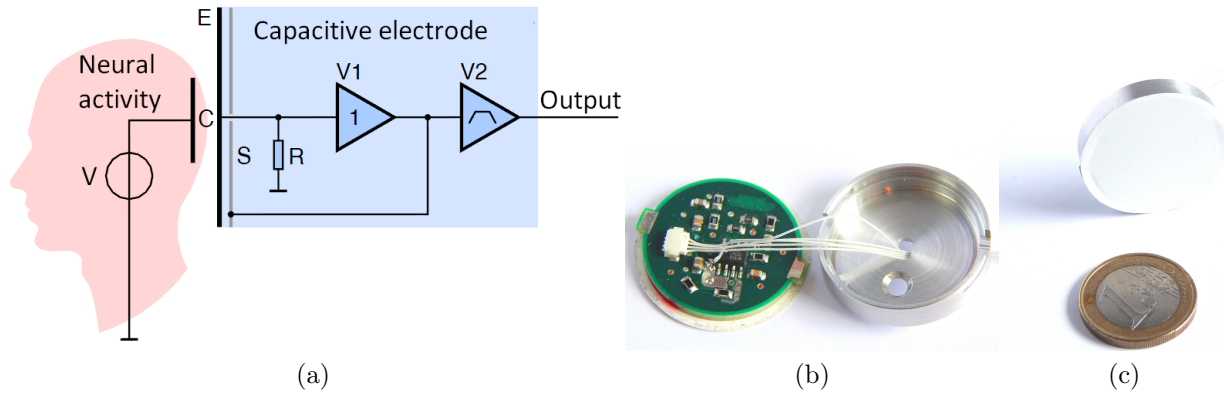


Figure 2.2.: Capacitive electrode's scheme (a) [13] and photographs (b) and (c).

The electroencephalography systems using this type of electrodes are called capacitively coupled EEG or simply capacitive EEG (cEEG). Figure 2.2.(a) shows how these electrodes register the neural activity of the brain. The measured voltage ( $V$ ) is coupled via the capacitance ( $C$ ) between the head and the electrode surface ( $E$ ). The bias resistor ( $R$ ) is below the operating point of the impedance converter ( $V1$ ) and forms with the coupling capacitance a high-pass. An active shield ( $S$ ) is used as a guard to alleviate the charging effects on the capacitance by maintaining an equal potential and shield the inner electrical

components against other disturbing signals. Finally, the signal passes through an active band-pass filter.

## BCI

A Brain-Computer Interface (BCI) establishes a bridge between mind and environment, allowing interaction through an interface with external stimuli. This response to stimulation can be achieved by Steady-State Visual-Evoked Potentials (SSVEP) and can be detected in neural waves, which present great potential for many applications such as allowing people who suffer from motor dysfunction in daily activities.

**SSVEP:** is a brain response to visual stimuli at a given fixed frequency (in the range of 3.5 Hz and 75 Hz [6]). When this type of stimuli is observed an EEG component at the same frequency appears in the visual cortex of the brain.

**Alpha waves:** are brain signals dominant in the occipital region of the brain and appear at about 10 Hz. They are particularly interesting and used in BCI because they can be triggered easily by closing eyes in a relaxed state by almost everyone.



### 3. State of art

Electroencephalography suffers from disturbances and artifacts that affect the integrity of the brain signals measurements [14]. For artifacts it is understood any potential difference registered which does not come from the brain, and also modifications due to the media surrounding [15]. They can be classified into three different groups, *biologic* (such as ECG, EOG, EMG and breathing, etc.), *technological* (such as a bad location of the electrodes, recording equipment, electrodes impedance, etc.) and *extrinsic* (such as line interferences, radio frequencies, electrostatic, etc.) [16, 17, 18].

The main influences seen in this thesis are [19]:

**Power line:** EEG measurements may be disturbed by the 50 Hz or 60 Hz of power line, fluorescent lights and other equipment in the nearby.

**Electrocardiography:** electrical activity of the heart (specially the QRS complex) may contaminate the EEG measurements.

**Electromyography:** muscular activity also produces electrical signals that can appear in the EEG measurements.

**Breathing, heart beat, muscles:** movement of the body, either from breathing, heart beats, eyes or muscle movements (volunteer or involuntary) may affect the EEG measurement by varying the impedance of the electrodes.

The introduction of capacitive electrodes [20, 21] presents new possibilities of how and where to use these electroencephalography systems [8], but it also comes with new and harder hold backs. The main concern working with the capacitive coupled EEG systems are the motion artifacts due to the movement of the non-contact electrodes [22, 23] and also the triboelectric noise (due to the electron interaction in the superficial layer) [24]. Low frequency signals produce similar coupling impedance as the input impedance of electrode's amplifiers. Thus, any variation in coupling capacitance, caused mainly by movements of the body, can

result in distortions due to signal attenuation and increase of noise levels [8]. Nevertheless, these artifacts appear also in the whole range of frequencies but with lower amplitudes [25].

To overcome motion artifacts in traditional EEG measurements several techniques have continuously been developed and tested [26]. Some of these approaches are adaptive filters [17], wavelets [27] [28], blind source separation techniques (BSS) [29, 30], Hilbert-Huang transform [18], morphological component analysis [31], comb filters [32], surface Laplacian [33], maximum noise fraction [34] and combination of them [35, 36].

Among the BSS techniques, Independent Component Analysis (ICA) is one of the most accepted one [37, 38]. It consists in finding the independent components of a measurement and eliminate those components which are not desired. Successful results have been obtained with different types of motion artifacts [39, 40].

Another usually used denoising method is the wavelet transform [41], in which the measurements are decomposed in different levels of frequency contents with spatial information, by means of dilatations (time information) and scaling (frequency information) from the projecting waveform—defining together an orthogonal basis in the space of all square integrable functions  $L^2(\mathbb{R})$  [42]. Both ICA and wavelets combined is one of the latest and promising approaches to reduce all sort of artifacts in EEG measurement. Once the independent components are found, wavelet thresholding [43, 44, 45] is used to cancel noise in the components and therefore it is not necessary to remove an entire source losing some of the EEG components [46, 47, 48].

Adaptive filtering is a common technique to remove other physiological signals [49] contaminating the EEG measurements such as EOG and ECG and also ambient noise as power line interferences [17, 50]. In order to achieve this goal a reference signal is required, which is correlated with the noise [51]. Usually the reference signal is obtained by sensing it with dedicated electrodes, for example with an electrocardiograph. Approaches less expanded are using auxiliary sensors (accelerometers and gyroscopes) to detect the movement of the electrode and evaluated the quality of the measurement [52, 53]. Hosseini *et al.* [54] used a double sensor provide reliable information of movement in capacitive ECG to later use it with an adaptive filter.

## 4. Research methodology and materials

### 4.1. Study of the acquisition system

In this section some characteristics of the acquisition system will be analyzed and tested, such as the effectiveness of referencing leads, the crosstalk between channels and some of the major noise sources.

The measurements were done with a 7 leads capacitive electroencephalogram built at Technische Universität Braunschweig by C. Wehrmann *et al.* (2012) [55] [56, 57]. It has 8 electrodes, one placed in frontal lobe (Fz) as reference and the rest placed to be the following leads O1, Oz, O2, Pz, C3, Cz and C4 (see Figure 4.1)

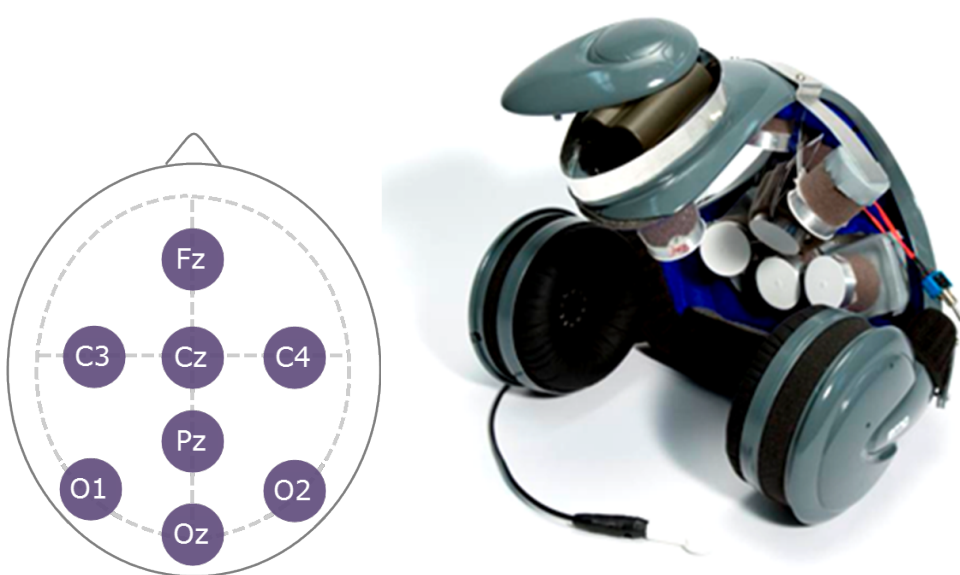


Figure 4.1.: Electroencephalography system with 8 electrodes and their location on the scalp

The specifications of this helmet are:

- Sampling frequency: 500 Hz
- $Z_{in} = 100 \text{ G}\Omega$  and  $\sim 20 \text{ pF}$
- Frequency response: high pass filter second order at 0.125 Hz and a first order low pass filter at 100 Hz
- Analogue to digital conversion: each channel is multiplexed and converted through ADS1258
- Interface: via Bluetooth® the system sends data to a computer

The helmet is supplied with 5 V split in two ( $\pm 2.5 \text{ V}$ ) and has two amplifications stages of gain 2 and gain 50. Therefore, the dynamic range of the channels is  $\pm 12.5 \text{ mV}$  in theory—it is lower due to the low drop voltage regulator used to stabilize the power supply.

For some particular measurements another helmet was used [58], which has 24 leads referenced to forehead.

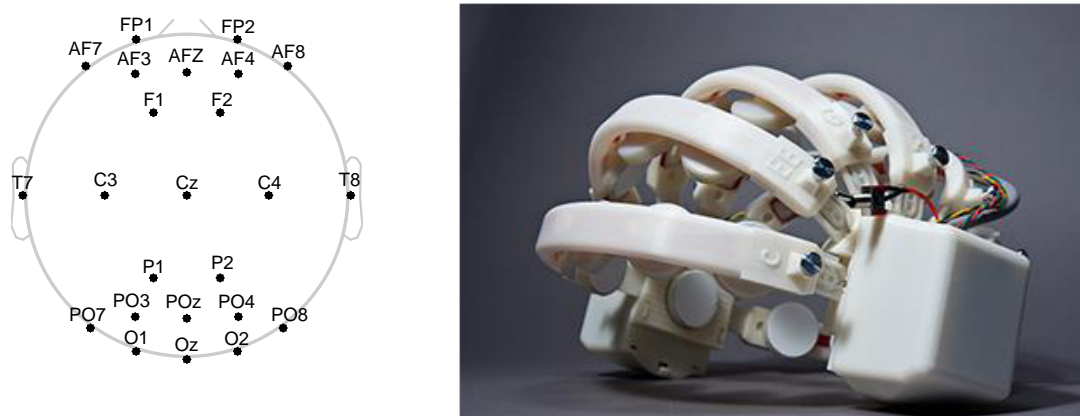


Figure 4.2.: Electroencephalography system with 24 electrodes and their location on the scalp

Every time it will be mentioned which helmet was used, denoting “7-Helmet” for the 7 leads system and “24-Helmet” for the 24 leads system.

#### 4.1.1. Analysis of leads

The system is based on different channels having each one an individual amplifier. Therefore, it is necessary to asses each lead to determine how they response and how they

interact with each other. In order to answer these questions four different types of measurements were done. The first two were done to evaluate the gain of each channel. Then, the relative influence of the reference lead was evaluated and finally the crosstalk between leads.

#### 4.1.1.1. All leads together

As each lead is referenced against a reference electrode, every variation affecting this electrode will act on the rest. Therefore, this reference electrode was used to compare the gain of all leads at the same time. The 7-Helmet was placed on a glass dummy head covered with aluminium foil so all electrodes have the same applied potential and the reference electrode, isolated from the foil, was connected to a test signal.

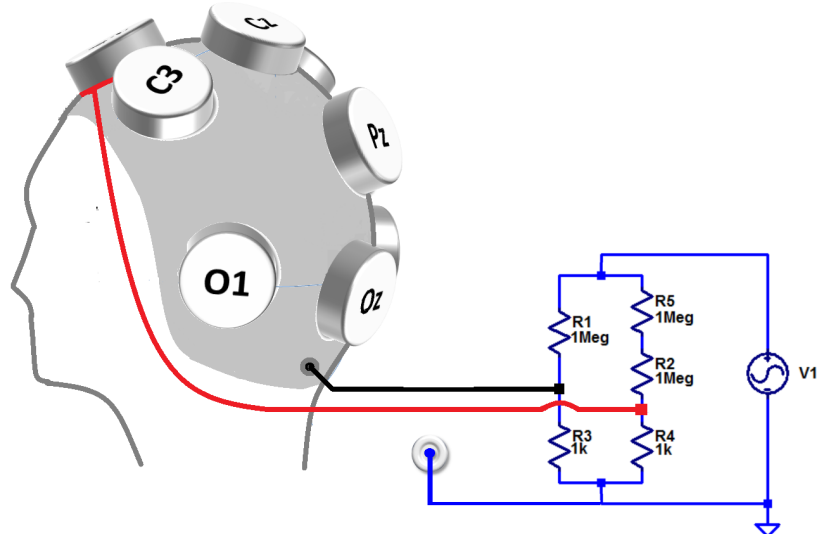


Figure 4.3.: Setup to measure gain in all leads together

In Figure 4.3 a diagram of the setup is shown, where the head is made of glass, the gray part is aluminium foil, and the electrodes represent the 7-Helmet. The electrodes which have a cable connection are isolated from the aluminium foil and a copper circular plate was used to apply a signal to them. A sinusoidal waveform of 75 Hz and 1 V amplitude generated with the Agilent 3322A signal generator [59] was used. The frequency was chosen because the noise floor at 75 Hz was more stable between measurements than at other frequencies. A resistor divider was used to avoid ground loops and to reduce instrument's error by using a higher amplitude range. The red cable applies a 0.5 mV amplitude sinus to the reference electrode and it is expected that the output of the other electrodes are -0.5 mV at 75 Hz.

#### 4.1.1.2. Each lead at a time

As the electrodes are capacitive it is not possible to establish a perfect and equal connection due to the differences in placement over the dummy head. Therefore, an individual test for each lead was performed, in which special attention to electrodes' placement was giving.

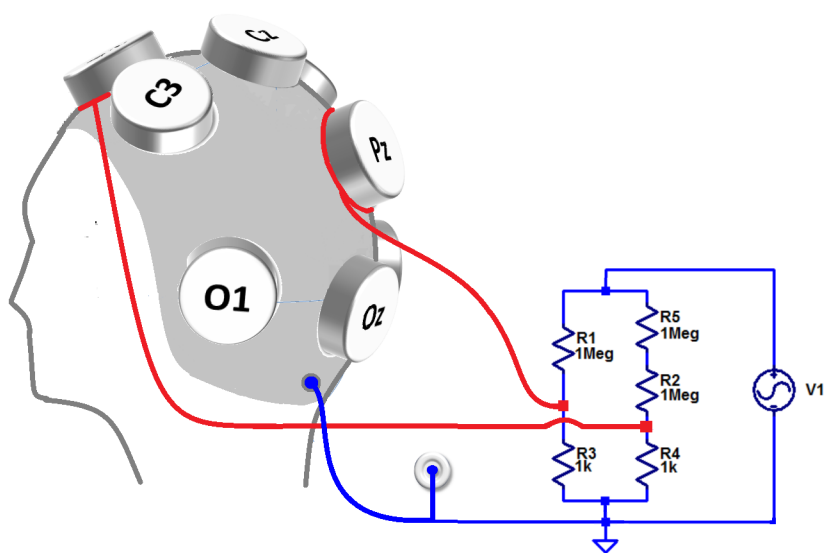


Figure 4.4.: Setup to measure gain in each lead at a time.

The same input signal from previous measurement was used, but in this configuration 1 mV is applied to the reference electrode and 2 mV are applied to the observed electrode. Therefore, the output in tested electrode will be  $2\text{mV} - 1\text{mV} = 1\text{mV}$ . The rest of the electrodes were connected to ground to minimize interferences.

#### 4.1.2. Common mode rejection

Opposite to previous measurements, here it was intended to test the effectiveness of the system to measure a zero when the same signal is applied both to reference electrode and leads. It is also expected to validate gain measurements, since the results for each electrode should be proportional to each lead gain.

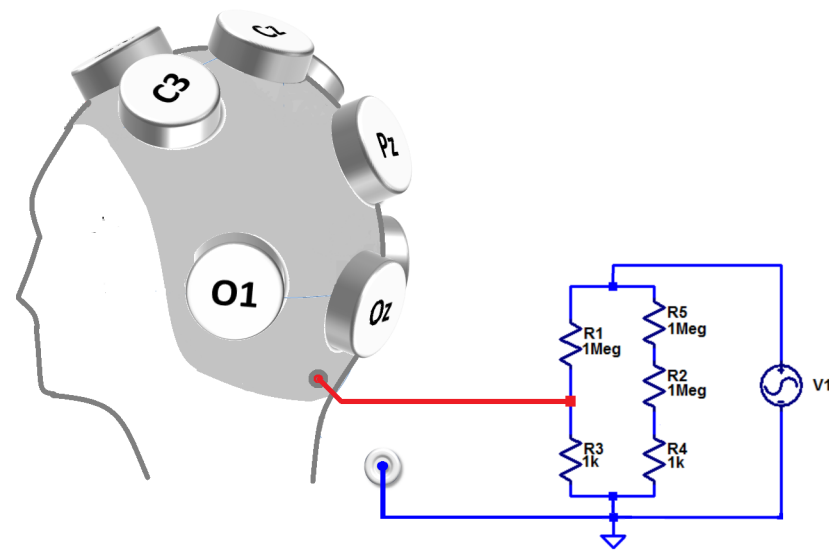


Figure 4.5.: Setup to measure zero in all leads together

The same sinusoidal signal was applied to the aluminium foil in the dummy head, in which all electrodes were placed including the reference electrode. There are a few factors to be analyzed in case the 0 V is not achieved. On the first hand, bad placement of electrodes will cause different sensed voltages. On the other hand, each channel has a different amplifier, so they can present slight differences in gain. Another possible cause could be that the crosstalk between channels may introduce some mismatches. Hence, some crosstalk measurements will also be done.

### 4.1.3. Crosstalk

Crosstalk measurements were done for three main reasons. First, the electrodes being capacitive can sense nearby signals, then the cables and circuitry may introduce some unwanted coupling specially because they are not shielded, and third the ADC specifies the crosstalk at 1 kHz but not at lower frequencies [60].

Two setup configurations were tested, the first one with the 7-Helmet placed on dummy head (see Figure 4.4) and the other one without the dummy head (see Figure 4.6). In the first case all electrodes have a well defined potential and it is closer to a real measurement when all the electrodes are well placed. In the second case electrodes are more susceptible to interferences being in free air, this is the case when the placement is not good and some electrodes are not in contact with the head.

The applied signal (4.2 mV) was greater than normal EEG components ( $\sim 10 \mu\text{V}$  –

$100 \mu\text{V}$ ) in order to measure crosstalk with higher accuracy.

The crosstalk was calculated in percentage as follows:

$$c_{ij} = \frac{v_j}{v_i} \cdot 100 \quad (4.1)$$

with  $c_{ij}$  being the crosstalk from electrode i to electrode j and  $v_i$  the voltage measured in electrode i.

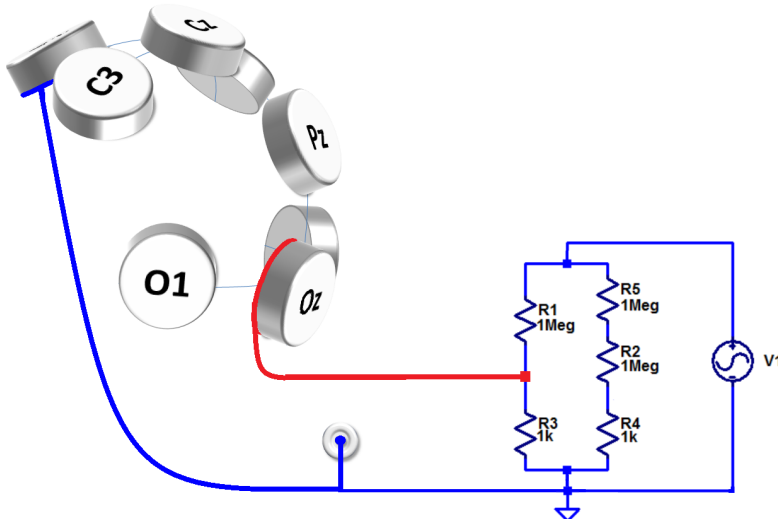


Figure 4.6.: Setup to measure crosstalk without the dummy head

The difference between these setups, besides one is using the dummy head and the other one is not, is the reference electrode connection. In the setup with the dummy head it was possible to connect the virtual ground of the 7-Helmet to the rest of the electrodes as it would happen in a real measurement where the virtual ground is connected to the body via a resistive electrode. But, without the dummy head it was not possible to do this, so the reference had to be connected to ground, otherwise (as explained in Section 4.1.1.1) the signal at the reference electrode would be replicated in each of the electrodes and the crosstalk measurement would not make sense. The drawback of this configuration is that possible ground loops may be formed due to different resistances in paths to ground. The consequences of this could be a higher crosstalk and poor common mode rejection.



Figure 4.7.: 7-Helmet on dummy head to illustrate how the aluminium is contacting all electrodes.

#### 4.1.4. Noise sources

In this section the term *noise sources* refers to inherent noises of 7-Helmet and not to EEG noise or movement artifacts. Notwithstanding, power line interferences are going to be studied in order to compare and understand the other noise sources.

Several test were performed in different conditions, so that ambient noise and inherent noise could be distinguished. To accomplish this, an isolation multilayer tank was used (see Appendix A.1). It has 4 layer (see Figure A.1) in the following order: permalloy, permalloy, copper and permalloy; it was placed over foam to absorb external vibrations and electrically grounded. The cable with the Bluetooth® dongle plugged in, was introduced inside the tank through small gaps between the cover and the body of each tank.

The following measurements were done:

- 7-Helmet inside the isolation tank with both covers (only two of the four layers have cover)
- 7-Helmet inside the isolation tank with copper covers only
- 7-Helmet inside the isolation tank with permalloy covers only
- 7-Helmet outside the isolation tank

- 7-Helmet outside the isolation tank with signal generator on nearby

In Figure 4.8 the three most important measurement setups can be seen.

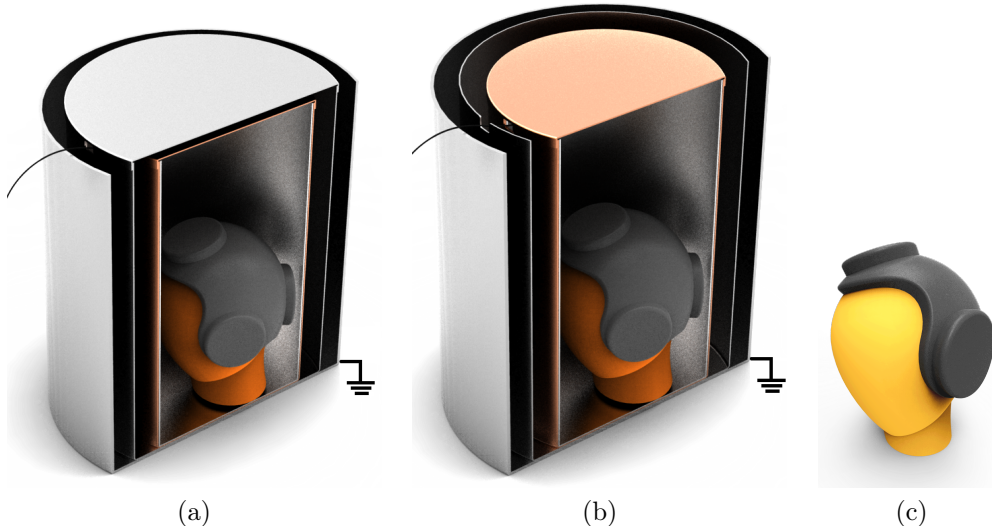


Figure 4.8.: Setup configuration for measuring noise in the 7-Helmet: (a) is using both covers, (b) using only copper cover and (c) measured outside the isolation tank.

The idea behind measuring the 7-Helmet inside and outside the isolation tank is to be able to differentiate inherent noise from ambient noise. It is expected that ambient noise will increase as the isolation decrease, while the inherent noise remains constant despite isolation variations.

The lack of wired interface on the 7-Helmet with the computer forced to have a configuration setup where the Bluetooth® dongle had to be placed inside with an USB cable. Therefore, these measurements inside the isolation tank could be not entirely isolated because this cable may act as an antenna.

## 4.2. Motion artifact analysis

Because motion artifacts caused by the movement of the electrodes are one of the main concern in the non-contact electrode system, a special analysis on them will be conducted. The idea is to reproduce this noise in order to understand it and thus be able to decide how to reduce its effect.

This section will be structured as follows. First an analytical analysis is of how a simple periodic movement affects the output of the channels. Then simulate this movement and try to reproduce it experimentally to validate previous simulation. Finally, a solution to counteract the effects of movement is evaluated.

### 4.2.1. Analytical

Given the electrical input model of the 7-Helmet [13] the output was calculated applying a sinusoidal displacement of the capacitor's plates.

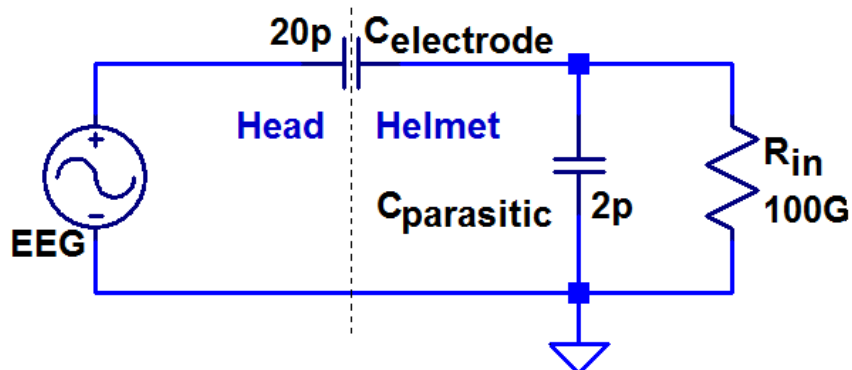


Figure 4.9.: Simplified schematic of 7-Helmet input

### 4.2.2. Experimental

To reproduce the sinusoidal displacement, the cone of a loudspeaker [61] was used as one of the capacitor's plates and as the reference potential. Then the loudspeaker was excited with a sinusoidal waveform so that the displacement of the cone would vary the distance between plates. The setup had a micrometer adjustment screw so it was possible to test it with different offsets.



Figure 4.10.: Setup to simulate the movement of the electrode by varying the distance with the reference potential.

The initial spacing between plates was 2.1 mm and a 8 V amplitude sinusoidal signal at 7 Hz excited the loudspeaker.

In order to confirm that the results were caused by the movements, analog measurements were conducted without exciting the loudspeaker but with the signal generator on (so no other possible noise source was removed).

Two different setups were tested differing only in using or not an isolation copper 'ceiling'. In Figure 4.11 both configurations can be seen. The idea of having this 'ceiling' is to connect it to ground and have higher isolation against outside noise.

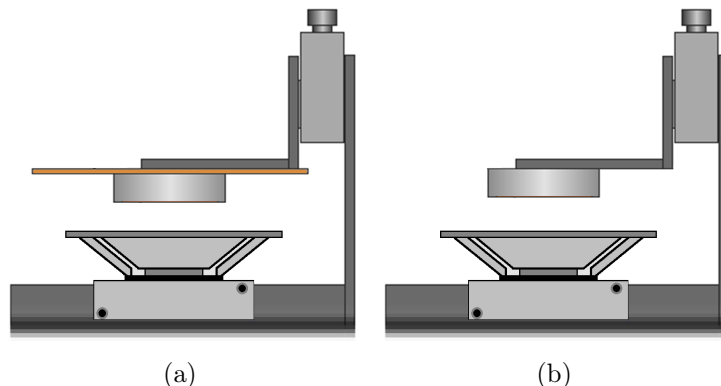


Figure 4.11.: Different setup configuration for the loudspeaker measurements. In (a) a copper "ceiling" connected to ground is used, while in (b) no "ceiling" is used.

### 4.2.3. Evaluation

Looking forward to understand how output and perturbing signal (sinus) interact and to determine how to reduce the effects of motion in the measured signals the correlation coefficients were calculated.

## 4.3. Algorithms

In the following sections different techniques are going to be used, which may not be of general knowledge. Therefore, they will be briefly explained. They are the wavelet transform, adaptive filter and independent component analysis.

### 4.3.1. Wavelets

The continuous wavelet transform transforms a function or signal of one independent variable  $t$  into a function of two independent variables  $a$  and  $b$ , related to dilation and translation of the mother wavelet.

$$x_a(t) = \int_{\mathbb{R}} WT_{\Psi} \{x\} (a, b) \cdot \Psi_{a,b}(t) \cdot db \quad (4.2)$$

Equation 4.2 is the projection of  $x$  into a subspace  $\Psi$  of scale  $a$  with coefficients  $WT$ .

Dilations and translations of the mother wavelet  $\varphi$  define an orthogonal basis in the Hilbert space  $L^2(\mathbb{R})$  of all square integrable functions, in which any signal can be represented as a linear combination of these basis functions. Unlike the Fourier transform, which is confined to the sine and cosine bases, the continuous wavelet transform can have many forms of mother wavelets to choose from. The main requirement is that they should integrate to zero, “waving” above and below the x-axis. Another and most important difference with the Fourier transform is that wavelets are located in both frequency/scale (via dilations) and time (via translations), which tries to overcome the main resolution time-frequency trade-off in spectrograms –here called scalograms [62, 42, 63].

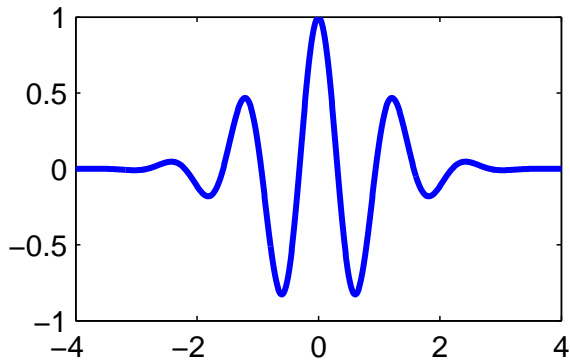


Figure 4.12.: Example of mother wavelets: Morlet

The wavelet transform can be used to get parameters of an original signal that are easily detected in one of its levels of decomposition. Also to apply some processing to the coefficients, like thresholding, and then reconstructing the signal.

A simple example is shown in Figure 4.13, where a signal (with smooth and sharp variations) is contaminated with white noise. After thresholding the coefficients (see Figure 4.14) of the wavelet transform it was possible to remove this noise that appears in every frequency without loosing information of the original signal (for more details of this example see Appendix A.3).

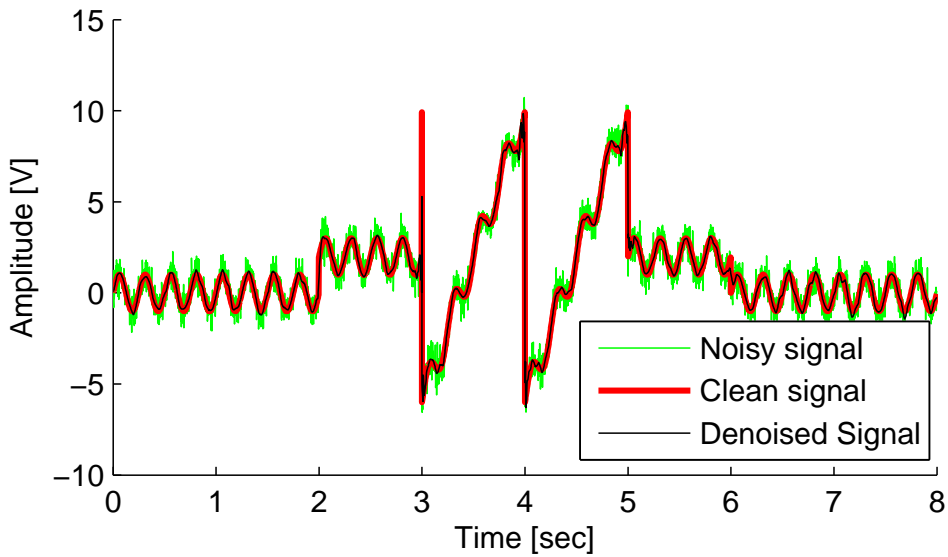


Figure 4.13.: Example of data processed with wavelets

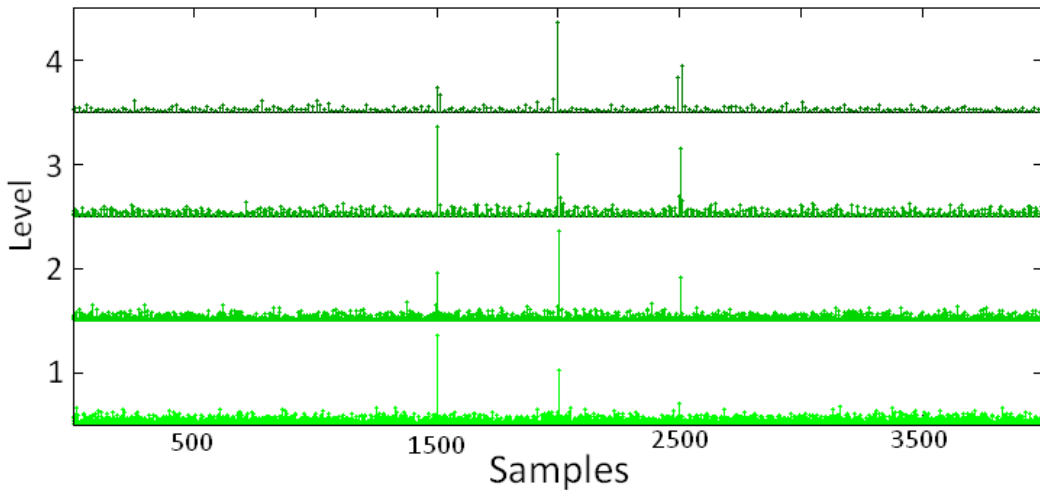


Figure 4.14.: Detail coefficients of the four level of decomposition

### 4.3.2. Independent component decomposition

When having different emitting sources interfering between each other, it could be desirable to recover the original sources. This is the main goal of blind source separation (BSS) techniques. The classical example is the cocktail party, where a lot of people are talking in one room and their voices are being recorded with several microphones. The aim is to separate each voice into a separate speaker channel. Because BSS is unsupervised, is like a black box in which many problems are encountered, for example time delay, different amplitudes, among others specifics fore each case [64].

Independent Component Analysis (ICA) is a BSS technique, which assumes that original underlaying sources are mutually independently distributed and non-Gaussian. Another characteristic is that it needs at least the same amount of signals as sources there were. It is a transformation which tries to maximize the separation between signals. In order to do that it finds a set of orthogonal axes and project the data onto them to decorrelate it, this is called *whiten the data*. Then, it rotates the axes and projects them to the original coordinate frame [64].

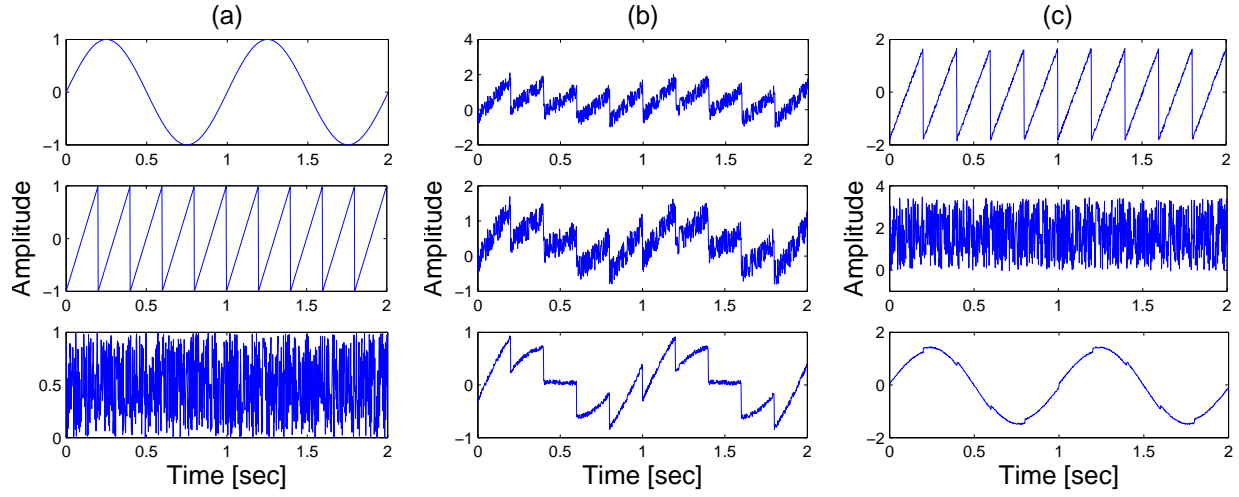


Figure 4.15.: Example of how ICA works. In (a) the original sources are shown. (b) are the measured signals from which the sources should be found; they are a linear combination of sources presented in (a). (c) shows the output of ICA, an estimation of the sources.

The signals used to estimate the sources should be a linear combination of them, as shown in Equation 4.3.

$$m_i(t) = \sum k_j \cdot s_j(t) \quad (4.3)$$

being  $m_i$  the mixed sources,  $s_j$  the sources and  $k_j$  a random number.  $i = 1, 2, \dots, N_m$  with  $N_m$  the amount of signals available to perform ICA, and  $j = 1, 2, \dots, N_s$  with  $N_s$  the amount of sources composing the signals.

Figure 4.15 illustrates the operations of ICA. It can be seen that the estimated sources approximate really good to the original sources.

Some of ICA disadvantages are:

- in theory it cannot estimate correlated sources. Nevertheless, in a majority of cases it has a good performance with non-Gaussian sources. Also, sub band decomposition ICA is a technique that separates the signals into narrower bands which are expected to have less correlation than those in the whole band.

- it cannot find more sources than the amount of input signals. One technique that attempts to overcome this issue is called *Overcompleted ICA*.
- when the input signals are many more than the sources it can be harder to estimate the sources. In this case, a dimensional reduction must be conducted.
- it assumes linear mixing of sources.
- it assumes stationary mixing of sources. This implies a time invariant mixing matrix.

### 4.3.3. Adaptive filters

An adaptive filter is a filter which adapts its transfer function while it is filtering. In order to do that, a close loop is needed as well as a weight function. A general scheme is shown in Figure 4.16. Depending on the application it could have variations, but one possible variable assignment could be  $x(n)$  as the reference signal,  $d(n)$  as the input signal containing both desired signal and unwanted noise and the output in this case would be the error  $e(n)$ . In order to this filter works,  $x(n)$  must present some correlation with the undesired noise present in  $d(n)$ .

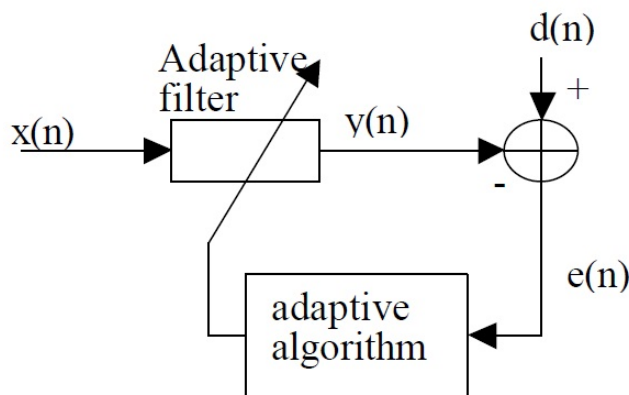


Figure 4.16.: General scheme of adaptive filter [65].

A classical example is reducing power line interference from a measurement. The most efficient approach would be measuring directly from power line to have an accurate frequency measurement, but using a sinus can also do a fine job. Though it is necessary to use two sinus waves with different phase shift so the initial phase of the measurement would not

matter.

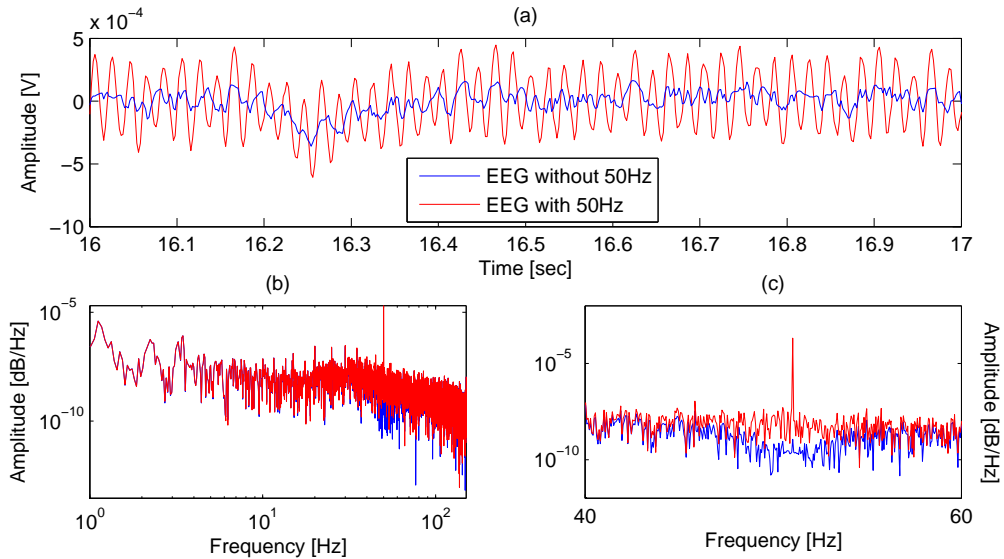


Figure 4.17.: Example how adaptive filter works. In (a) the measurement with power line interference and the denoised signal is shown; (b) shows the spectrum in the whole range and (c) in the 50 Hz band.

Figure 4.17 shows how 50 Hz interference can be canceled from a real EEG measurement and Figure 4.17.(b) shows how only the hum is removed and not other important data.

## 4.4. Denoising methods

### 4.4.1. Auxiliary sensors: gyroscope and accelerometer

The first approach was using the already built-in auxiliary sensors of the 7-Helmet. They are a triaxial accelerometer and a triaxial gyroscope located on top of the 7-Helmet as shown in Figure 4.18. Correlations between sensors and leads were calculated in order to know if it would be possible to apply the sensor information into denoising the EEG measurements, specially for motion artifacts caused by the movement of the electrodes. To improve the correlation a correction of delays between signals was conducted, and both cases were compared.



Figure 4.18.: Accelerometer and gyroscope in 7-Helmet and their corresponding axes.

If the results in Section 4.2 show that it is possible to counteract the effects of movement in the measured signals with some information of how the movement was, these sensors could be useful to apply the same concepts in the EEG measurements.

### 4.4.2. Pre-processing

Prior to further denoising algorithms some pre-processing filtering techniques were applied. They were not always the same due to particular requirements of each algorithm, therefore they will be mentioned each case.

#### 4.4.2.1. Bandpass filter

More important than removing unwanted components was not disturbing the actual EEG, therefore Butterworth filters were used in order to minimize the ripple in the passband. The cutoff frequencies depend on each case and not always the same were used.

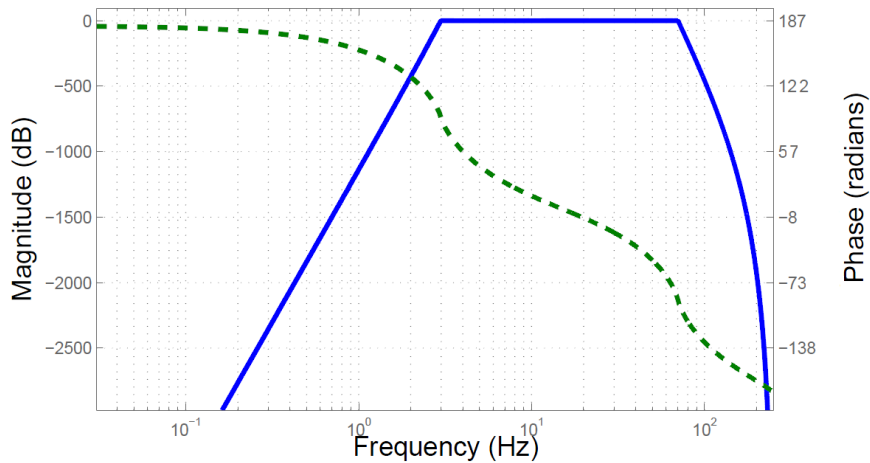


Figure 4.19.: Frequency response of band pass filter used to pre-process the measurements

#### 4.4.2.2. Notch filter

To remove power line interference a notch filter at 50 Hz was used.

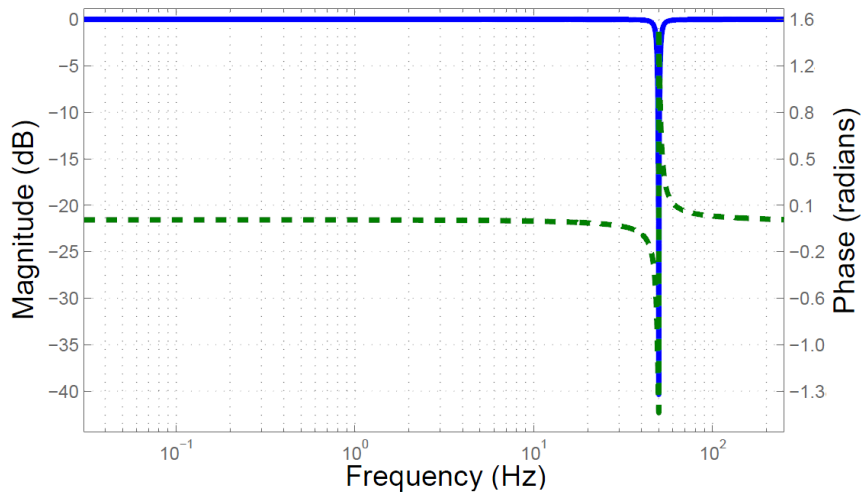


Figure 4.20.: Frequency response of notch filter (at 50 Hz) used to pre-process the measurements.

#### 4.4.2.3. Adaptive filter

In order to remove unwanted 50 Hz hum also an adaptive filter was used (see Section 4.3.3 for more details). The selectivity of the adaptive filter is higher but the notch filter is faster.

### 4.4.3. Motion artifacts

Due to the fact that motion artifacts are the main concern when using a capacitive acquisition system, several denoising attempts were made with different techniques.

#### 4.4.3.1. Linear filter

The first and simplest approach is to use a band pass filter or just a high pass filter, due that most artifacts with higher amplitude are below 4 Hz, for example breathing.

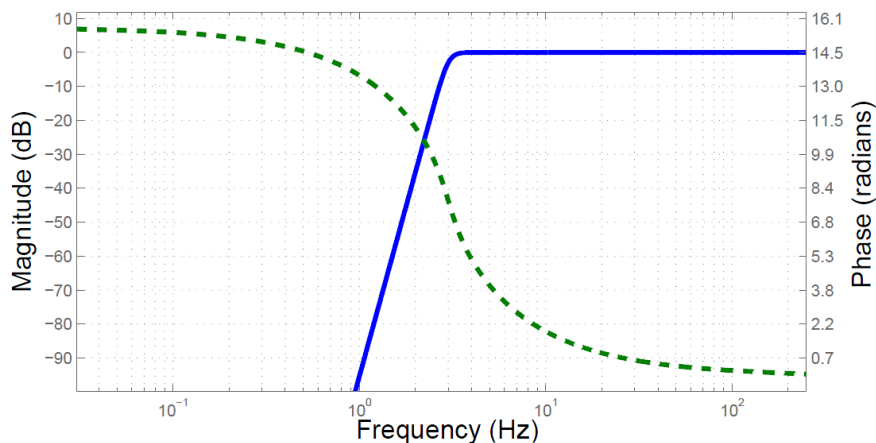


Figure 4.21.: Frequency response of high pass filter used to remove unwanted artifacts

#### 4.4.3.2. Wavelet

Matlab's<sup>®</sup> toolboxes and functions were used to evaluate the signals.

As a first step, a visual study of wavelet coefficients was done, testing how divers mother wavelets and levels of decomposition work. Then, wavelet denoising was performed by using **wden** function with universal thresholding rule ( $\sqrt{2 * \log d}$  [66]), 8 levels of resolution and soft-thresholding. Afterwards, **cmddenoise** was tested under a simple programmed GUI (see Figure 4.22) in order to see which artifacts could be detected by thresholding the coefficients.

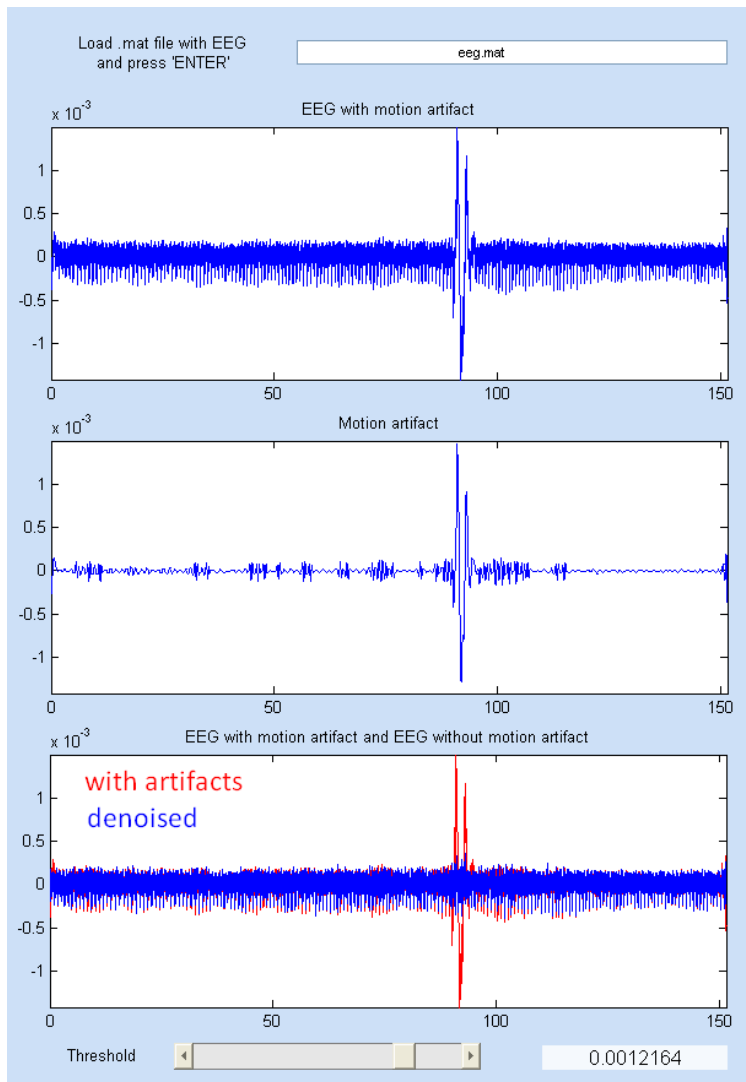


Figure 4.22.: Simple GUI to test the effects on threshold variations

Finally, a translation invariant wavelet transform was tested. To address the shift invariance in critically-sampled wavelet transform a cycle spinning was done before and after making the transformation, following directions from Misiti *et al.* [63].

As the highest motion artifacts are mostly located in lower frequencies, at first glance of the denoised signal spectrum, it could be thought that a simple high pass filter could be used. In order to verify that the performance is better and more reliable than a high pass filter both techniques are going to be compared. Moreover, a fake low frequency and low amplitude sinus wave was added to the noisy signal and, after denoising it, the sinus is expected to remain intact using wavelet thresholding –while the low pass filter will certainly remove both sinus and noise.

#### 4.4.3.3. ICA

Different ICA methods and algorithms were tested in order to obtain the sources that composed the EEG measurement. The most important ones were:

- Second order blind identification (SOBI) [67]
- Kernel ICA (KDICA) [68]
- Fast ICA (FASTICA) [69]

After having the signal decomposed (in the same amount of sources as the amount of input leads), the sources containing mostly noise and artifacts were not included in the recomposition.

Being  $S$  the sources from  $X$  (input signals) obtained by  $M$  (demixing matrix) such that  $S = M \cdot X$ , noisy signals in  $S$  are set to zero and  $X$  denoised is reconstructed,  $X_{denoised} = M^{-1} \cdot S$

#### 4.4.3.4. Comparison of ICA, wavelets and the combination of both

A more effective approach is to apply some denoising techniques before reconstructing the signals, and not simply to cancel sources because EEG components may be also lost. Therefore, wavelet thresholding is combined with ICA.



Figure 4.23.: Diagram of how ICA works in combination with wavelet thresholding.

To compare the effectiveness of only using wavelets or ICA or this combination, an EEG containing alpha wave components was used. In this way a visual analysis in time can be easily done because of the higher amplitude of alpha waves. The measurement was done alternating open eyes (low alpha waves) with closed eyes (high alpha waves) every 20 seconds.

#### 4.4.4. ECG artifacts

Similar approaches were used to denoise the measurements from ECG contaminations.

#### 4.4.4.1. Linear filter

As the sensors (gyroscope and accelerometer) register the ECG activity, they were employed to remove it. Main frequency of the ECG can be obtained from sensors spectrum and therefore use it to apply three adapted notch filters in that frequency and in the first two harmonics.

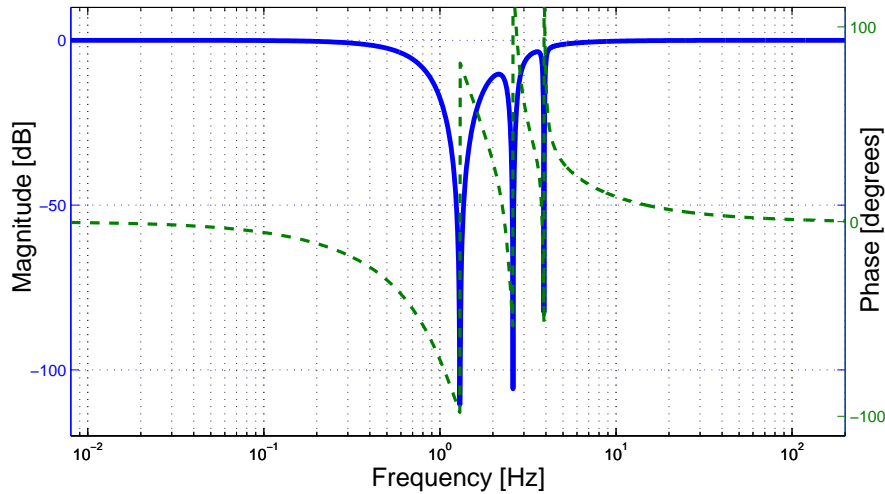


Figure 4.24.: Frequency response of 3 notch filters used to remove ECG components.

#### 4.4.4.2. Wavelet thresholding

Using same methods as Section 4.4.3.2 but setting the threshold to modified higher coefficients of the wavelet transform, so ECG could be detected and afterwards canceled.

### 4.4.5. SSVEP enhancement: bipolar lead and SNR

The last denoising method was focused on SSVEP enhancement. To measure the quality of a SSVEP measurement, signal to noise ratio (SNR) was used. The SNR of a SSVEP component in  $y(t)$  at frequency  $f$ , being the Power Spectral Density  $Y(f)$  was computed as:

$$SNR = \frac{\sum_{f_i=f-\Delta s}^{f+\Delta s} N \cdot Y(f_i)}{\sum_{f_i=f-\Delta n}^{f+\Delta n} Y(f_i)} \quad (4.4)$$

where  $\Delta s = 0.3$  Hz is the tolerance range to locate the SSVEP maximum and  $\Delta n = 2$  Hz is the frequency range to measure noise nearby the SSVEP.  $N$  is the length of the used samples.

#### 4.4.5.1. Time span selection

Given a long duration SSVEP measurement where it is highly possible that the volunteer using the 7-Helmet had concentrated more in some time spans than in others, the power spectral density (PSD) will have higher SSVEP components if it is only computed from those time spans rather than from the whole measurement. Therefore, an automatic algorithm was programmed to find those time spans, in which the volunteer had higher concentration. Periods of time no shorter than 10 seconds were chosen, due to they would not be representative of the measurement. A normalization of the SNR was done, so a measurement with SNR above 1 was declared as good and below 1 as not-good.

#### 4.4.5.2. ICA enhancement

Once the time span with higher SNR was found, the signals sources in that time were estimated using ICA and only the ones containing mostly noise were removed. The idea behind this is to enhance the SNR of a SSVEP measurement and be able to determine if in fact the volunteer was concentrated in certain visual stimulations. A comparison was made between using this method and without it with different signals and time spans.

#### 4.4.5.3. Bipolar lead selection

The following algorithm is an adaptation of a procedure presented by Wang *et al.* (2004) [70]. This algorithm aims to find two electrodes which share a similar background noise and only one of them has SSVEP component. Thus, when creating together a bipolar lead the noise would be canceled and consequently the SNR of the SSVEP would be higher.

This implementation would work successfully only with the 24-Helmet because it has enough leads to find the appropriate match among them. It is expected to find the electrode with high SSVEP in the area of the visual cortex, while the reference electrode in the nearby. Therefore, no more than the 13 electrodes closer to the visual cortex were used. In order to select this two leads the following sequence of steps were followed:

1. Calculate for each electrodes's sources (obtained by ICA) the SNR of SSVEP.
2. With the four (approximate one third of the amount of sources) sources of higher SNR a new signal is reconstructed, named  $S_{signal}$ , which will be the part of the electrodes containing only SSVEP components and no noise.

3. With the rest of the sources a new signal is reconstructed, named  $S_{noise}$ , which will be the part of the electrodes containing only noise and no SSVEP component.
4. The four (approximate one third of the amount of channels) channels from  $S_{signal}$  with highest SNR will be the possible main lead.
5. Correlate  $S_{noise}$  signals between the same channels from previous step and the rest.

$$\rho_{noise_{s_i r_j}} = \text{cov}(EEG_{noise_{s_i}}, EEG_{noise_{r_j}}) \sqrt{\text{var}(EEG_{noise_{s_i}}) \cdot \sqrt{EEG_{noise_{r_j}}}} \quad (4.5)$$

with  $i = 1, 2, 3, 4$  and  $j = 5, 6, \dots, 13$ , being  $EEG_{noise_{s_i}}$  the four channels with greater SNR in descending order and  $EEG_{noise_{r_i}}$  the remaining channels.

6. The channels with highest noise correlation will be the possible reference lead.
7. Visually inspect the best bipolar lead (main lead - reference lead).

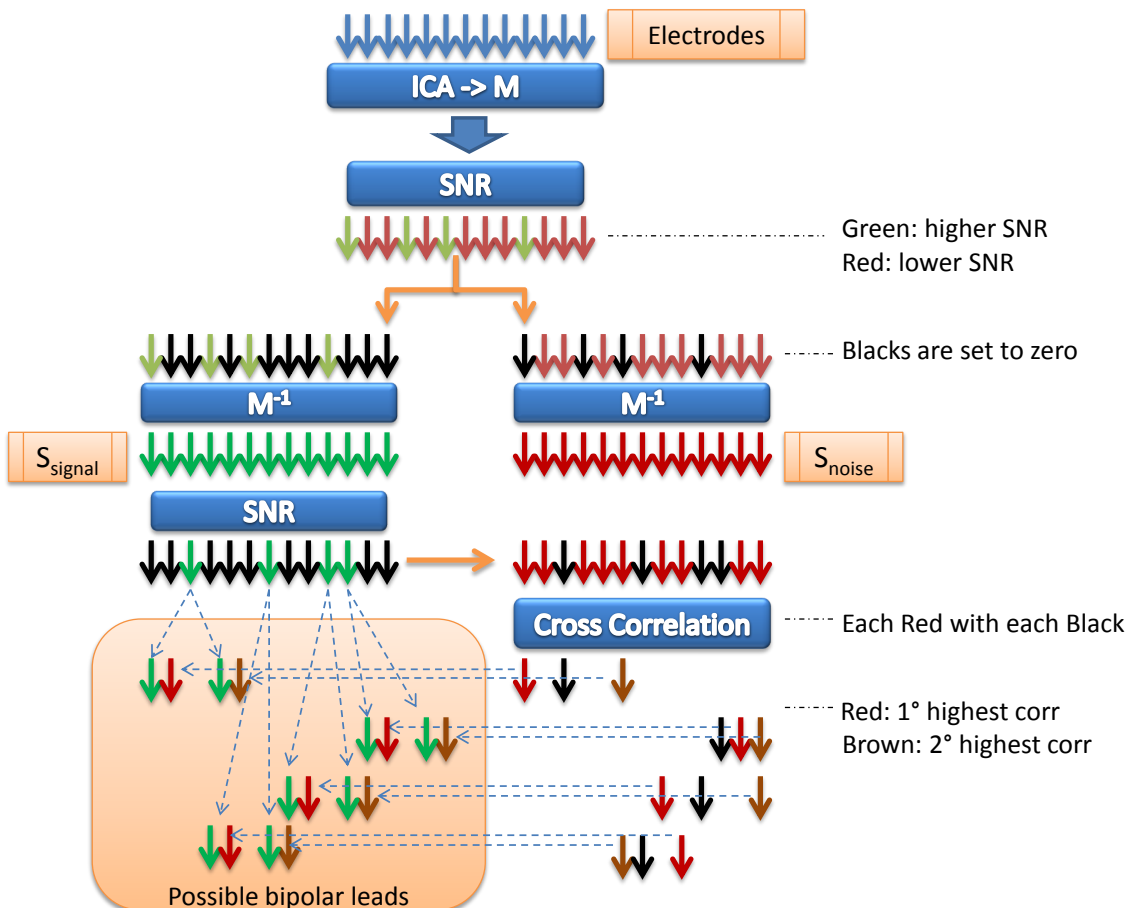


Figure 4.25.: Scheme of bipolar lead selection algorithm flow

# 5. Results

The spectrum of the measurements presented in this chapter were calculated using Welch's power spectral density estimate and a Blackman window.

## 5.1. Study of the acquisition system

### 5.1.1. Analysis of leads

#### 5.1.1.1. All leads together

In Figure 5.1 the spectrum of the measurement as explained in Section 4.1.1.1 applying a sinusoidal waveform of 0.5 mV at 75 Hz on the reference electrode is shown. Two unexpected results can be seen, first a frequency component at 24.54 Hz appeared which will be later analyzed, and second the 50 Hz component had more deviation between leads than the components at 75 Hz and 24.54 Hz.

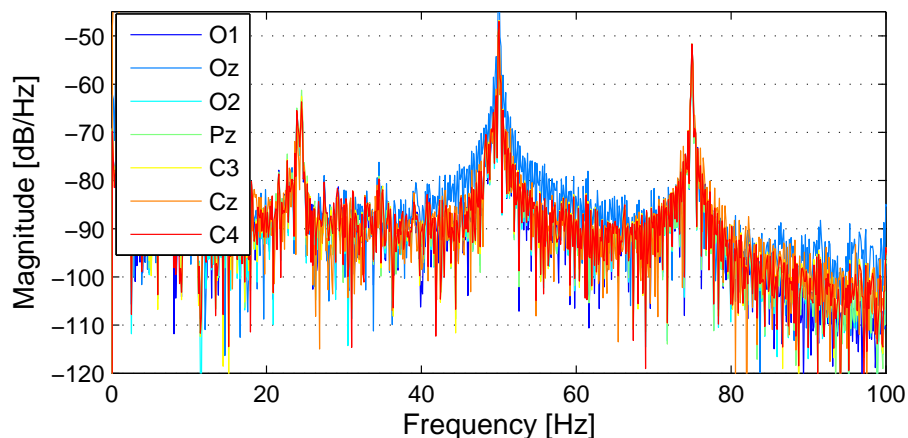


Figure 5.1.: Spectrum of the gain measurement of all leads

A detailed statistic of measurements is presented in Figure 5.2.

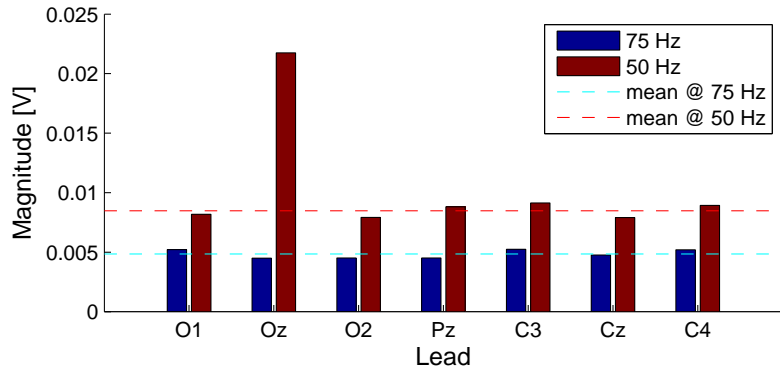


Figure 5.2.: Spectrum's peaks at relevant frequencies in gain comparison measurement with an applied signal of 5 mV at 75 Hz; the mean of 50 Hz component was computed without Oz measurement.

All electrodes have similar gain with a deviation lower than 10%, except Oz, which has, at 50 Hz, three times more amplitude than the rest. The non-direct proportionality between 50 Hz and 75 Hz components that can be seen in Figure 5.2, for example between O1 and Pz can be caused to the anti-aliasing filter.

#### 5.1.1.2. Each lead at a time

The measurement explained in Section 4.1.1.2 was repeated 7 times, one time for each lead, but only the measurement for lead O2 is shown in Figure 5.3 to represent how the results look like (the complete result can be seen in Appendix A.4).

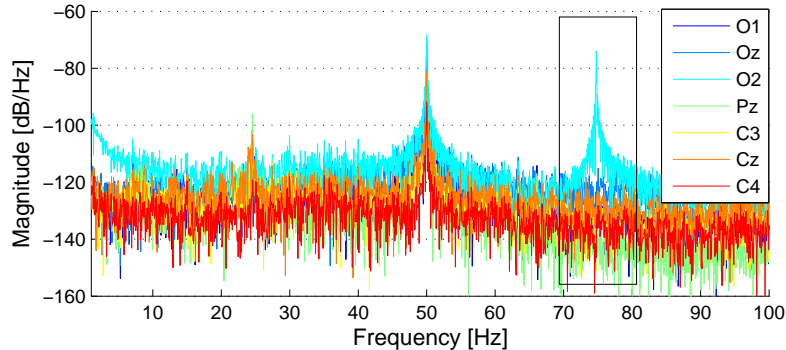


Figure 5.3.: Measured signals of all electrodes applying 1 mV amplitude sinus at 75 Hz only on O2

The statistic in Figure 5.4 is the result of the 7 measurements, it is an average from two simulations per lead. A dispersion of 16% from the optimal calibration level calculated as the measured amplitude over the theoretical output can be seen.

$$\text{Relative gain deviation} = \frac{\text{signal}_{\text{measured}}}{\text{signal}_{\text{applied}} \cdot \text{gain}_{\text{theoretical}}} \quad (5.1)$$

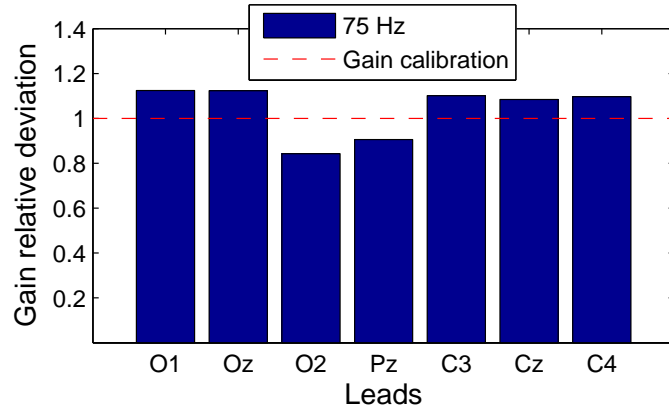


Figure 5.4.: Statistic of gain calibration at 75 Hz for each lead

### 5.1.2. Common mode rejection

The results of the measurements from Section 4.1.2 present greater dispersion compared to previous results (Section 4.1.1.1). Again, Oz has higher amplitude at 50 Hz than the rest, and the component at 24.56 Hz (refer to Section 5.1.1.1) appeared only in 4 electrodes: O2, Pz, C2 and C4.

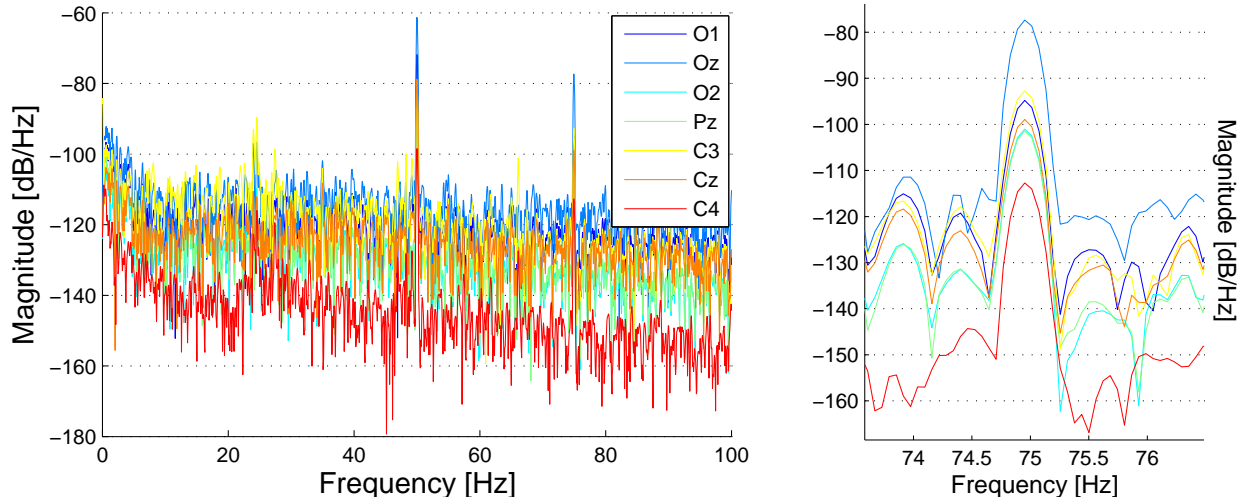


Figure 5.5.: Spectrum of each lead with the common mode input signal at 75 Hz

An average of two measurements is shown in Figure 5.6, where the components at

75 Hz and 50 Hz of each lead are compared. The variations at 50 Hz were higher than at 75 Hz, where only Oz presents a higher deviation compared to the other leads. A possible reason could be that the contact to the foil in the dummy head was not good compared to the others.

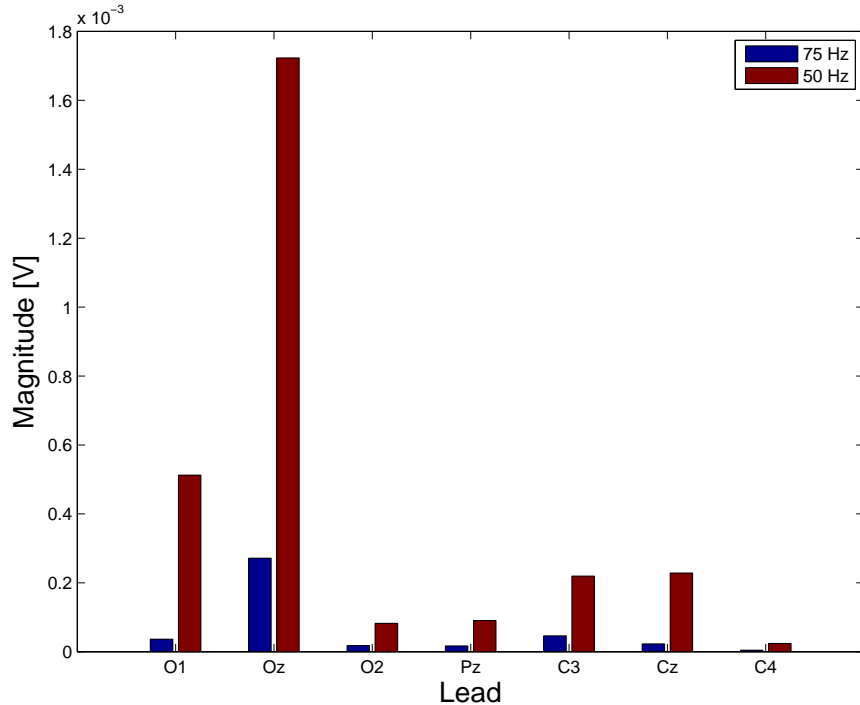


Figure 5.6.: Statistic of signal rejection at 75 Hz and 50 Hz for each lead

To present an approximation to a standardized value, the Common Mode Rejection Ratio (CMRR) was computed only at 75 Hz.

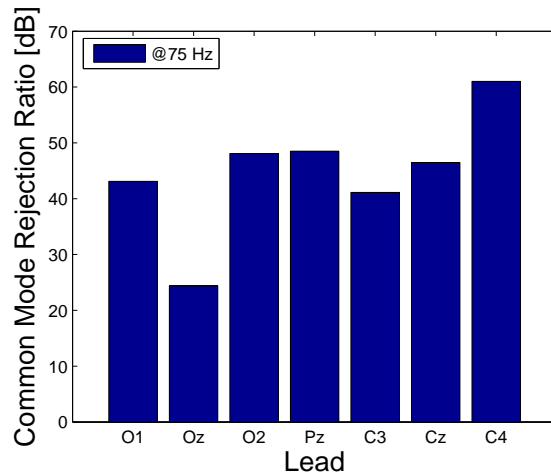


Figure 5.7.: Common Mode Rejection Ratio calculated at 75 Hz

### 5.1.3. Crosstalk

All results presented in this section are an average of two measurements.

#### 5.1.3.1. Crosstalk with dummy head

A measurement of 10 second long was made applying a signal of 4.2 mV on an electrode and then it was compared with the signals sensed in the rest of the electrodes. Only the result of applying signal in Oz is shown (see Appendix A.5 for the complete results), but for every frequency the crosstalk was below 1%.

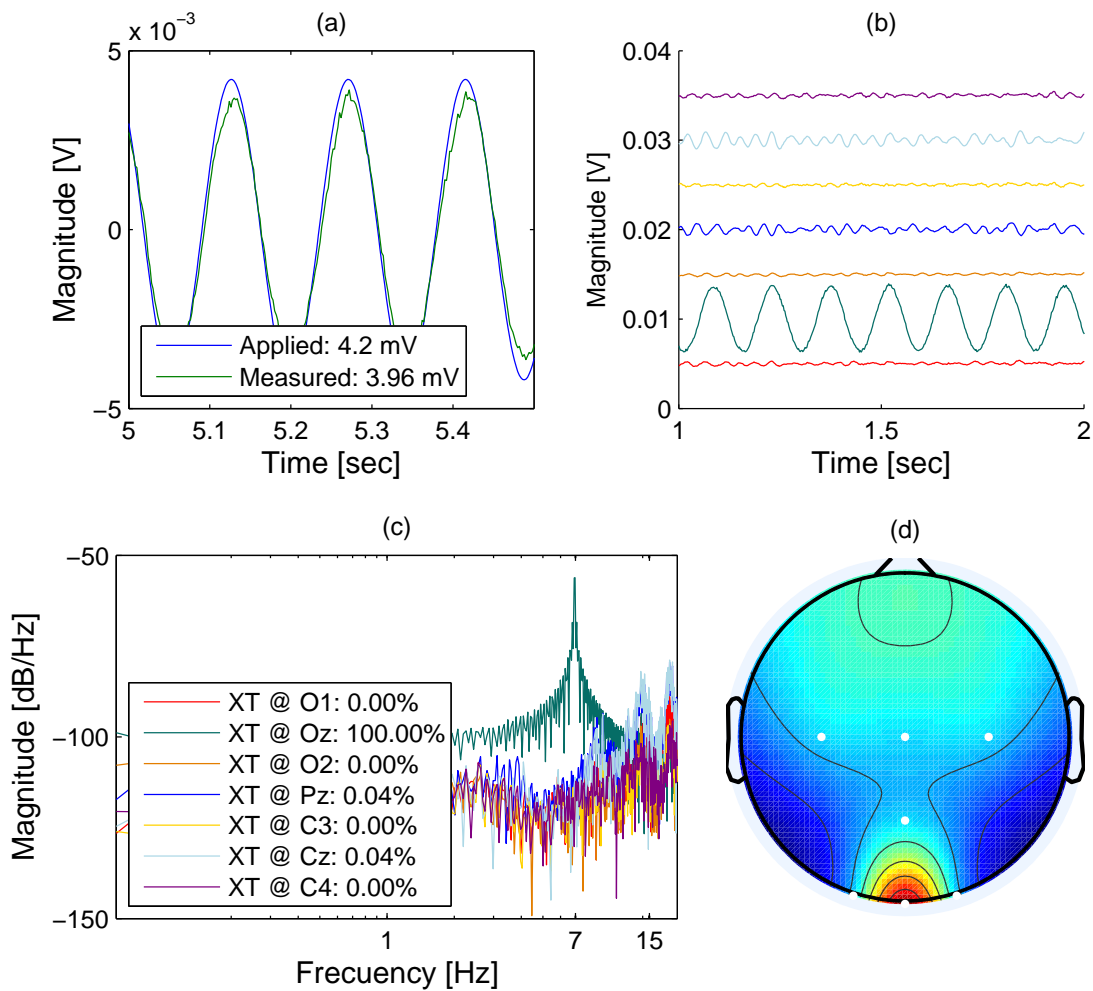


Figure 5.8.: Crosstalk from electrode 2 (Oz) to the other leads. (a) shows the applied signal and the measured signal in Oz. In (b) are all lead outputs in descending order (C4, Cz, C3, Pz, O2, Oz, O1) shown. (c) shows the spectrum of each lead and the crosstalk in percentage. (c) is the topographic plot [71] with a scale from red to blue in descending power density.

### 5.1.3.2. Crosstalk without dummy head

A measurement of 15 second long was made applying a signal of 42 mV to an electrode and then it was compared with the signal sensed in the rest of the electrodes. The crosstalk measured without the dummy head was over 100% at least in one electrode for each measurement (mostly in Pz). The other channels present no consistent pattern between measurements and they spread along the whole range. A comparision of crosstalk was done repeating the measurement five times and then another five times previous reacomodation (re-setting up) of the electrode which applied the signal. The results can be seen in Figure 5.10. While the electrodes remain constant in the same setup configuration, with a slight variation the crosstalk presents variations and even the order of electrodes with more crosstalk changes.

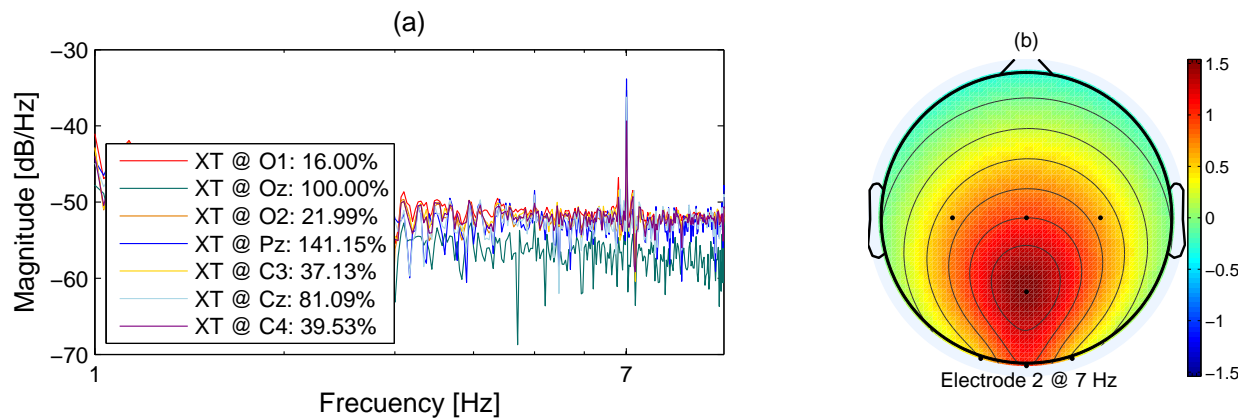


Figure 5.9.: Spectrum of each lead with the crosstalk in percentage and the topographic plot

In Figure 5.9.b, the topographic plot presents higher activity at lead Pz rather than at Oz, where the signal was applied.

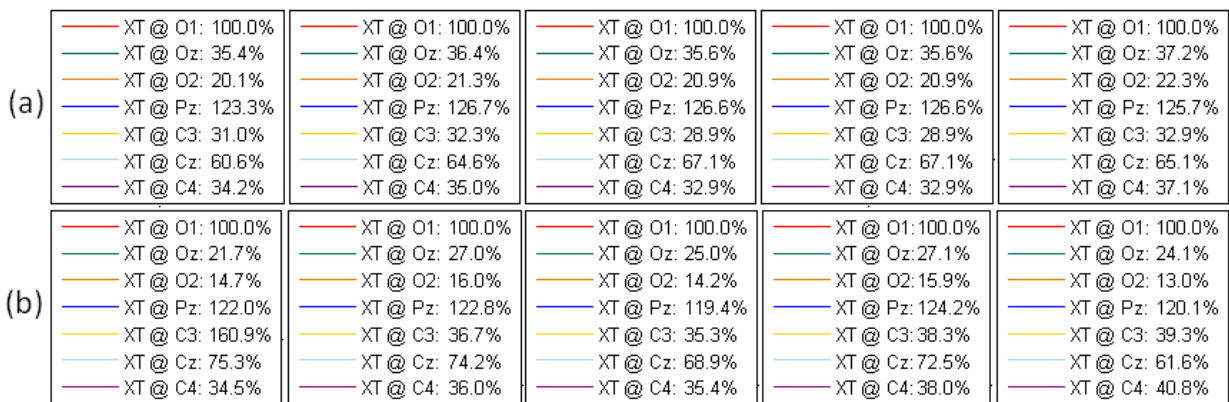


Figure 5.10.: Crosstalk measurement repetition over O1, re-setting up the measurement configuration from (a) to (b) after a while

After repeating the measurements with different accommodations of the 7-Helmet no consistent pattern could be found. In Figure 5.10 it can be seen that not only the levels of crosstalk variated from one 'accommodation' to another but also the order of influenced channels.

#### 5.1.4. Noise sources

All results are an average of six measurements repetitions. With high isolation (using copper and permalloy covers) low amplitude component at 50 Hz was measured as it was expected, because it is known to be an outside source. Using only the copper cover a low peak at 24.56 Hz appeared (see Figure 5.11.(b)) and without isolation it had higher amplitude. In every case the average noise density was below  $10 \mu\text{V}/\text{Hz}$ .

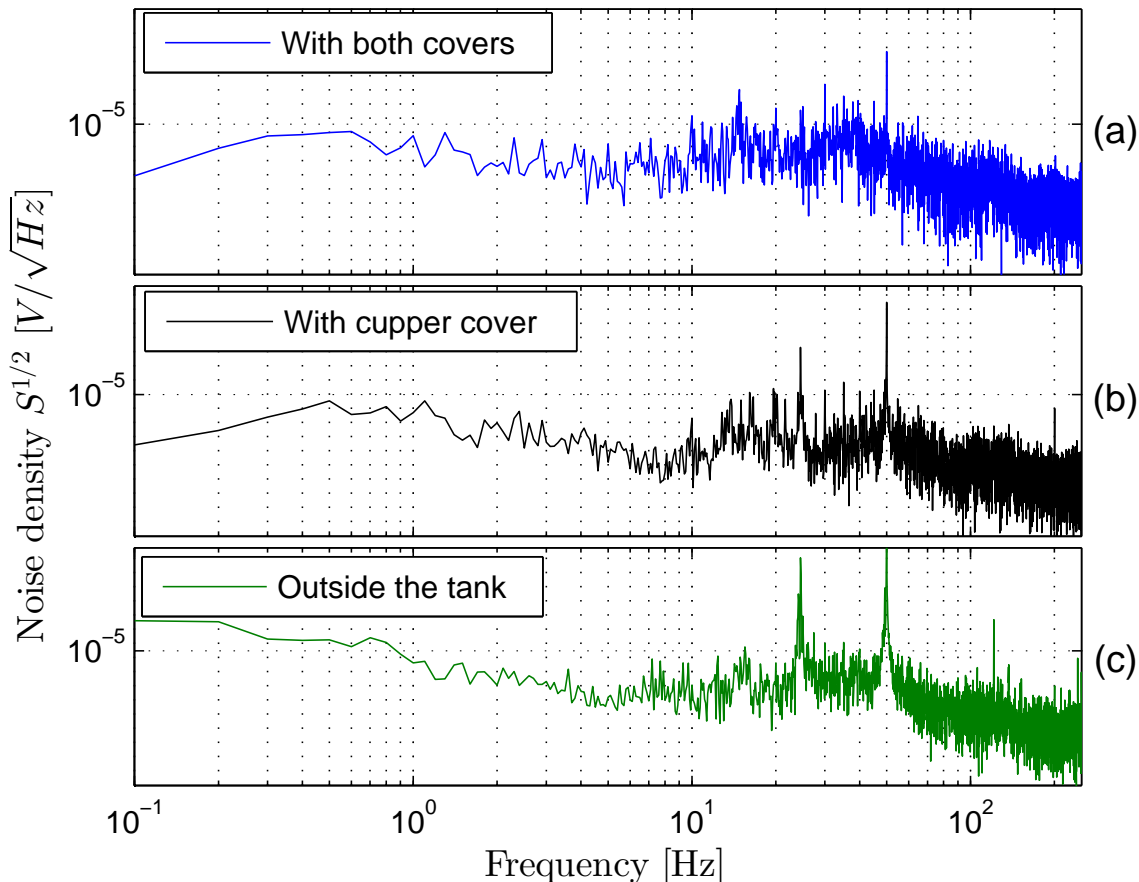


Figure 5.11.: Noise measurement of the 7-Helmet: (a) was measured with 7-Helmet inside the tank and using both cover. (b) was covered only with permalloy cover, and (c) was measured outside the tank.

## 5.2. Motion artifact analysis

### 5.2.1. Analytical

#### 5.2.1.1. Analysis

The impulse response of the circuit (see Figure 4.9) is:

$$T(s) = \frac{\frac{1}{s \cdot C_1 + \frac{1}{R}}}{\frac{1}{s \cdot C_1 + \frac{1}{R}} + \frac{1}{s \cdot C_2}} = \frac{C_2 \cdot R \cdot s}{R \cdot s \cdot (C_1 + C_2) + 1} \quad (5.2)$$

Then, the sinus response is calculated anti-transforming the impulse response multiplied by the sinus transformation.

$$\begin{aligned} \mathcal{L}_s^{-1} \left[ \frac{C_2 \cdot R \cdot s}{R \cdot s \cdot (C_1 + C_2) + 1} \cdot \frac{\omega}{s^2 + \omega^2} \right] (t) = \\ \frac{C_2 \cdot R \cdot \omega \cdot (R \cdot \omega \cdot (C_1 + C_2) \cdot \sin(\omega \cdot t) - \exp -\frac{t}{R \cdot (C_1 + C_2)} + \cos(\omega \cdot t))}{(C_1 \cdot R \cdot \omega)^2 + 2 \cdot C_1 \cdot C_2 \cdot (R \cdot \omega)^2 + (C_2 \cdot R \cdot \omega^2) + 1} \end{aligned} \quad (5.3)$$

Evaluated on estimated values may simplify the understanding:

$$\begin{aligned} C_1 = 2 \text{ pF}, \quad C_2 = 20 \text{ pF}, \quad R = 100 \text{ G}\Omega \\ \frac{10 \cdot \omega \cdot (11 \cdot \omega \cdot \sin(\omega \cdot t) + 5 \cdot \cos(\omega \cdot t) - 5 \cdot \exp -5 \cdot \frac{t}{11})}{121 \cdot \omega^2 + 25} \end{aligned} \quad (5.4)$$

#### 5.2.1.2. Simulation

The sinus response of the circuit was compared with a constant and a variable  $C_2$  (electrode capacity):

$$C_2 = \frac{\epsilon_0 \cdot \epsilon_r \cdot \text{Area}}{\text{distance}_0} \quad \text{and} \quad C_2(\text{distance}) = \frac{\epsilon_0 \cdot \epsilon_r \cdot \text{Area}}{\text{distance}_0 + \text{distance}}$$

When the distance is variating at the same frequency of the input signal, in time domain the output seems to be the same as the input but with lower amplitude. Instead, in frequency domain peaks can be seen at the harmonics.

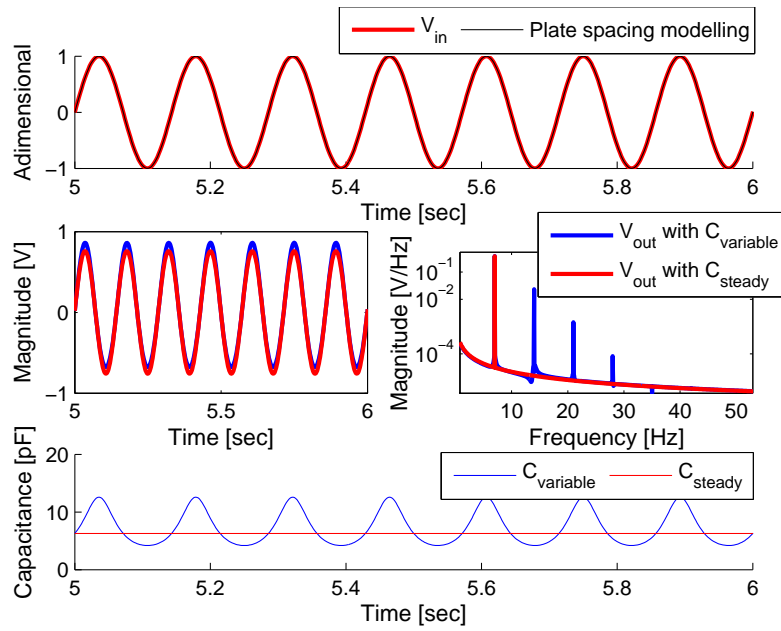


Figure 5.12.: Simulation of electrode input circuit with variable and constant electrode's capacity: an sinus waveform at 7 Hz was used, both to excite the input and to variate the distance of the capacitor  $C_2$ .

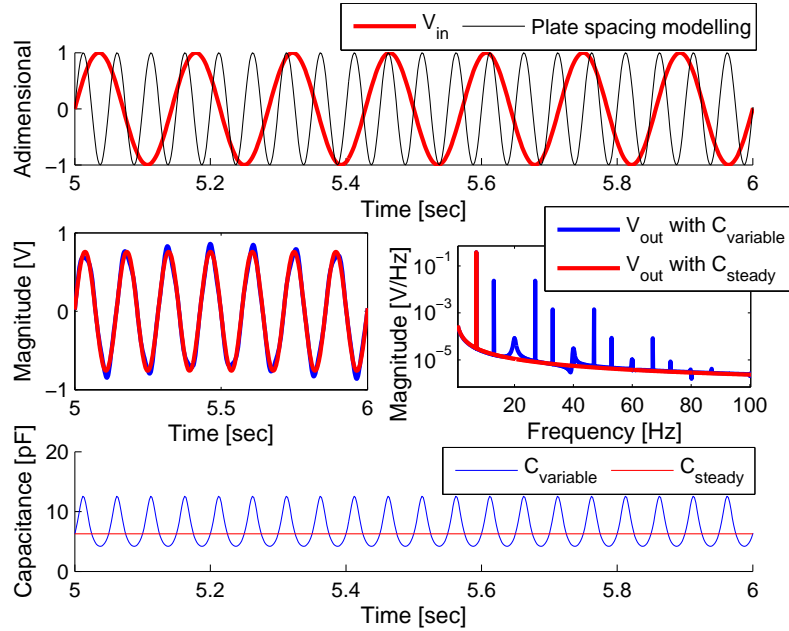


Figure 5.13.: Simulation of electrode input circuit with variable and constant electrode's capacity: an sinus waveform at 7 Hz was used to excite the input and a sinus at 20 Hz to variate the distance of the capacitor  $C_2$ .

When the excitation signal and movement of the electrodes differ, the output results in

a modulation. The capacitance is variating as the inverse of a sinus ( $\propto \frac{1}{\sin(2 \cdot \pi \cdot t \cdot f)}$ ) changing both time constant of the circuit and magnitude of the output.

After simulating the effects of movement of an electrode, an experimental reproduction of this was conducted. Because the setup does not allowed a different signal as excitation and distance variation, only the results in Figure 5.12 will be experimentally compared.

### 5.2.2. Experimental

Applying a 7 Hz sinusoidal waveform to the loudspeaker a sinusoidal variation of the capacitor's plates was reproduced. The sensed signal showed analog behavior to previous simulation where there is a peak in every harmonic (see Figure 5.12).

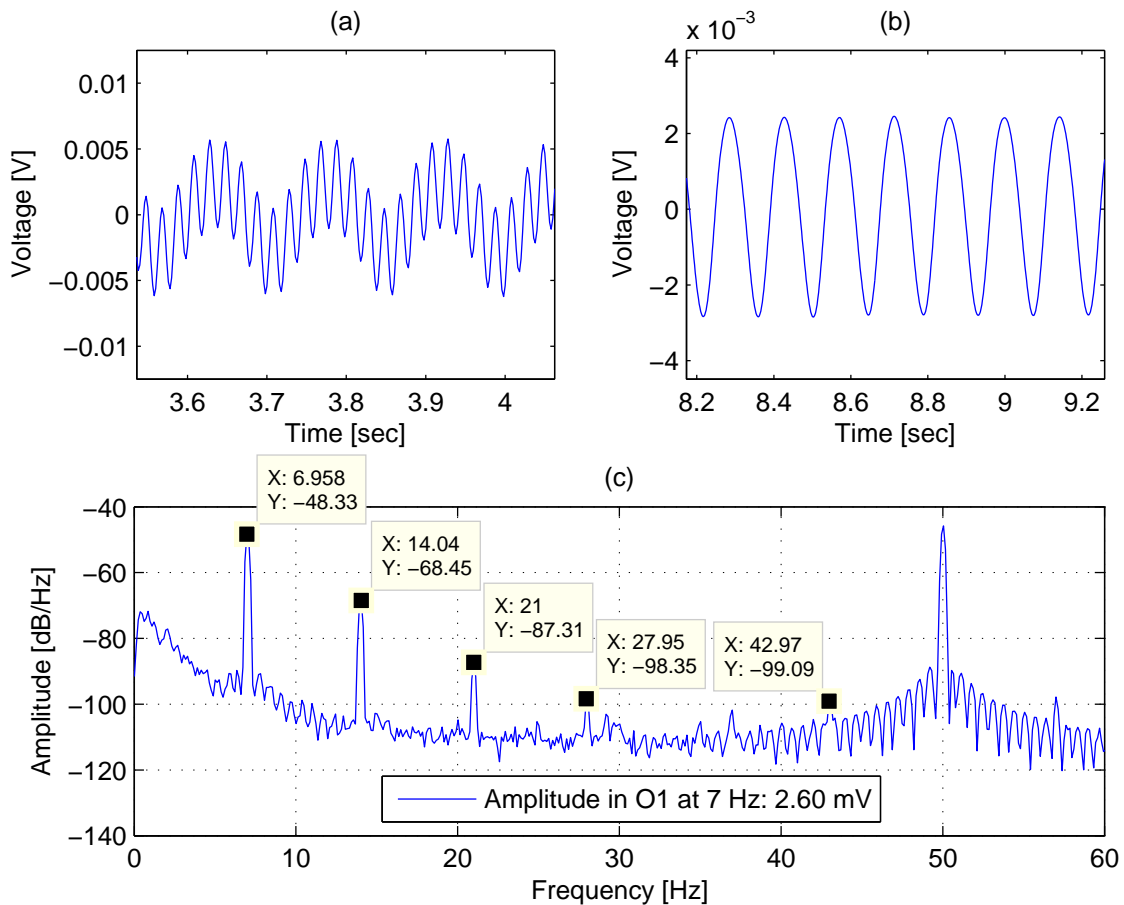


Figure 5.14.: In (a) is the sensed signal with the loudspeaker excited and in (b) also, after a notch filter at 50 Hz. (c) is the spectrum of the measurement with a tick label in each harmonic (it contains the 50 Hz component).

Figures 5.14 and 5.15 compare both situations with the loudspeaker excited or not. In the second case, where the idea was not to have a variation in the capacitance, the signal was applied to the capacitor's plate attached on the loudspeaker's membrane. Without the loudspeaker excitation none of the harmonics appeared as in the simulation shown in Figure 5.12.

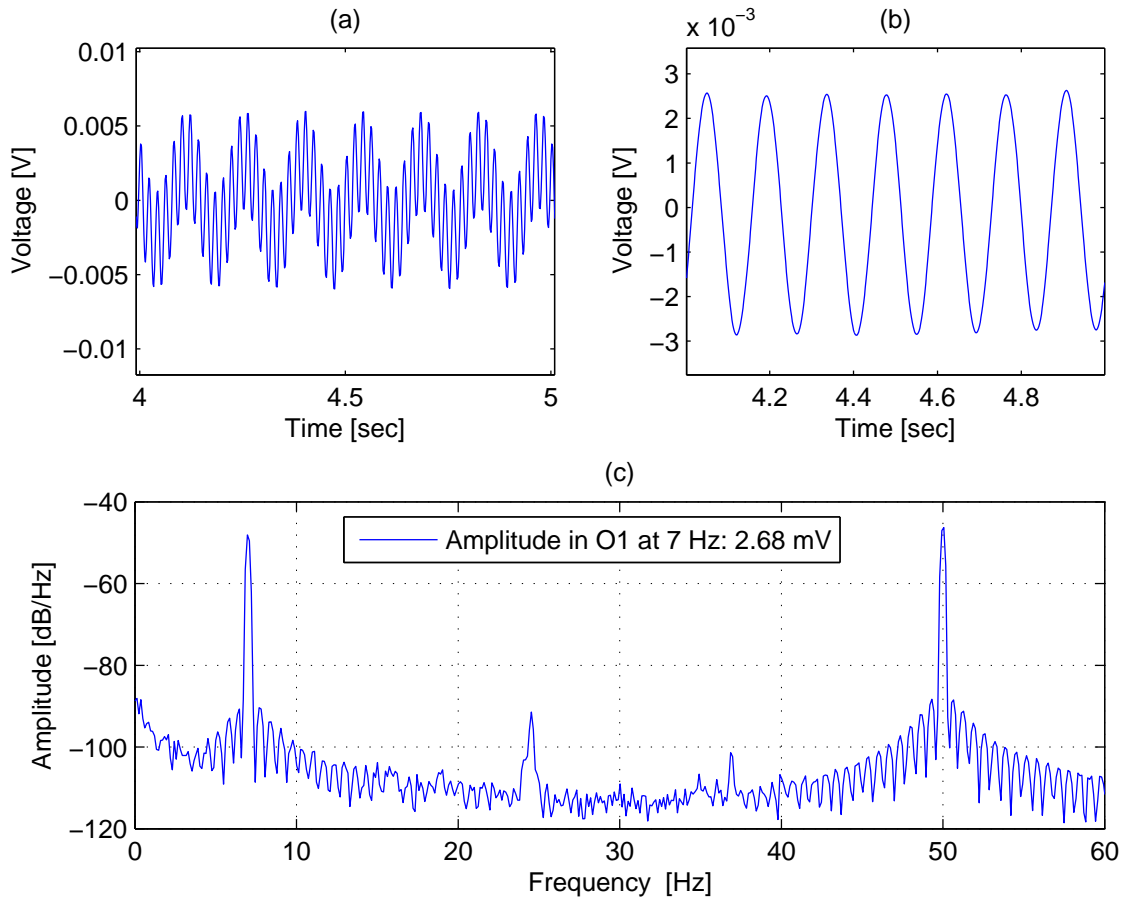


Figure 5.15.: In (a) is the sensed signal without the loudspeaker excited but the capacitor plate attached on the loudspeaker (see Figure 4.10). (b) is the signal in (a) after a notch filter at 50 Hz. (c) is the spectrum of (a).

No specific analysis on the magnitude of the peaks was made because of two reasons: the noise present in the 7-Helmet and the mechanical secondary effects of the loudspeaker such as inertia.

### 5.2.3. Evaluation

Once the simulation in Section 5.2.1.2 was validated the correlation between input signal and motion of the capacitor's plates was computed. When both input signal and movement are the same (case presented in the loudspeaker measurement) the correlation coefficient is high ( $r = 0.98$ ), but when they are different (for example in Figure 5.13) it becomes non-linear and neither with Spearman and Kendall correlations (non-linear correlation) correlation coefficients higher than zero were obtained.

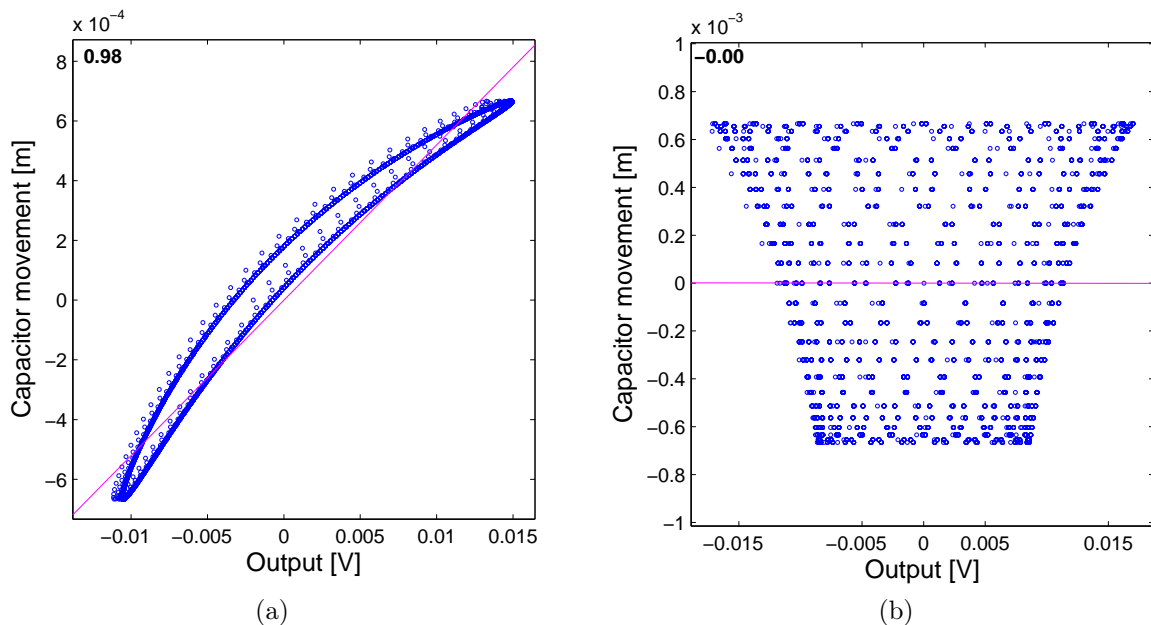


Figure 5.16.: Pearson correlation between the sensed signal and the movement of the capacitor's plates: (a) correspond to simulation presented in Figure 5.13 and (b) correspond to simulation presented in Figure 5.13

The non-linearity effects produced by a modulation are beyond the scope of this thesis, therefore no further analysis was pursued in this subject.

## 5.3. Denoising methods

### 5.3.1. Auxiliary sensors: gyroscope and accelerometer

Measurements making fast and wide movements with the head were done and the correlation between sensors and leads was calculated. In time domain they seem to be highly correlated but none correlation coefficient was higher than 0.4.

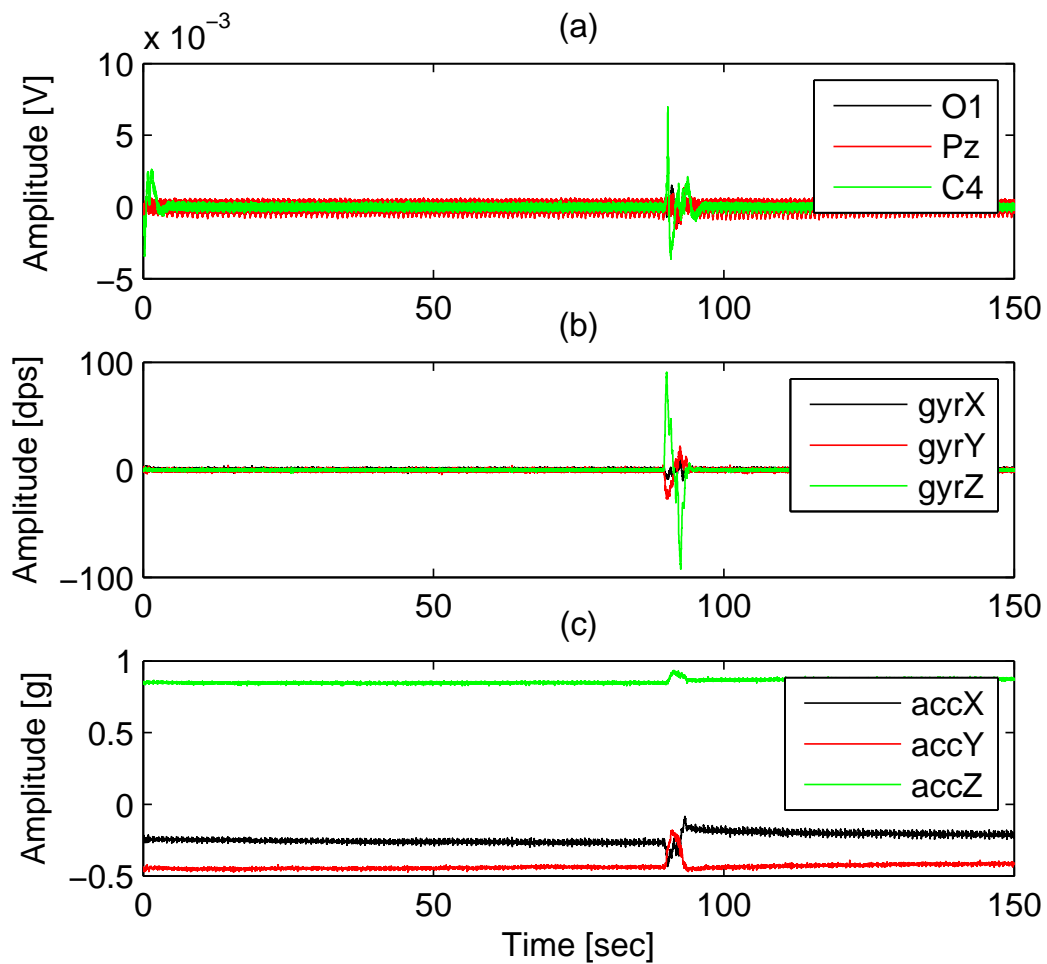


Figure 5.17.: Time domain comparison of a measurement with one big shake of the head at 90 seconds: in (a) are the central leads of the 7-Helmet, in (b) the gyroscope output and in (c) the accelerometer output.

In the cross covariance shown in Figure 5.18 some small delays ( $< 1$  sec) can be seen so an alignment was done without having any improvement.

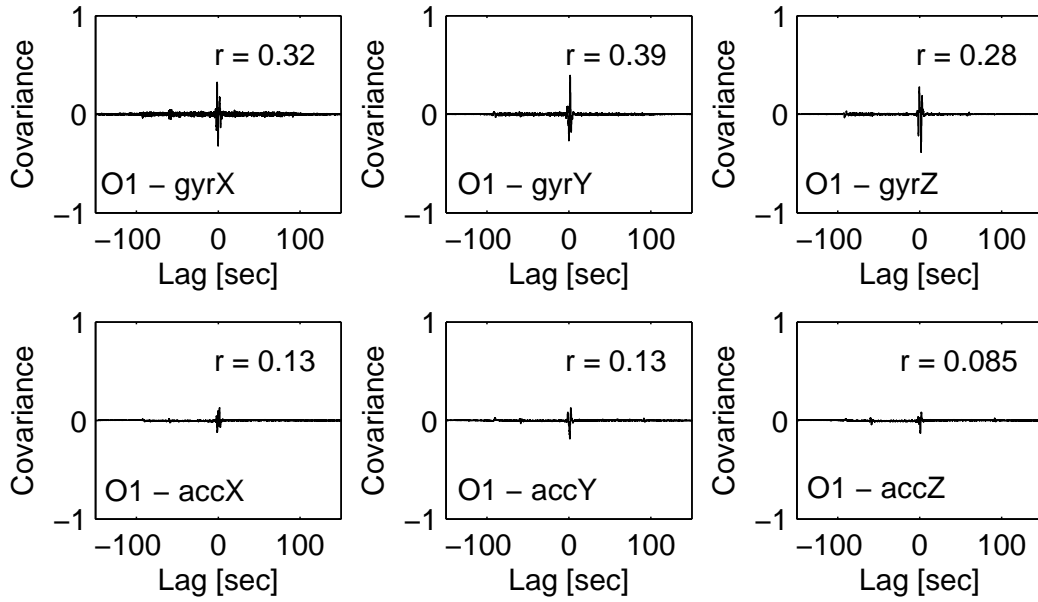


Figure 5.18.: Cross covariance of the sensor with lead O1 and the correlation coefficient

Nevertheless ECG influence can be seen (Figure 5.19) in the spectrum of the sensors and therefore this information can be used to remove it. How this has been done is explained later in Section 5.3.3.1

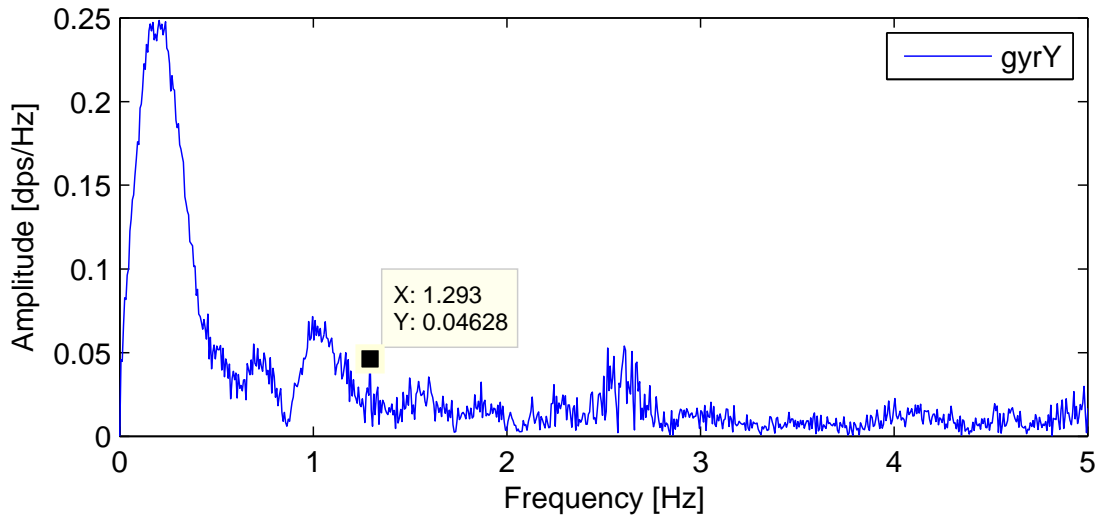


Figure 5.19.: PSD of the gyroscope in axes Y with the ECG components marked

### 5.3.2. Motion artifacts

#### 5.3.2.1. Wavelets

The measurement in Figure 5.20 shows that a big motion artifact can be isolated and later removed using wavelet thresholding. The comparison between the wavelets method and a high pass filter shows that the first one only removes the motion artifact, while the other also affects the ECG components.

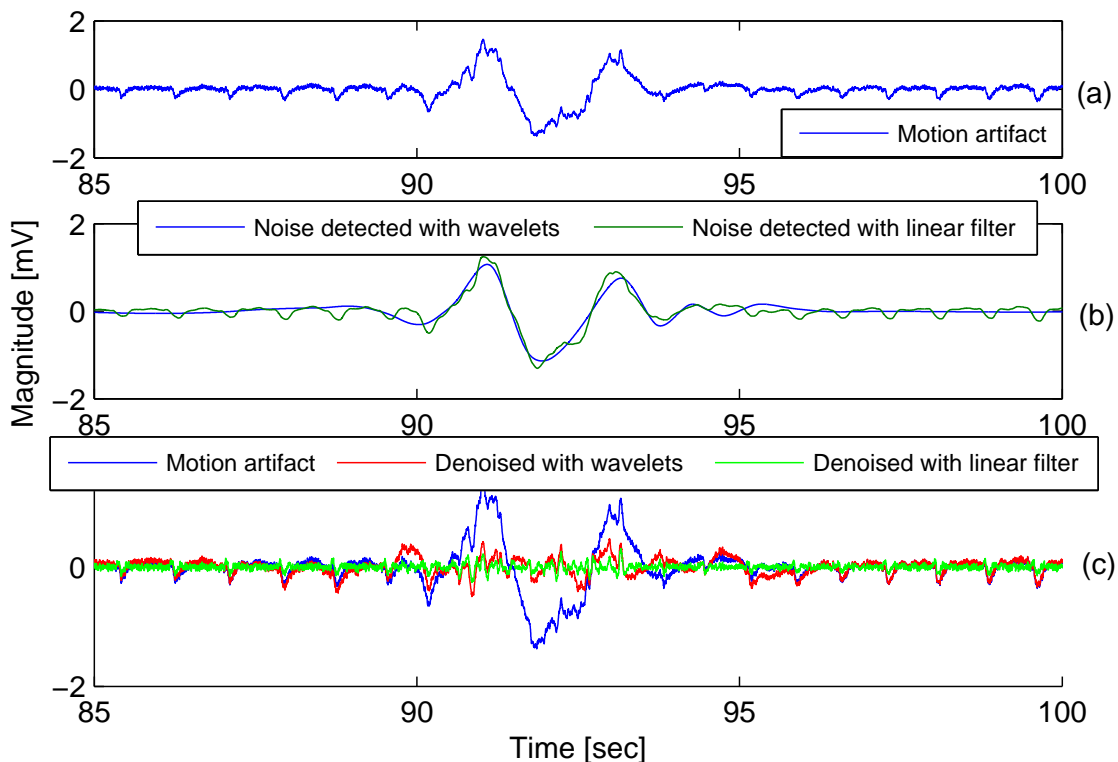


Figure 5.20.: Detection of motion artifacts using wavelet thresholding and linear filters: (a) is the EEG measurement with a motion artifact between 90 sec. and 95 sec. In (b) are the motions detected by both techniques and in (c) the denoised signals compared to the original measurement.

To assure that wavelet thresholding does not act as a linear filter, the following signal was tested:

$$\text{Test Signal} = \text{Gaussian noise (simulating EEG)} + \text{real motion artifact} + \sin(\pi \cdot t)$$

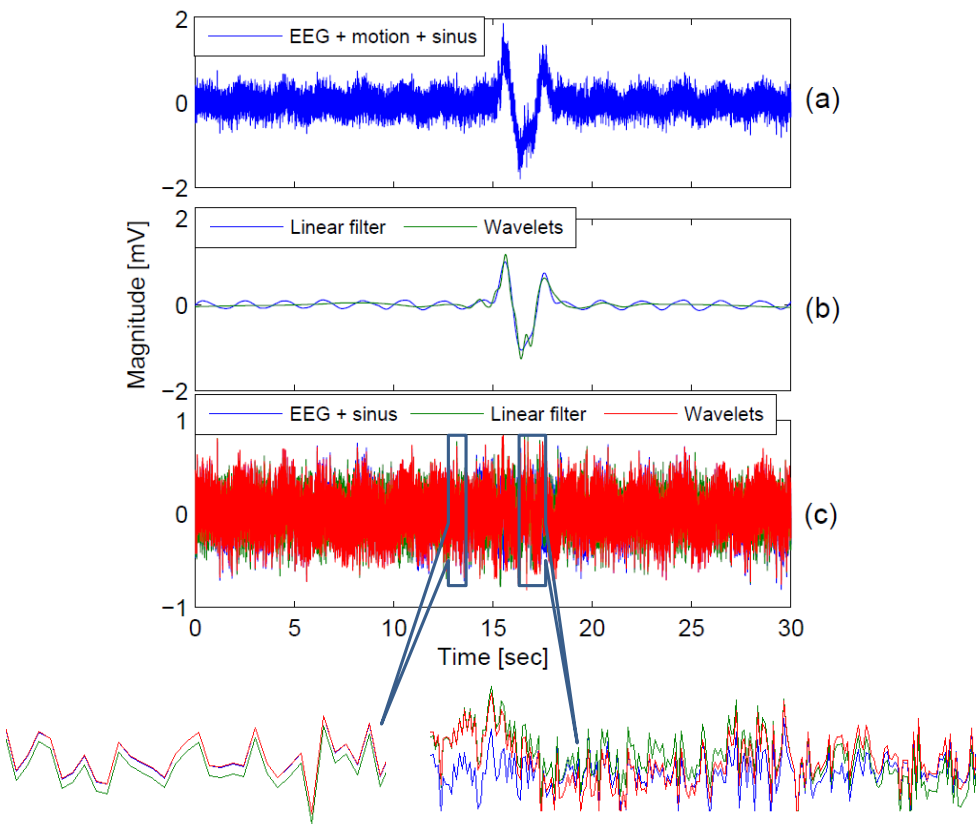


Figure 5.21.: Comparison of wavelet thresholding with linear filters: in (a) the test signal is shown, in (b) the noised detected and in (c) both denoised signals and the test signal without the motion artifacts.

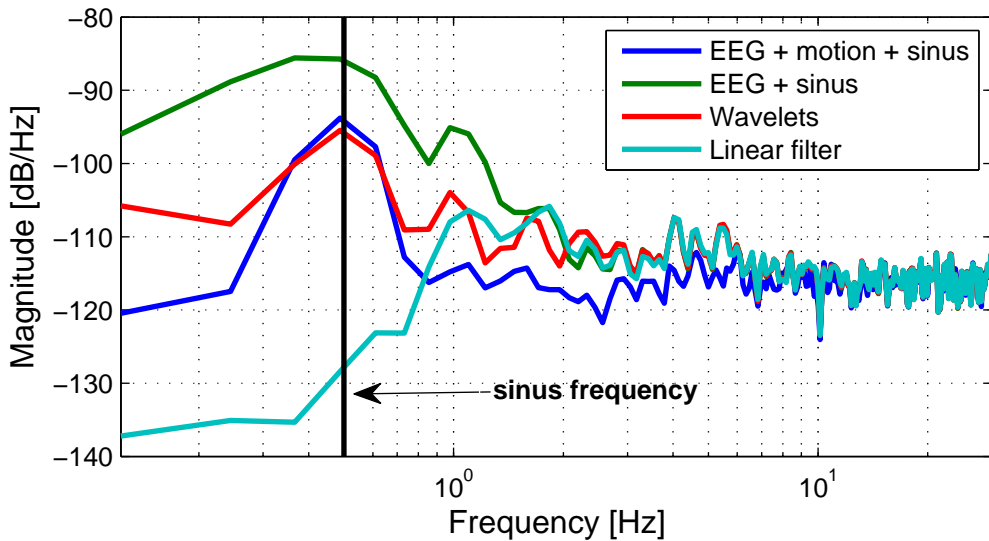


Figure 5.22.: Comparison of PSD from the artificial test signal and the denoised signals. The black vertical line is the frequency of the sinus components.

In Figure 5.22 the sinus can be seen both in original and wavelet filtered signal, but not in the low pass filtered, proving that wavelet thresholding does not act as a linear filter.

### 5.3.2.2. Comparison of ICA, wavelets and the combination of both

The three techniques compared here were tested with the same EEG measurement (see Section 4.4.3.4) which contains alpha waves (see Chapter 2). The first method consists in decomposing the measurement with ICA and removing the sources containing mostly noise. The second one only uses wavelet thresholding to reduce the noise, and the last method uses wavelet thresholding on the sources obtained by ICA.

The measurement was made alternating closed eyes with open eyes, which will result in a variation of amplitude in electrodes's signal. In those times with closed eyes the power in the alpha frequency range increases and so does the amplitude of the signal, and with open eyes the alpha components are lower.

Only the first four channels are shown for illustration purpose, the complete results can be seen in Appendix A.2.

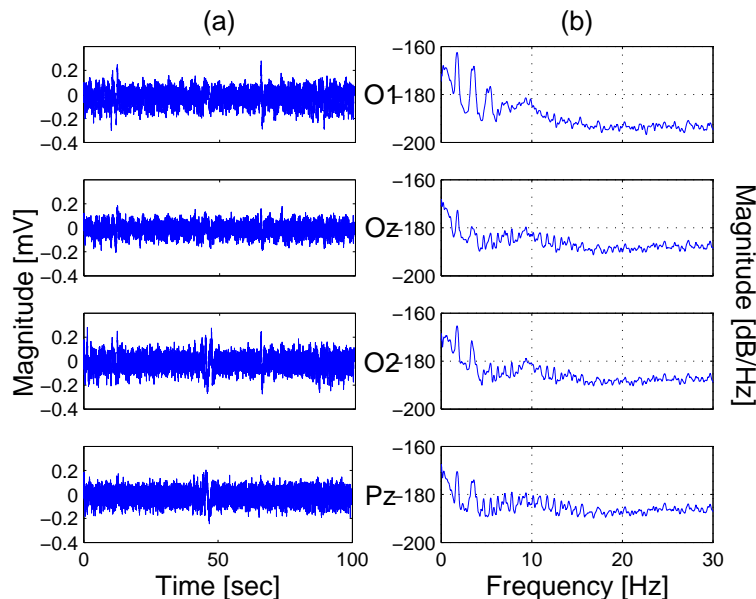


Figure 5.23.: EEG measurement with alpha waves components: alternating open eyes with closed eyes every 20 seconds, starting with open eyes.

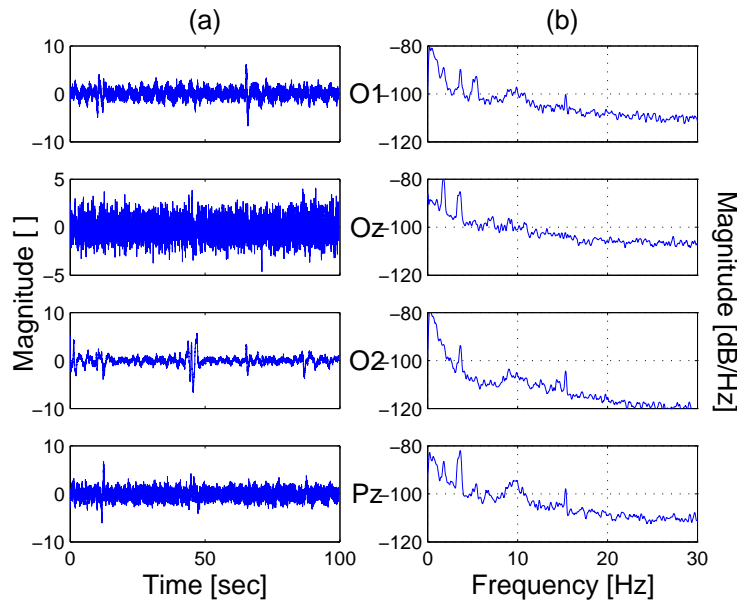


Figure 5.24.: EEG's sources estimated by ICA. Because ICA does not give information about amplitude the results are unit less.

### ICA

As seen in Figure 5.24 the second and third source have high artifacts so they are removed previous reconstruction. Particularly, the third source has also alpha components which will be lost.

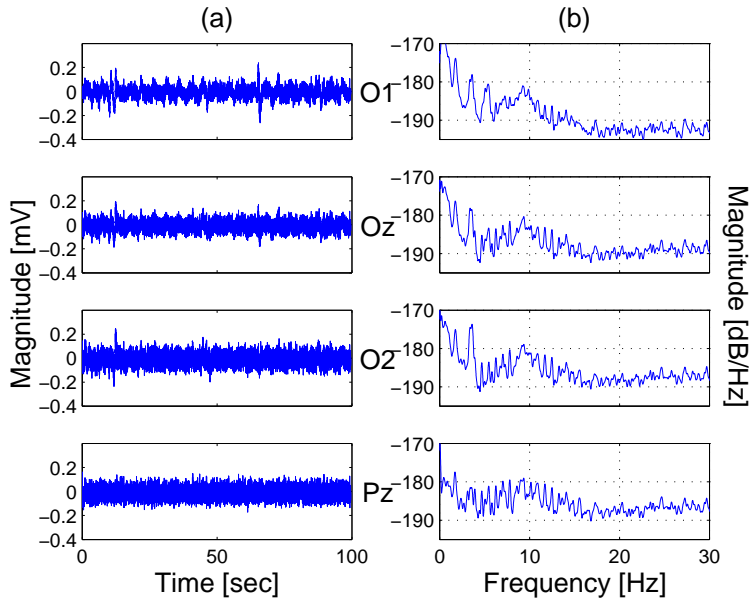


Figure 5.25.: EEG reconstructed eliminating sources 2, 3 and 7.

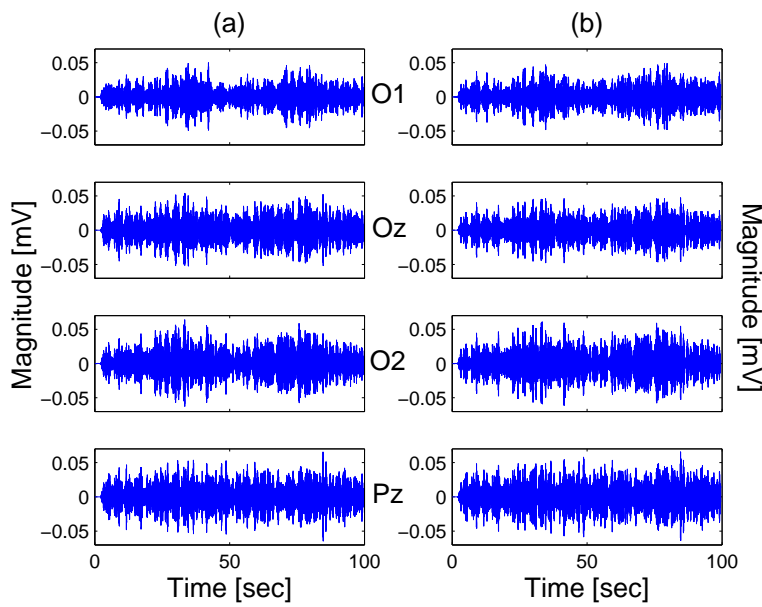


Figure 5.26.: Both (a) EEG and (b) EEG denoised band passed between 8 Hz and 12 Hz to verify that alpha waves were not affected

It can be seen that the alpha components, when comparing Figure 5.26.(b) against 5.26.(a), remained almost intact but in O2 some information was lost.

### WAVELETS

In this case, the alpha components remained intact and all the low-frequency artifacts have been reduced but also the EEG in that frequency range.

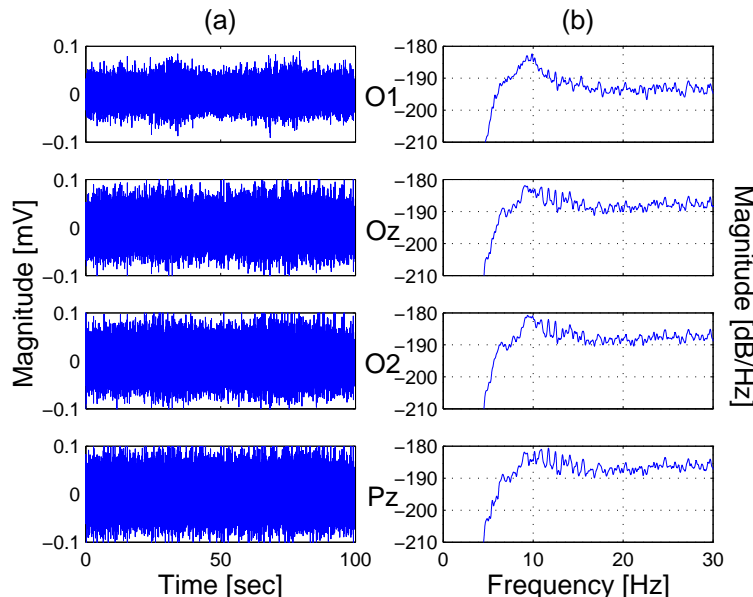


Figure 5.27.: EEG's sources denoised with wavelet thresholding

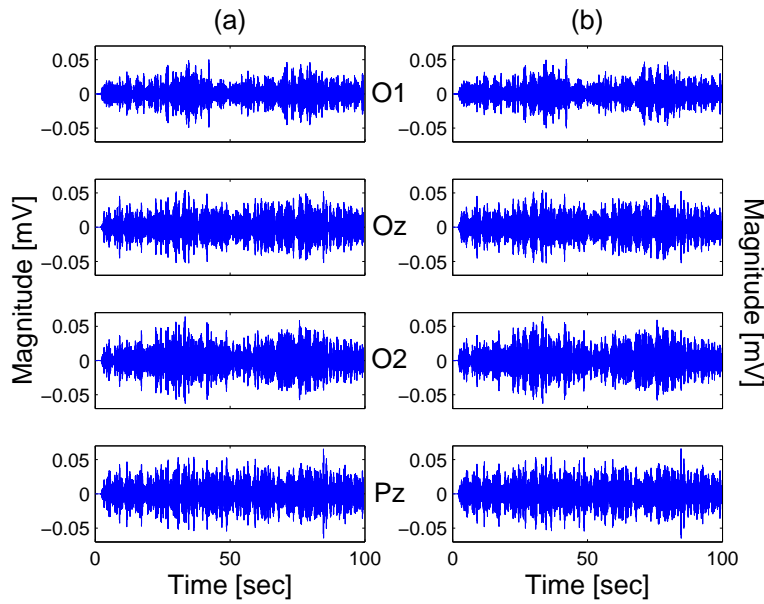


Figure 5.28.: Both (a) EEG and (b) EEG denoised band passed between 8 Hz and 12 Hz to verify that alpha waves were not affected.

### ICA AND WAVELETS

When combining both techniques an intermediate point was reached, in which artifacts have been reduced but the EEG components in low frequency remained intact. It can be seen in the PSD of Figure 5.29.(b) that also some low frequency noise components were not canceled.

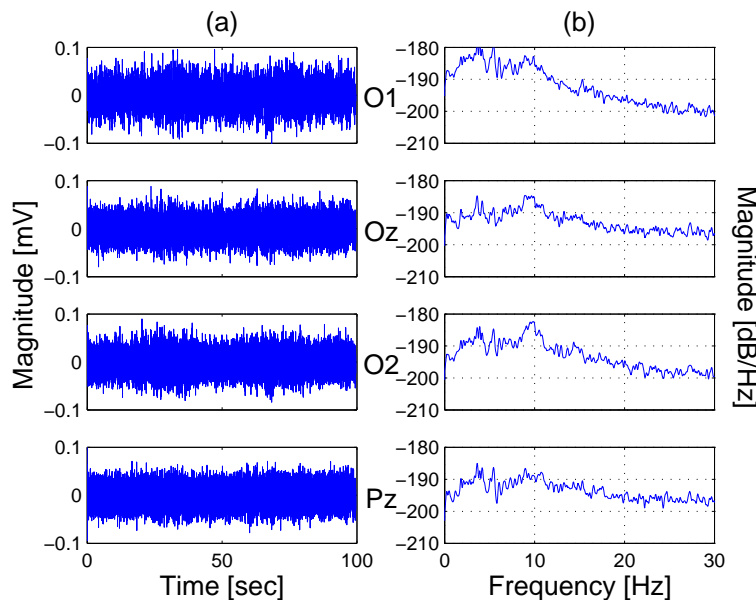


Figure 5.29.: EEG's sources denoised with wavelet thresholding

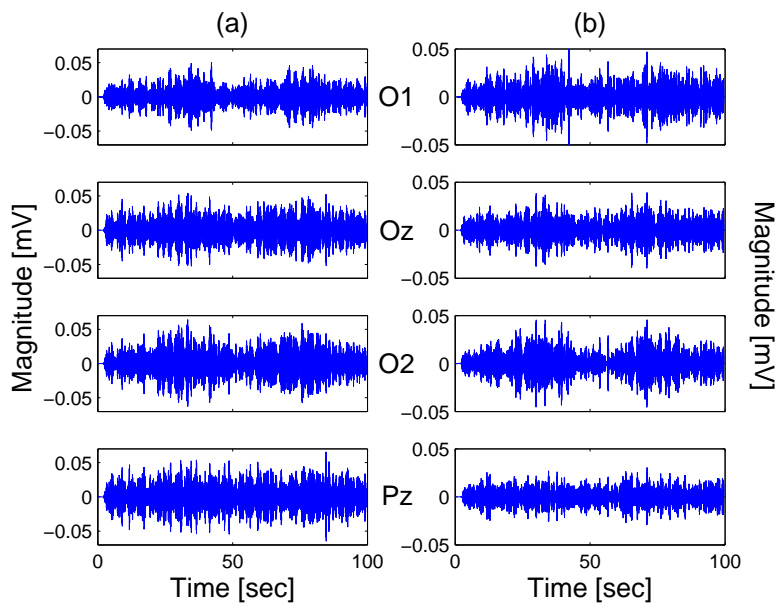


Figure 5.30.: Both (a) EEG and (b) EEG denoised band passed between 8 Hz and 12 Hz to verify that alpha waves were not affected

Alpha components were not only not reduced, but enhanced. Leads Oz, O2 and Pz show a clearer boundary between open eyes and closed eyes.

### 5.3.3. ECG artifacts

#### 5.3.3.1. Linear filter

Using the information obtained with the gyroscope in Section 5.3.1 three adapted notch filter were applied to the EEG measurement contaminated with ECG components. The first filter was at the heart beat frequency and the other two at the harmonics.

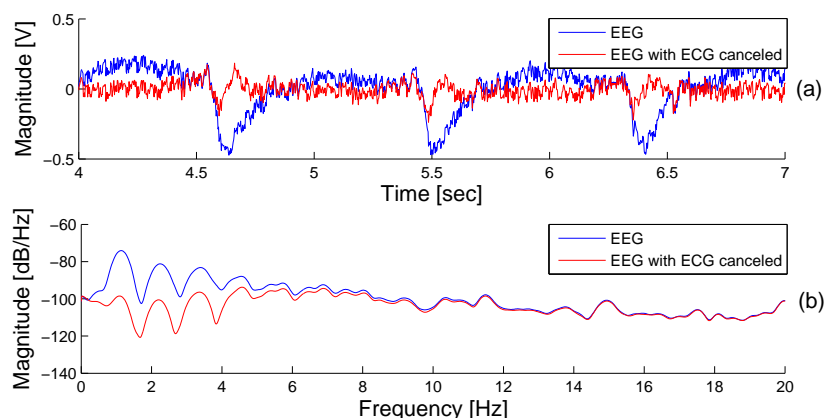


Figure 5.31.: EEG measurement on Cz denoised applying 3 adapted notch filters at frequencies found with auxiliary sensors.

It is still possible to see some ECG components, but at the same amplitude as EEG and not higher.

### 5.3.3.2. Wavelet

Wavelet transform was useful to detect the ECG components and most important the harmonics. After these results it is possible to apply previous method (notch filters) or to remove directly these detected components.

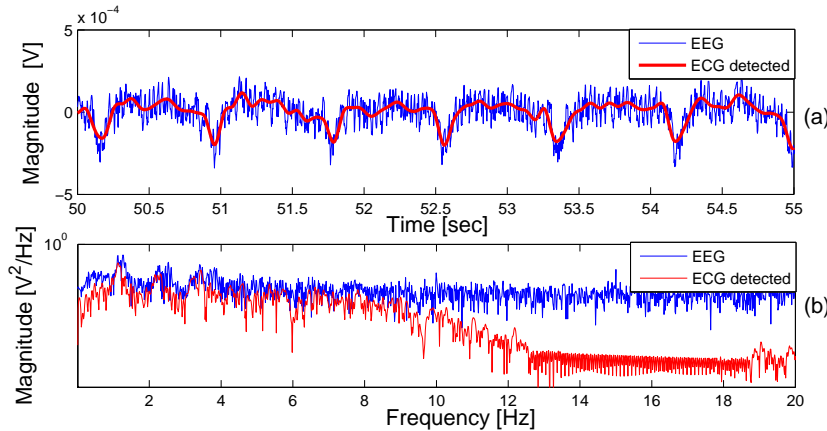


Figure 5.32.: ECG component detection using wavelet thresholding

### 5.3.4. SSVEP enhancement

#### 5.3.4.1. Time span selection

Time spans of a SSVEP measurement, where the volunteer had higher concentration, were successfully selected and afterwards two enhancement techniques could be tested.

Longer time spans were prefer to shorter time spans with higher SNR to test the processing techniques. The reason of this decision was that these longer time spans are more representative of the SSVEP measurement and the false positives, when deciding whether the volunteer was focus on certain pattern or not, are reduced.

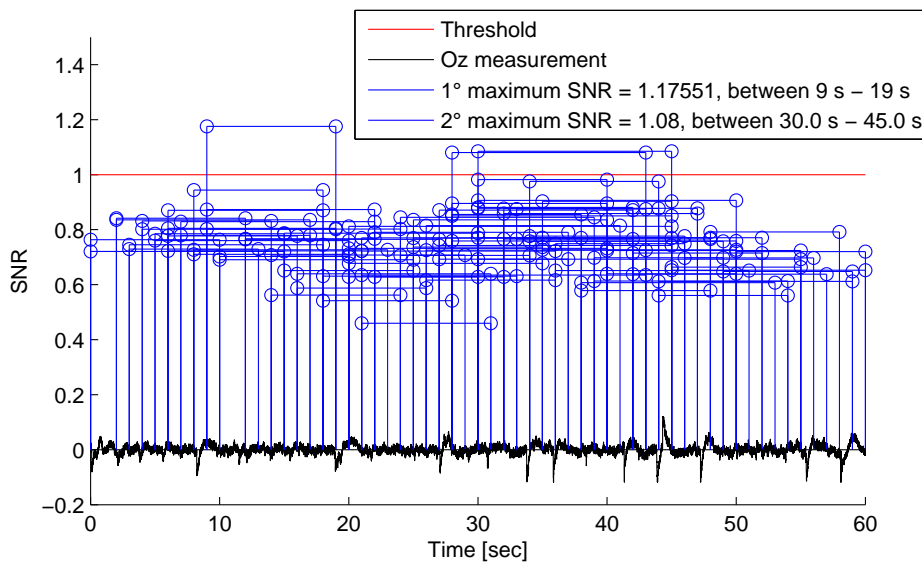


Figure 5.33.: SNR at SSVEP frequency of time spans tested: red line represents the SNR threshold to determine the quality of a SSVEP signal.

Figure 5.33 shows the SNR for each tested time span (a brief explanation of the algorithm is in Appendix A.7).

#### 5.3.4.2. SNR enhanced by ICA

Once the time span was selected and cut, it was decomposed into its sources and reconstructed without the noise sources. These approach enhanced the SNR from 1.09 to 1.18 and did not work when the whole signal from Figure 5.33 was used.

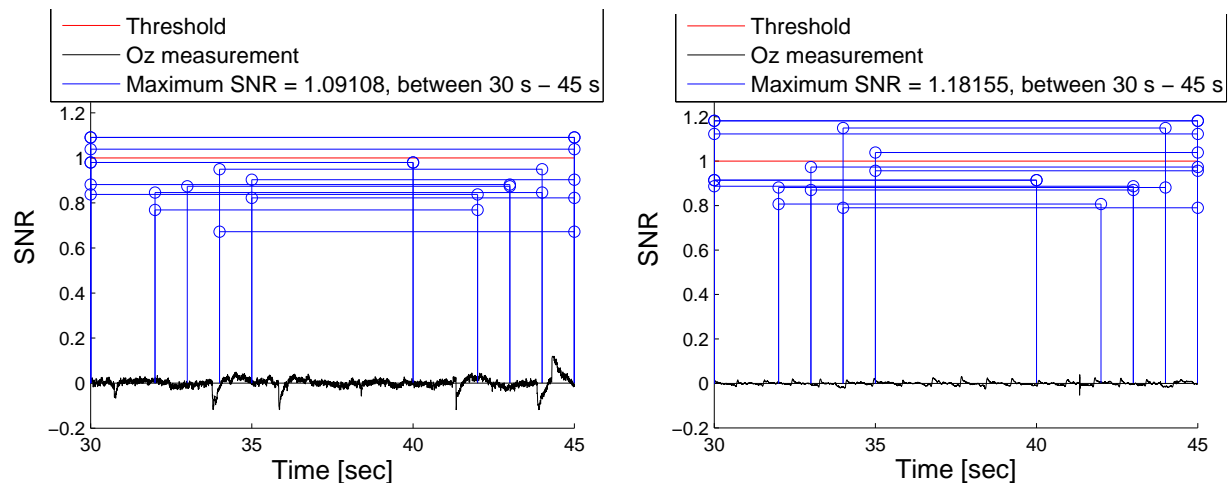


Figure 5.34.: Enhancement of SSVEP SNR using ICA in an already selected time span

### 5.3.4.3. SNR enhanced by bipolar lead

The last enhancement technique was selecting a bipolar lead. For this, the algorithm previously described in Section 4.4.5.3 was used and Figures 5.36 and 5.37 show the results.

The SSVEP components of PO3 (in black in Figure 5.36) was higher than in P1 (blue), but the noise components of both were similar. Therefore, when they are subtracted creating a bipolar lead (PO3-P1) the noise will be reduced but not the SSVEP components.

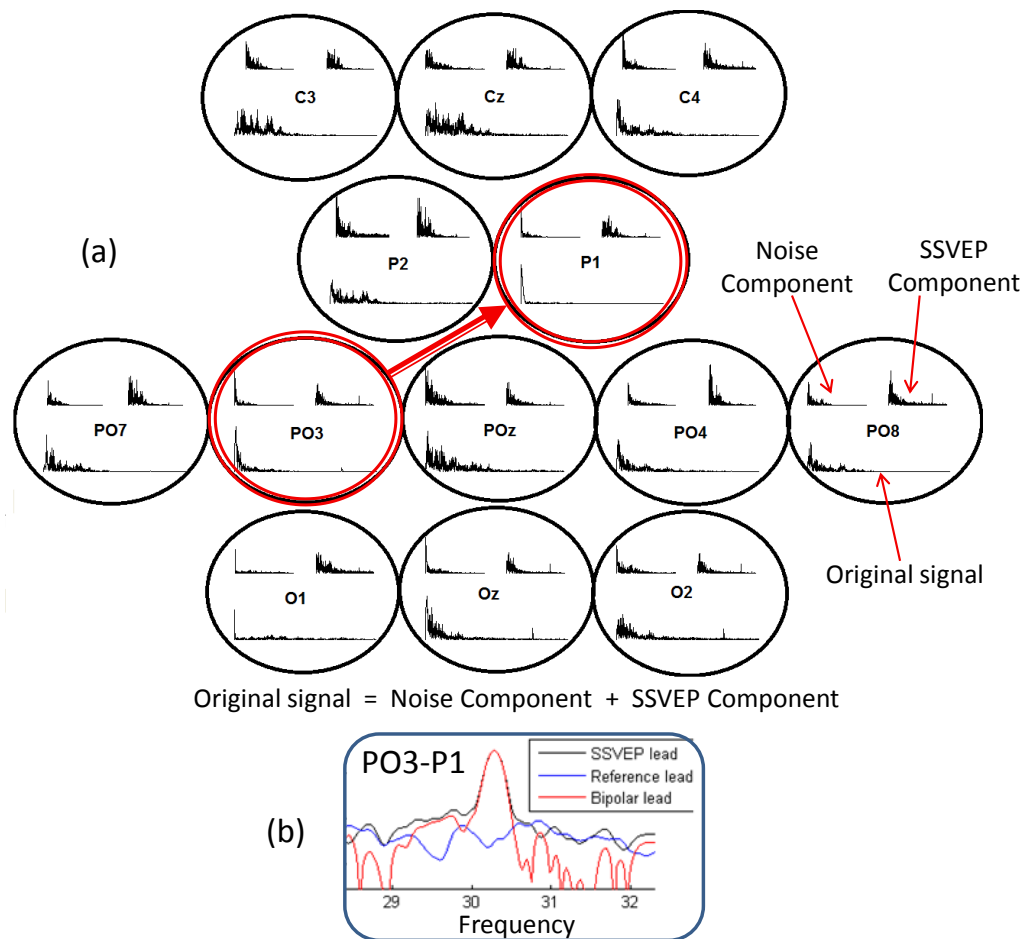


Figure 5.35.: Graphical example of bipolar lead selection algorithm: in (a) local PSD of original signal, noise and SSVEP components is shown and one bipolar lead selected.(b) shows the reduction of noise in the bipolar.

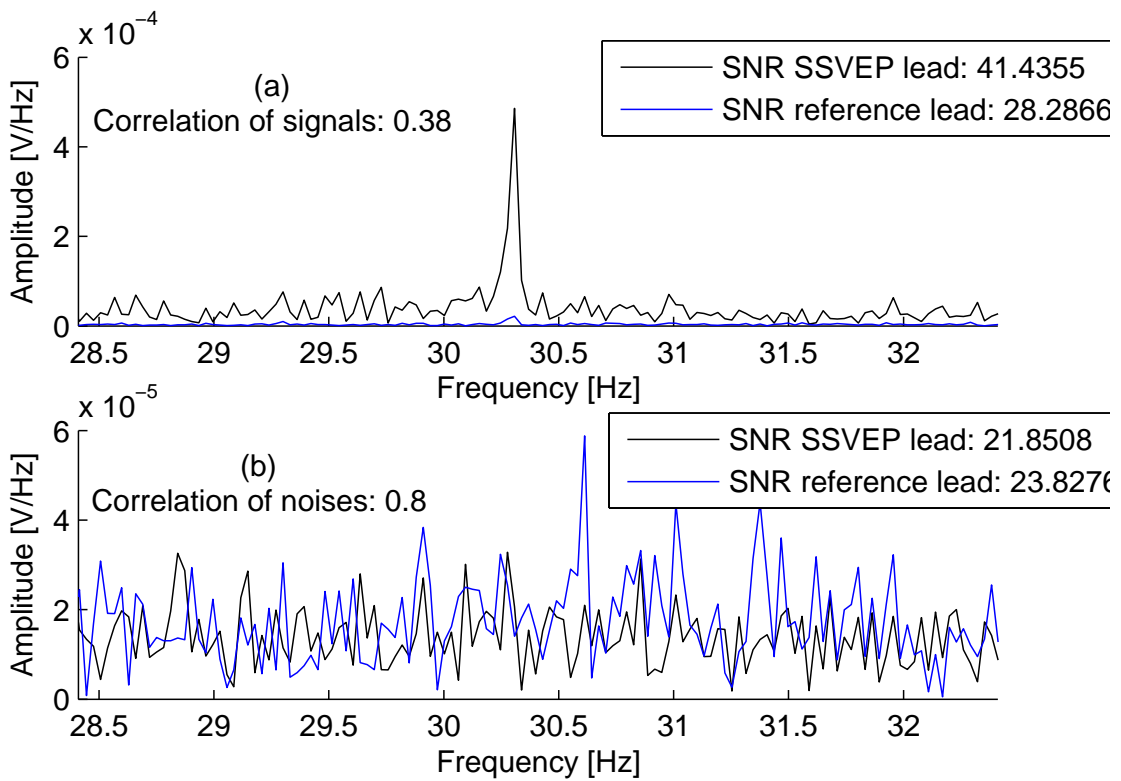


Figure 5.36.: (a) SSVEP components of PO3 (black) and P1 (blue). (b) Noise components of PO3 (black) and P1 (blue)

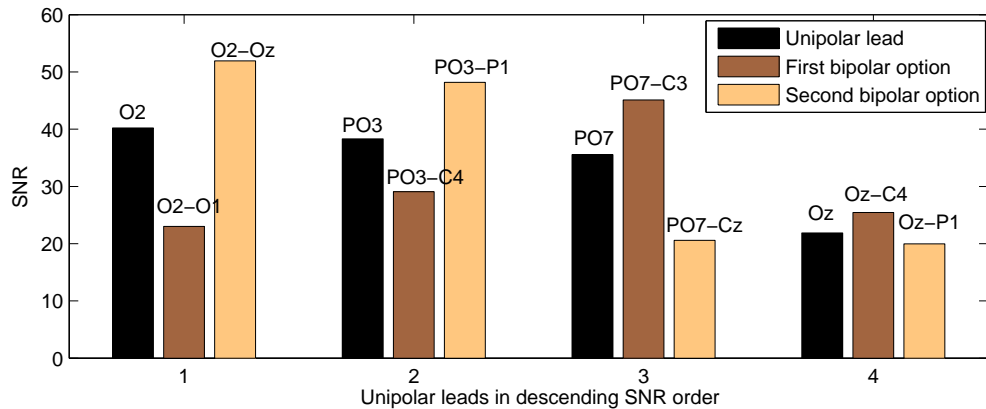


Figure 5.37.: Four unipolar leads and the two possible bipolar leads formed with them

Bipolar leads with higher SNR than the unipolar leads were found. Figure 5.37 shows that for each lead an enhancer reference lead was successfully found.



## 6. Discussion

The aim of this research was to assess some of the most effective algorithms used in traditional EEG to denoise it, paying special attention to motion artifacts and SSVEP signals. In the first place, wavelets seem to be a good approach to overcome motion artifacts at low frequencies, while ICA could be used effectively in combination with other filtering techniques. On the other hand, it was not possible to find a usefulness to auxiliary sensors –gyroscope and accelerometer–for denoising motion artifacts. Finally, SSVEP could be enhanced with help of ICA and the proper bipolar lead selection.

It was found out that the reference electrode does not reject common signal as it was expected, and mainly that it was not possible to achieve the same behavior on all electrodes at the same time with minimum dispersion. Also, an unexpected component at 24.54 Hz appeared in several measurements, thus further measurements were conducted with the isolation tank. Unfortunately no solid conclusion could be drawn from these measurements and so far this component at 24.54 Hz is thought to come from an outside source.

An incorrect placement of the electrodes –this means differences between the spacing between head and electrodes–will produce in general:

- mismatch with the reference and therefore poor common mode rejection
- difference in sensed amplitude between electrodes
- increase of probabilities of electrodes's movement

but particularly, the measurements of crosstalk show that when the placement is not good the interferences between channels will mix entirely the signal and probably with ambient noise.

The simulation of motion artifacts was validated with the experimental measurements, but unfortunately the correlation between the sensed signal and the movement of the electrode was non-linear and no direct technique was able to be applied to reduce the effects of movements on the measured signals.

Some of the tested denoising techniques present promising results, but not all of them. The approach with auxiliary sensors—gyroscope and accelerometer—did not work as expected. The sensors at first look seemed to have high correlation with the electrodes but actually the correlation coefficient was always below 0.4. The first thought was that the slight delay between these signals was reducing the correlation, but after aligning them the correlation did not improve. One possible explanation of these results could be that the coordinate axis of the sensors is not the same as the coordinate axis of each electrode. Despite this, it was possible to use some of the information from the sensors, particularly the gyroscope, to create a series of adapted notch filters to remove ECG components.

It was probed that wavelet thresholding can be used to remove high amplitude motion artifacts, and particularly that it does not act as a linear filter but as a selective filter leaving undisturbed the EEG components in the same frequency band as motion artifacts. The drawback of this technique is that it is limited to those artifacts that have higher amplitude than the EEG components—it could sometimes also be used for reducing the ECG components. It was not possible to find the most efficient threshold automatically nor to differentiate the threshold of wavelet coefficients for different levels of decomposition.

The results of applying Independent Component Analysis to the measurements of this non-contact electrode system differ from the literature [39, 40]. The estimation of the sources was in general not good because in every estimated source a mix of several sources was found. One possible reason to this could be the fact that the acquisition system has seven electrodes and the sources are more (ICA requires at least the same amount of signals as sources). To verify if the performance of ICA was affected by this, measurements done with the 24-electrode helmet were tested but the results did not improved. Another possibility could be the implementation of the ICA algorithm, so ICALAB [67] was used, in which different algorithms of ICA and other blind source separation techniques are available. With some of them, particularly SOBI [72] implementation, the results were improved but not overly. This may infer that motion artifacts, caused by the movement of the electrodes, disturb the signals in a way in which *whitening* the data is not completely possible, perhaps because it increases the correlation between measured signals.

Despite the poor effectiveness of ICA, it was possible to use it to reduce the noise of the EEG measurements in exchange of losing some EEG components. But when it was combined with wavelet thresholding good results were obtained, not only noise was reduced but also the alpha measurements were enhanced. This worked even when the EEG measurement was made alternating alpha components and non-alpha components, i.e. the EEG signals were

non-stationary. Particularly, it was found that using it on SSVEP measurements will reduce some of the noise and improve the SNR, but only when the signal has already a relative good SNR. For this reason, an algorithm to select the best time span in a SSVEP measurement was programed, which worked successfully.

Finally, the bipolar lead selection algorithm is an effective technique to enhance the SSVEP components without deleting any information of the measurements, but only referencing the electrodes between each others. With this algorithm it is possible to find two different electrodes which share similar background noise, but only one of them has SSVEP components. So when they are composed together one lead the noise will be reduced but not the SSVEP, resulting in an enhancement of the desired signal.



## 7. Conclusion

The first step to understand the effects of motion artifacts caused by the movement of the electrodes was accomplished by successfully reproducing the simplest oscillatory movement. Non-linear relations were found between the movements and the sensed signals.

Wavelets and independent component analysis combined present promising results having successfully reduced the amount of artifacts in the EEG measurements. Particularly, ICA alone seems to be less effective than in traditional EEG system measurements, probably due to the modulation that the movement does to all the involved signals.

Finally, it was found that SSVEP can be enhanced by means of selecting an appropriate bipolar lead.

### 7.1. Prospect for future researches

- To reduce the disturbances of 50 Hz and avoid a possible saturation of the sensors some additional guarding (as used in Figure 4.11.(b)) may be used around the electrodes.
- Integrating the gyroscope and accelerometer into one Inertial Measurement Unit (IMU) may result in higher correlations with the motion artifacts. Also, making the proper coordinate axis correction for each electrode will normalize the use of the sensors.
- Another possible option to sense the motion is to use a dummy electrode. The idea of this is to have electrodes distributed in the helmet, and they should not sense signals from the brain but only the effects of motion. One possible implementation is giving a well defined potential isolated from the head.
- To restrict the effects of motion only to those electrodes in which they have occurred, Surface Laplacian technique may be used. Increasing the spatial resolution of the EEG

measurement will probably mitigate the influences of one electrode movement to the surrounding electrodes.

- Implement and standardize the algorithm of bipolar lead selection in the software of the host research institute.
- Make further investigations about the movements of the electrodes. In this thesis only the variation of the capacitance due to distance variations was shown, but not due to area variations. An advisable work line would be, first reducing the effects of movement in an analytical way, and then (if the movement information was successfully sensed) test the same techniques with experimental measurements.
- To reduce artifacts in general implement a common mode electrode which gives the common mode signals as feedback to the body.

# A. Appendix

## A.1. Noise sources

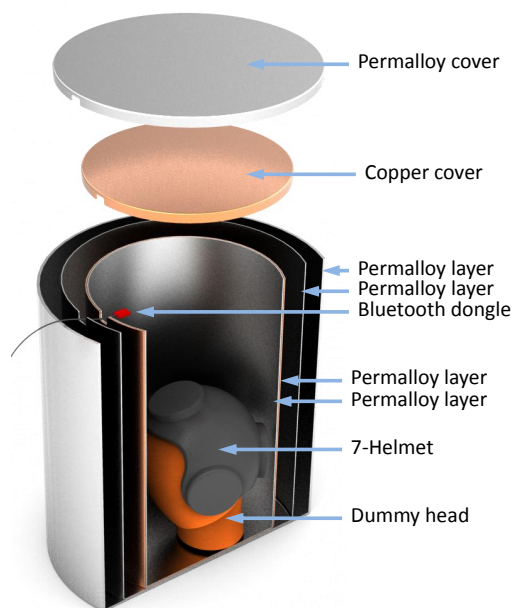


Figure A.1.: Photography of the isolation tank with the helmet inside and a diagram to explain the setups

## A.2. Comparison of ICA, wavelets and the combination of both

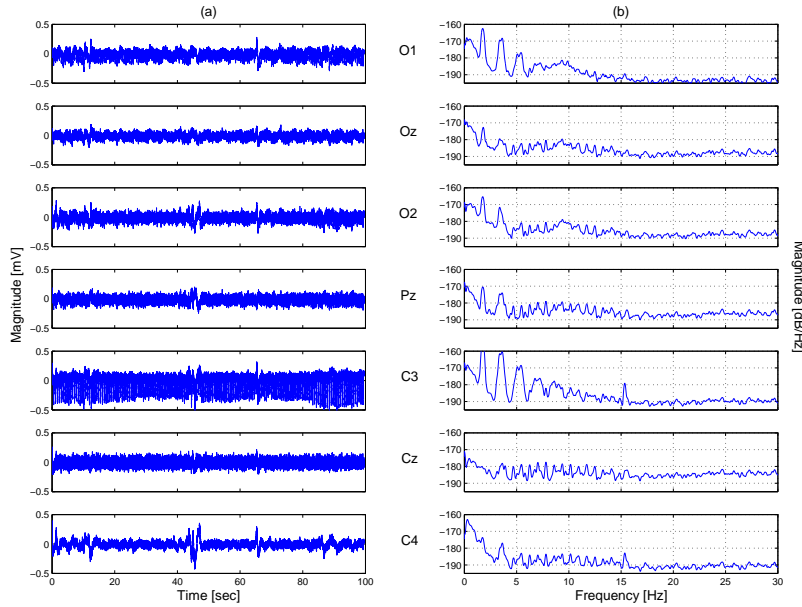


Figure A.2.: EEG measurement with alpha waves components. First 20 seconds with open eyes, then 20 sec. with closed eyes and so on.

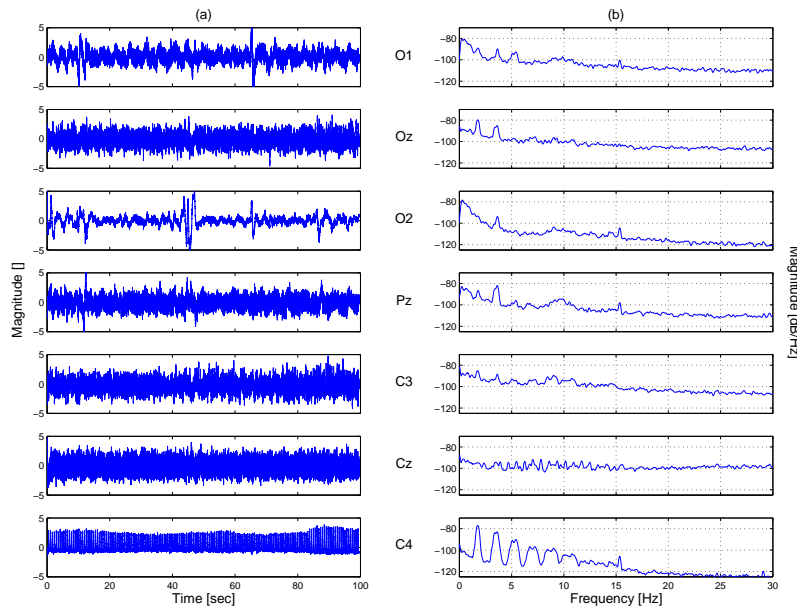


Figure A.3.: EEG sources estimated by ICA

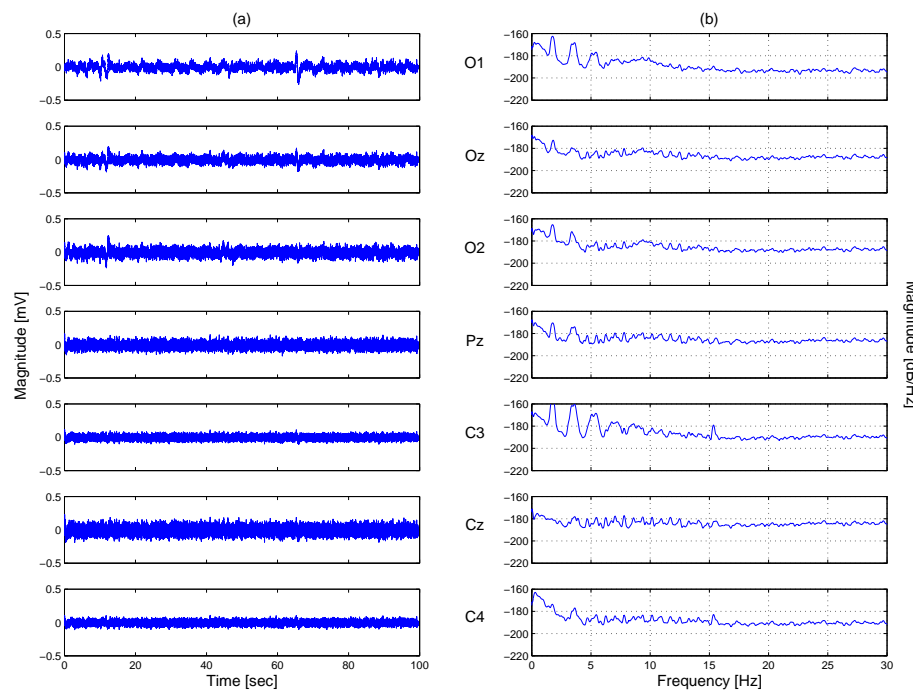


Figure A.4.: EEG reconstructed eliminating sources 2, 3 and 7.

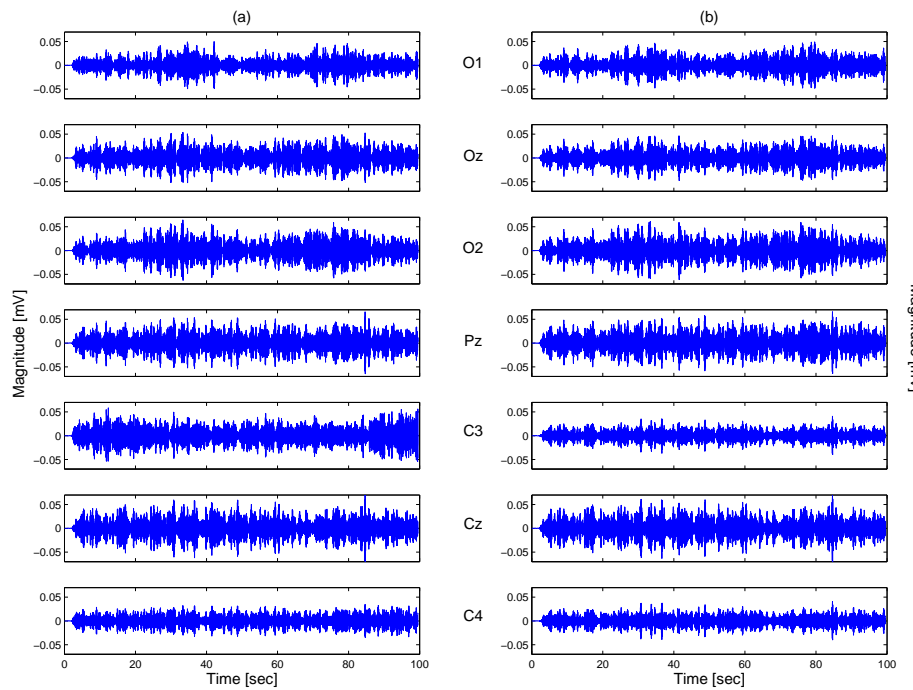


Figure A.5.: Both (a) EEG and (b) EEG denoised band passed between 8 Hz and 12 Hz to verify that alpha waves were not affected.

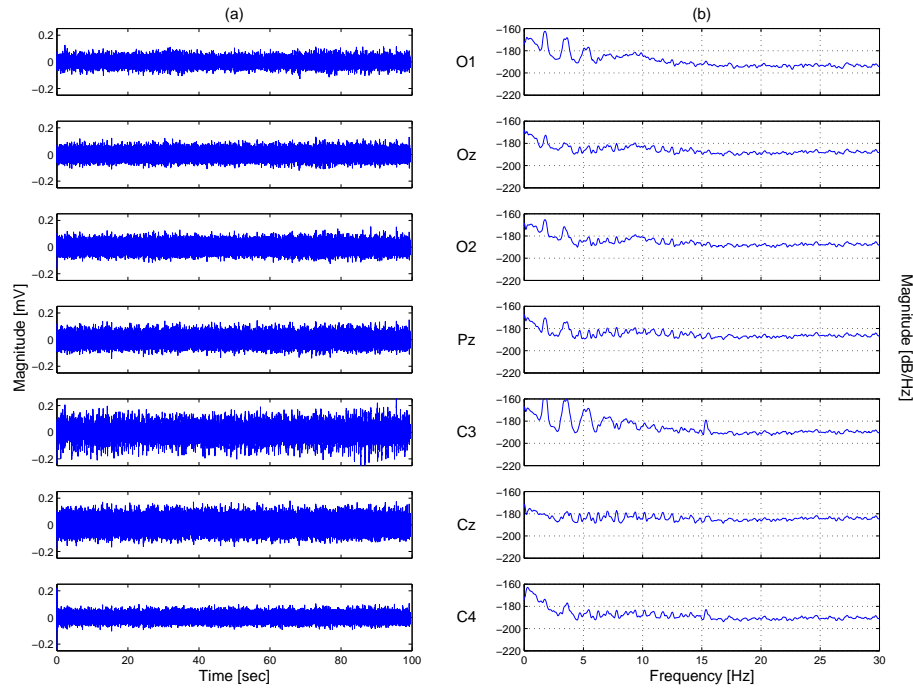


Figure A.6.: EEG denoised with wavelet thresholding.

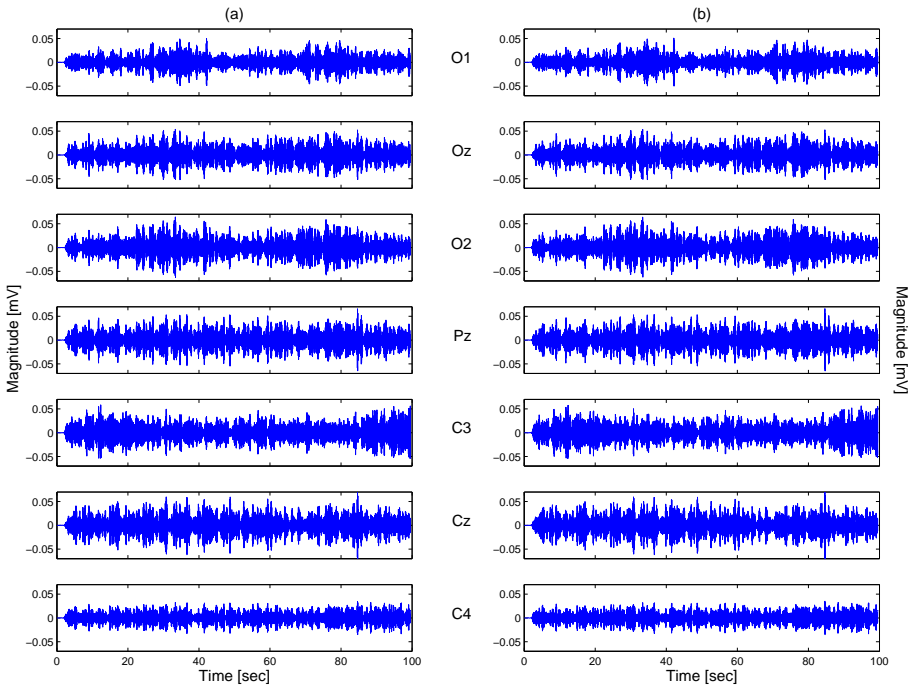


Figure A.7.: Both (a) EEG and (b) EEG denoised band passed between 8 Hz and 12 Hz to verify that alpha waves were not affected.

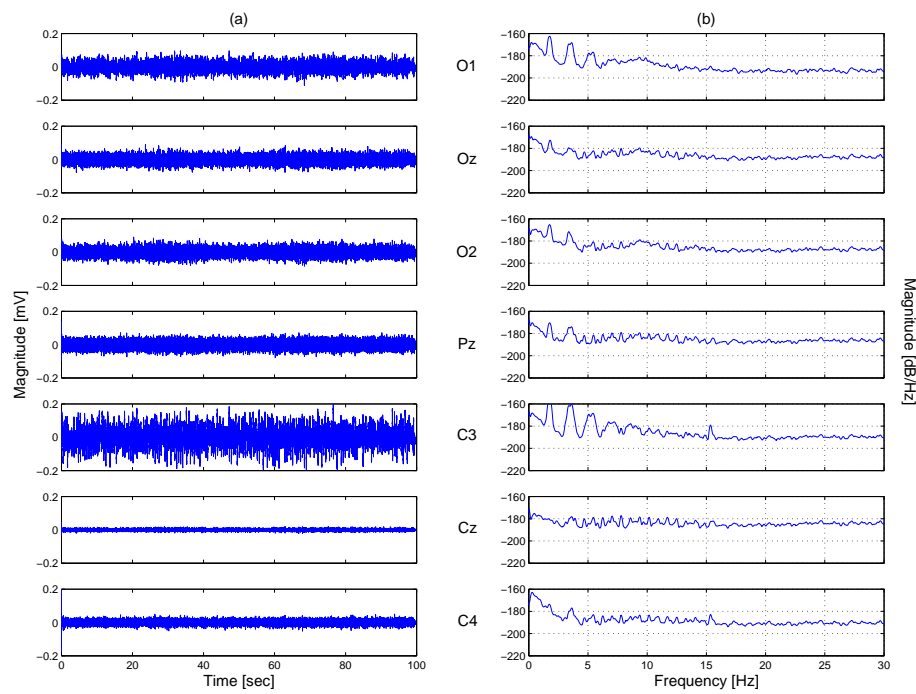


Figure A.8.: EEG sources denoised with wavelet thresholding.

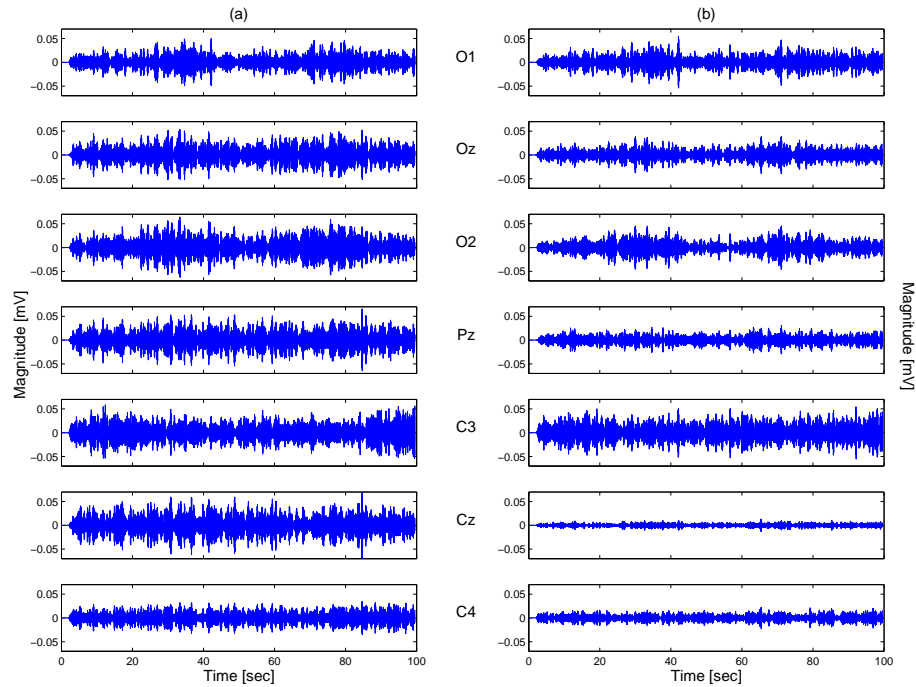


Figure A.9.: Both (a) EEG and (b) EEG denoised band passed between 8 Hz and 12 Hz to verify that alpha waves were not affected.

### A.3. Wavelet example

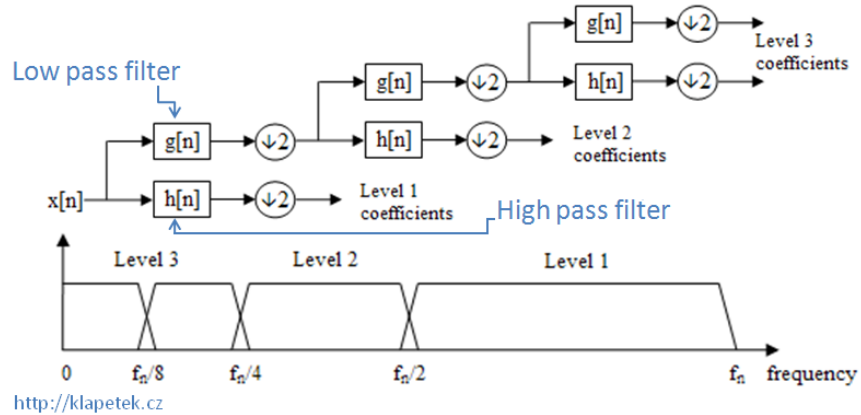


Figure A.10.: Graphical example of how wavelet coefficients are obtain. It high passes and low passes the signal. Then repeat this 2 more times the low pass part with half the frequency filters.

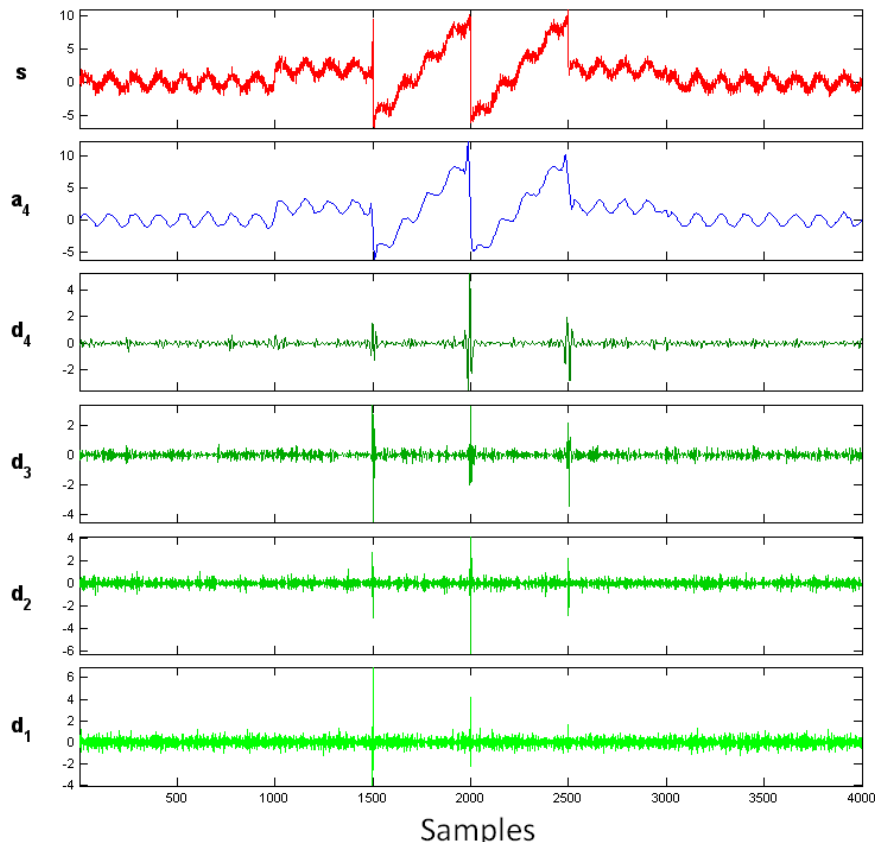


Figure A.11.: The signal and its decompositions.  $S$  is the original signal,  $a_4$  the last approximation decomposition and from  $d_4$  to  $d_1$  all the detail decompositions.

#### A.4. Each lead at a time

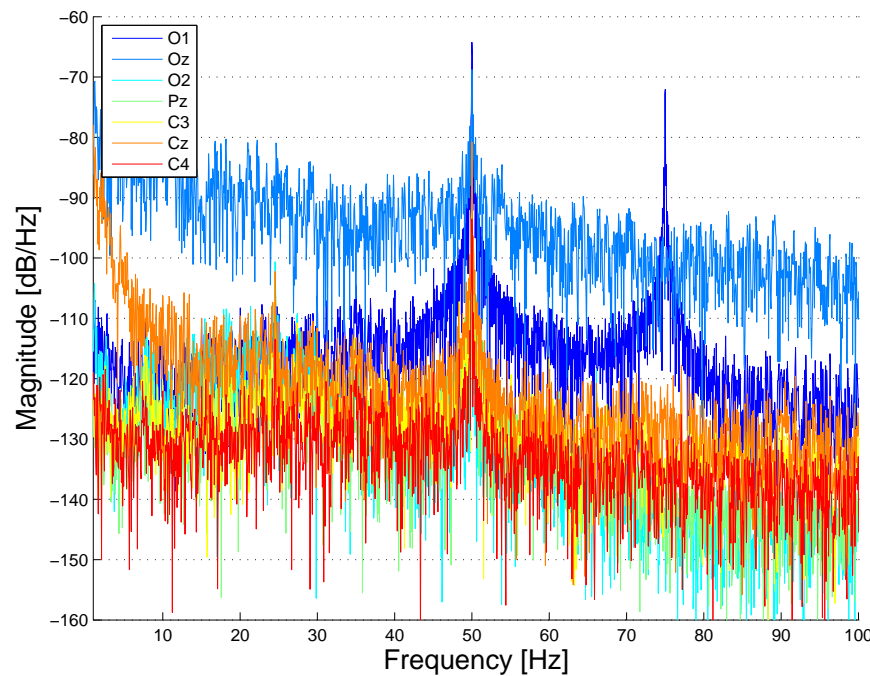


Figure A.12.: Measured signal on all electrodes applying 1 mV amplitude sinus at 75 Hz only on O1

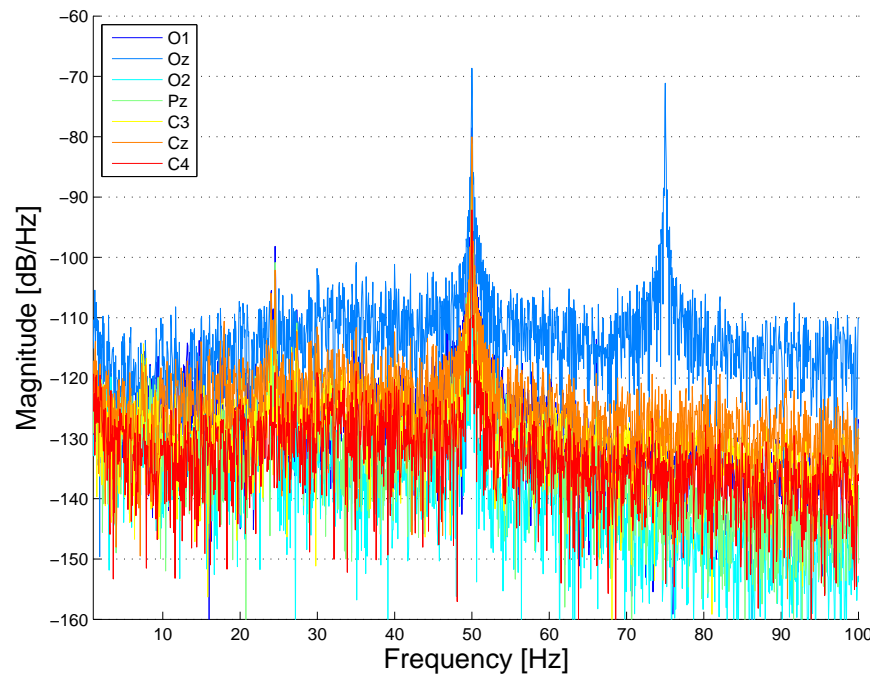


Figure A.13.: Measured signal on all electrodes applying 1 mV amplitude sinus at 75 Hz only on Oz

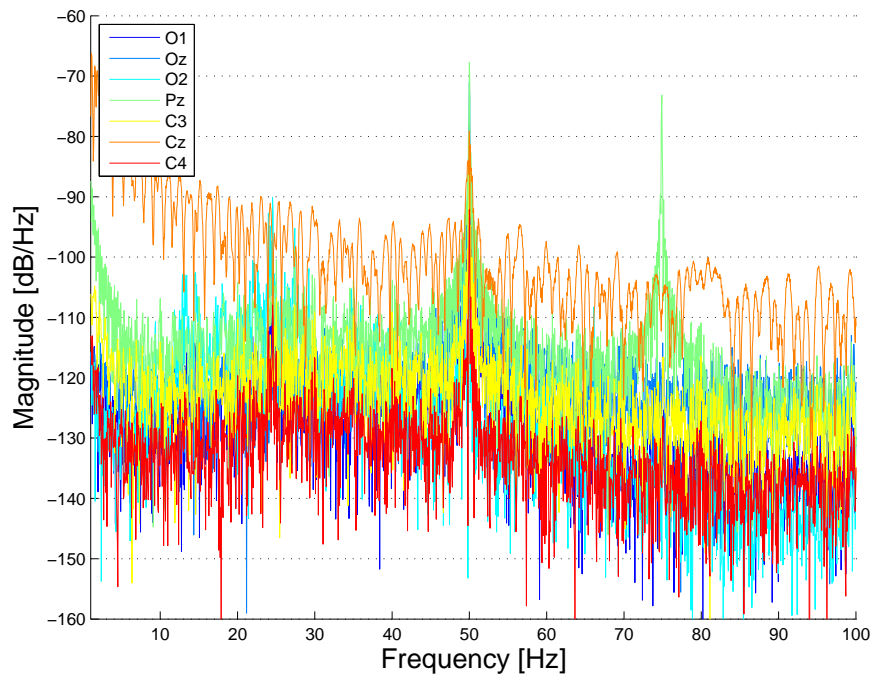


Figure A.14.: Measured signal on all electrodes applying 1 mV amplitude sinus at 75 Hz only on Pz

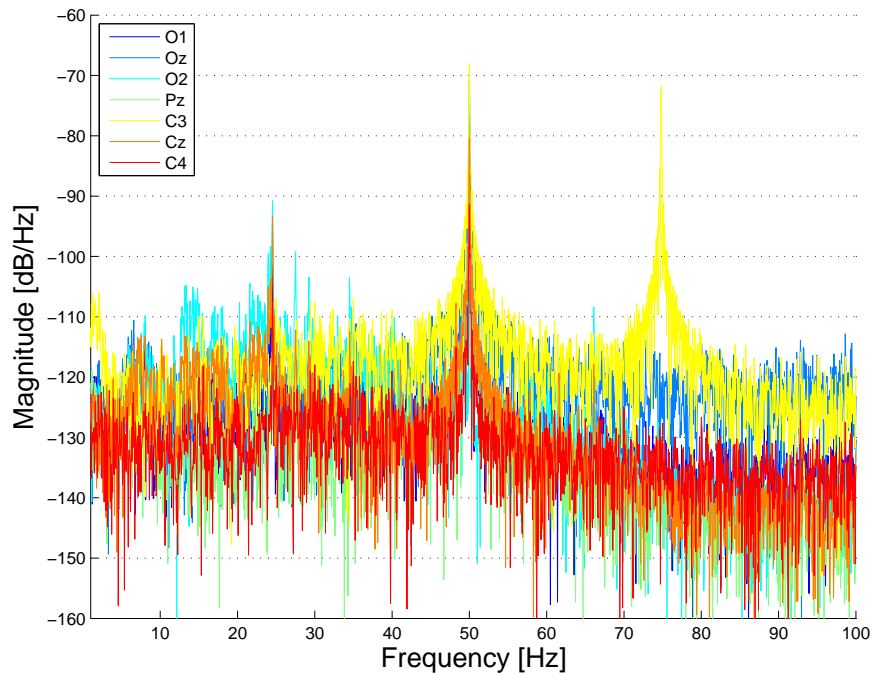


Figure A.15.: Measured signal on all electrodes applying 1 mV amplitude sinus at 75 Hz only on C3

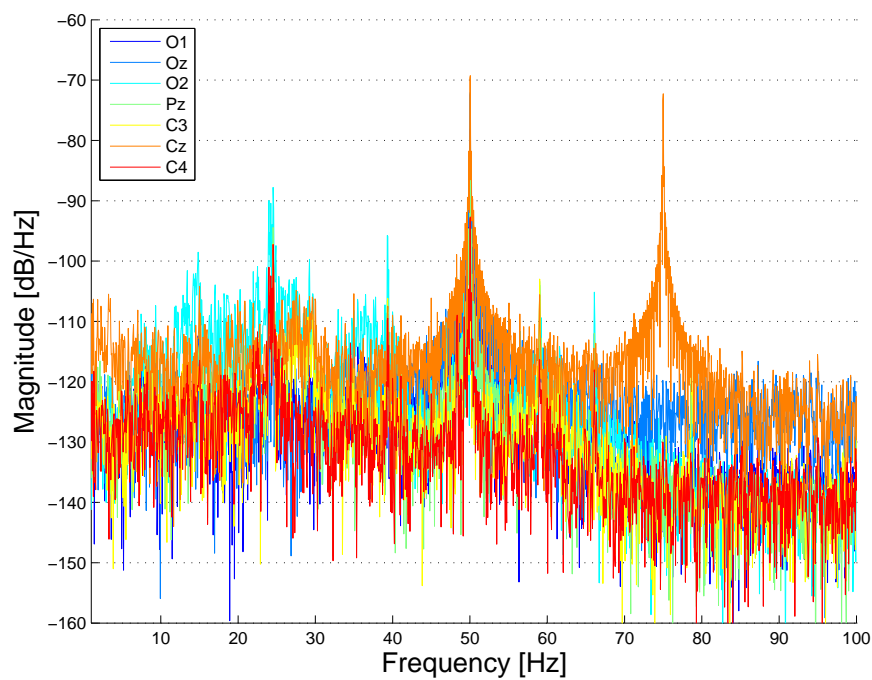


Figure A.16.: Measured signal on all electrodes applying 1 mV amplitude sinus at 75 Hz only on Cz

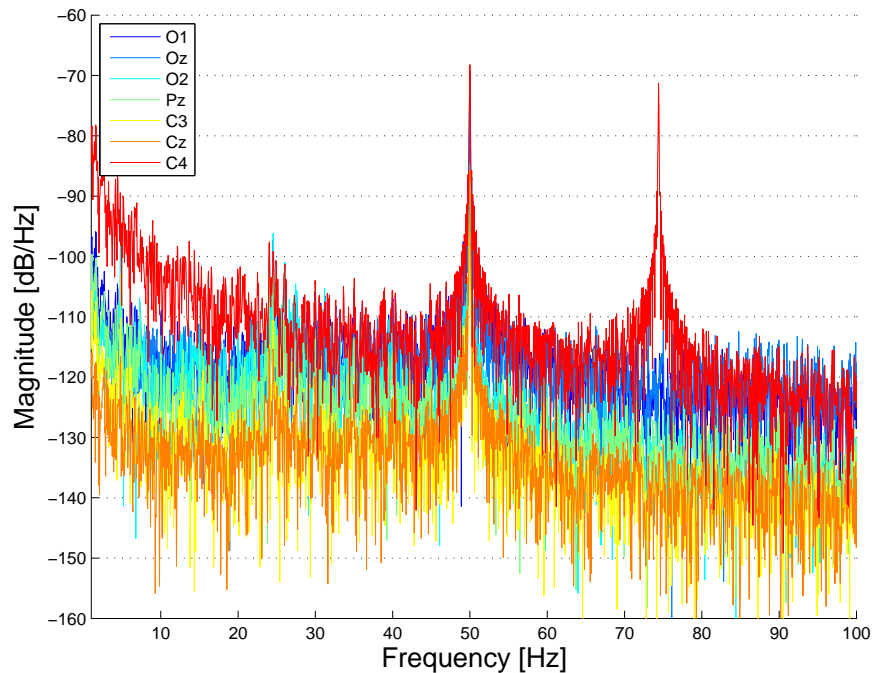


Figure A.17.: Measured signal on all electrodes applying 1 mV amplitude sinus at 75 Hz only on C4

## A.5. Crosstalk with dummy head

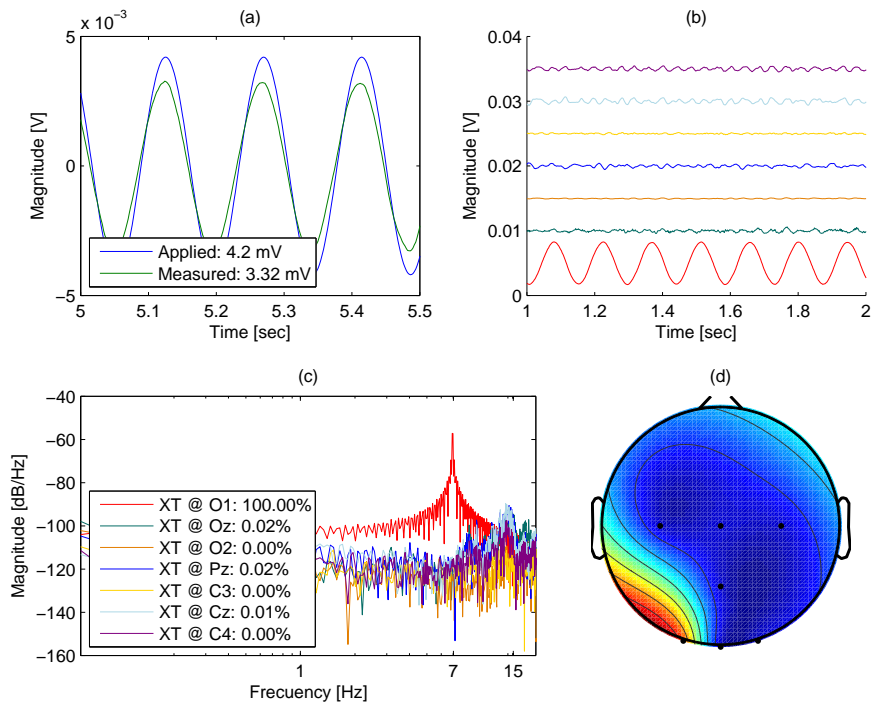


Figure A.18.: Crosstalk from O1 to the other leads

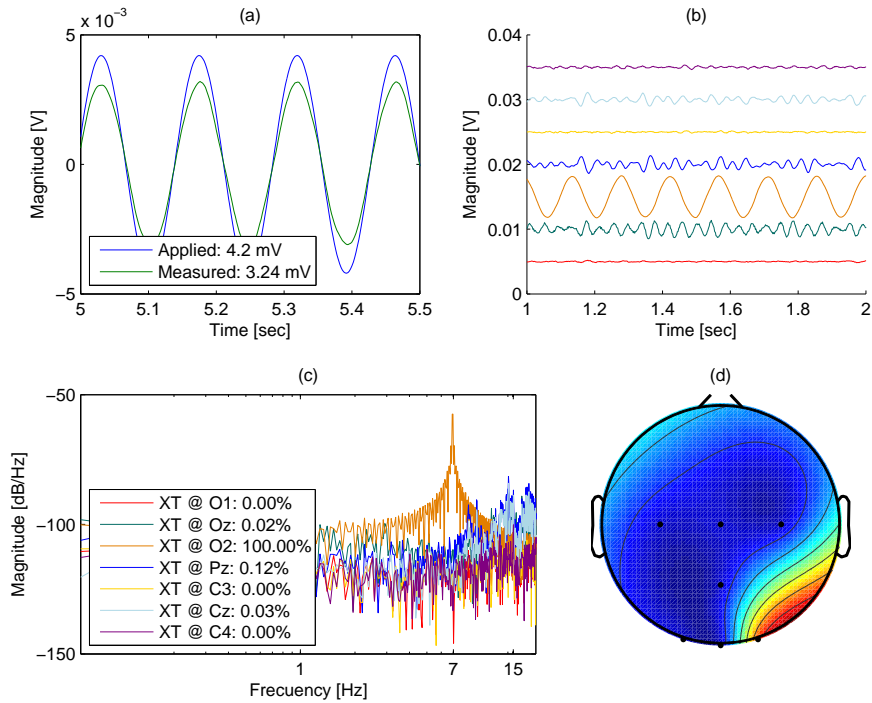


Figure A.19.: Crosstalk from O2 to the other leads

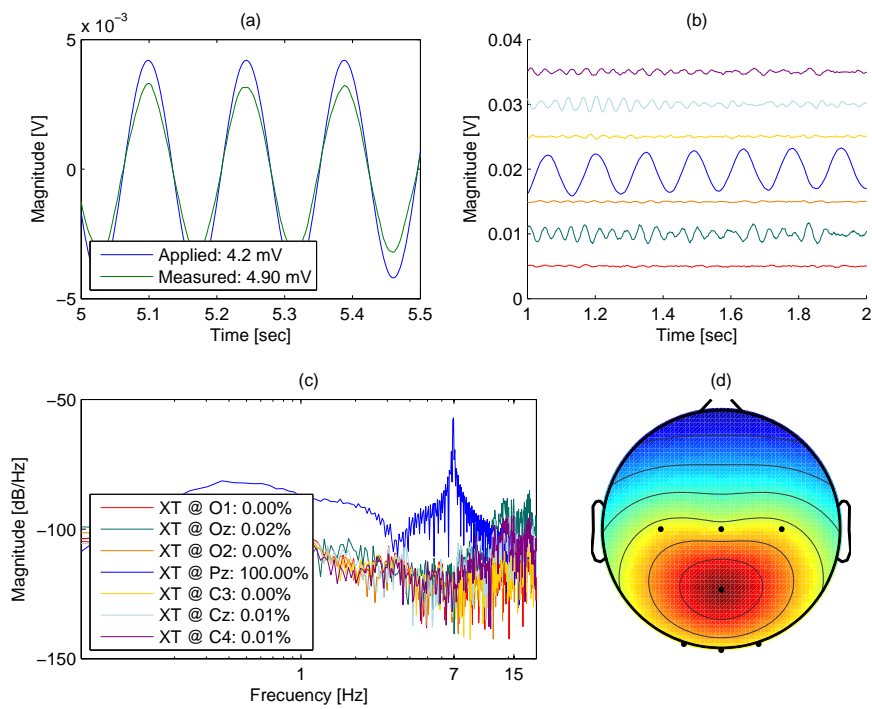


Figure A.20.: Crosstalk from Pz to the other leads

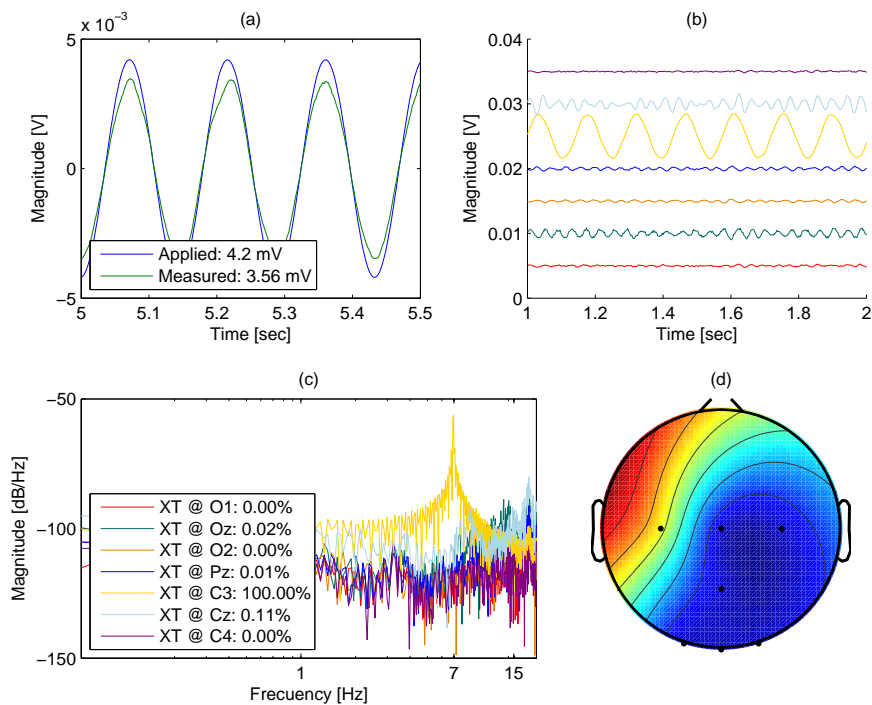


Figure A.21.: Crosstalk from C3 to the other leads

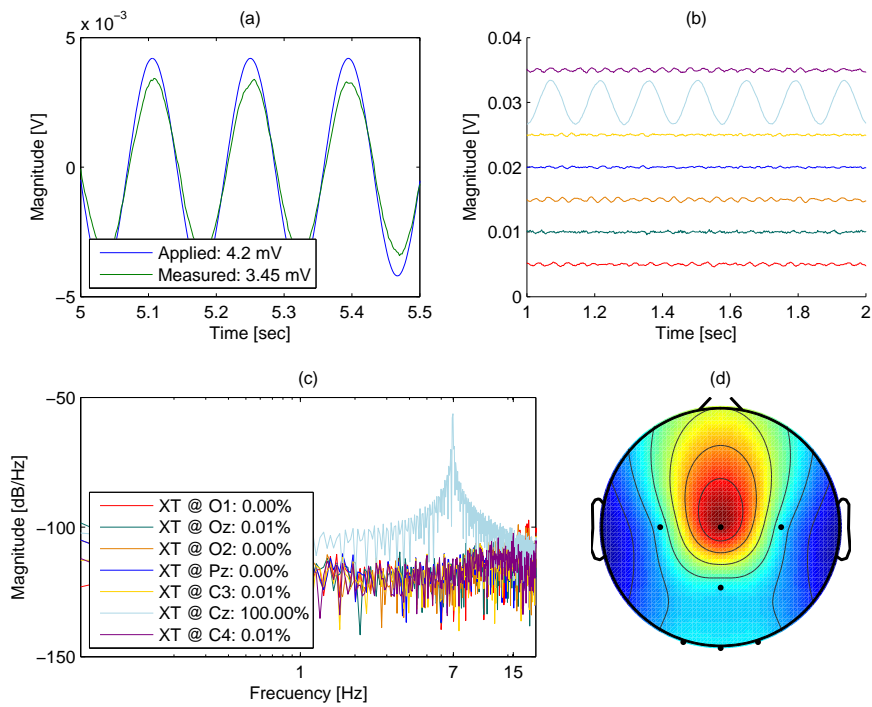


Figure A.22.: Crosstalk from Cz to the other leads

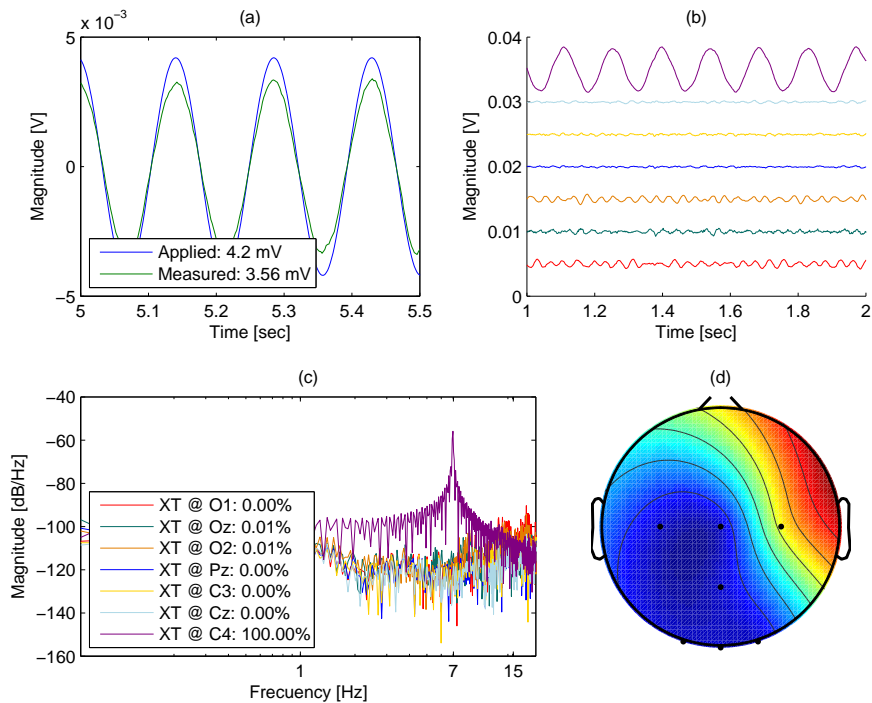


Figure A.23.: Crosstalk from C4 to the other leads

## A.6. Crosstalk without dummy head

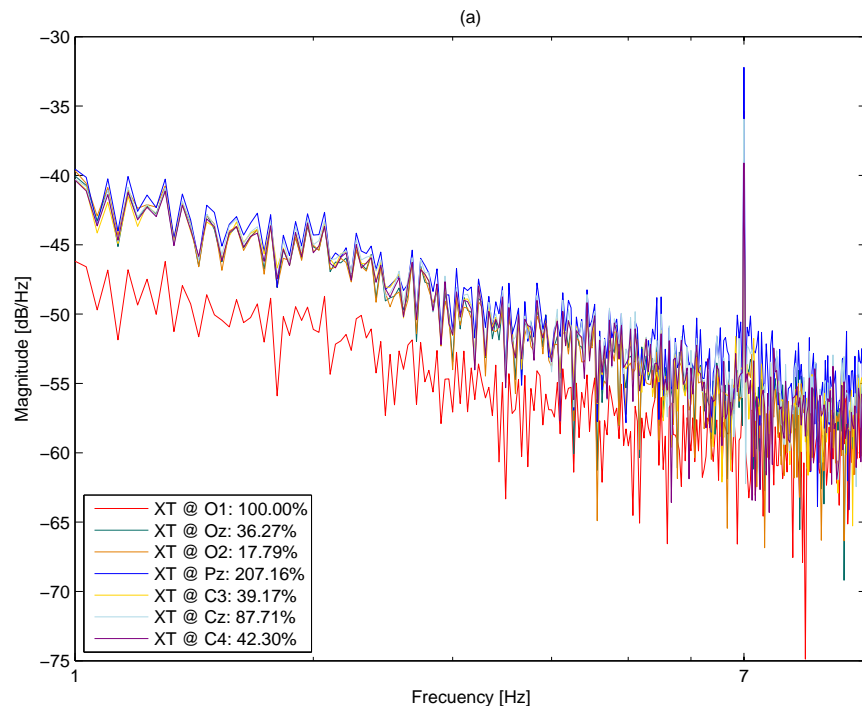


Figure A.24.: Spectrum of each lead with the crosstalk against lead O1 in percentage

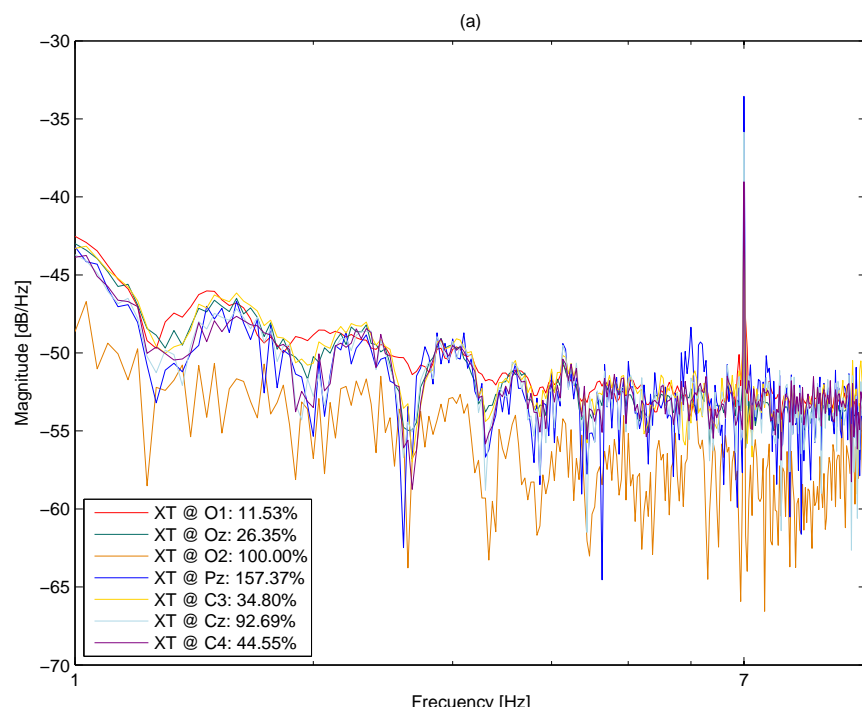


Figure A.25.: Spectrum of each lead with the crosstalk against lead O2 in percentage

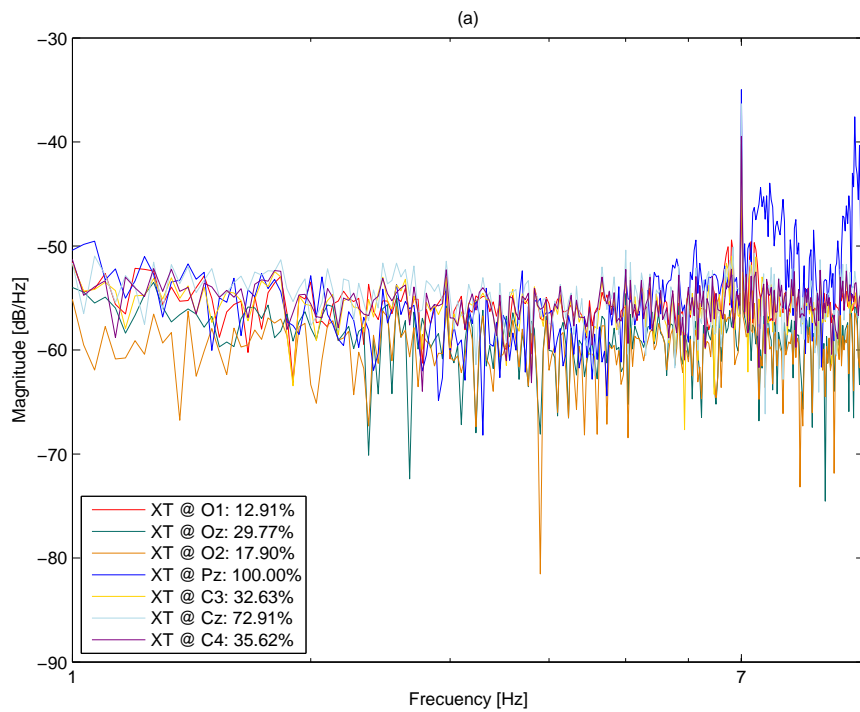


Figure A.26.: Spectrum of each lead with the crosstalk against lead Pz in percentage

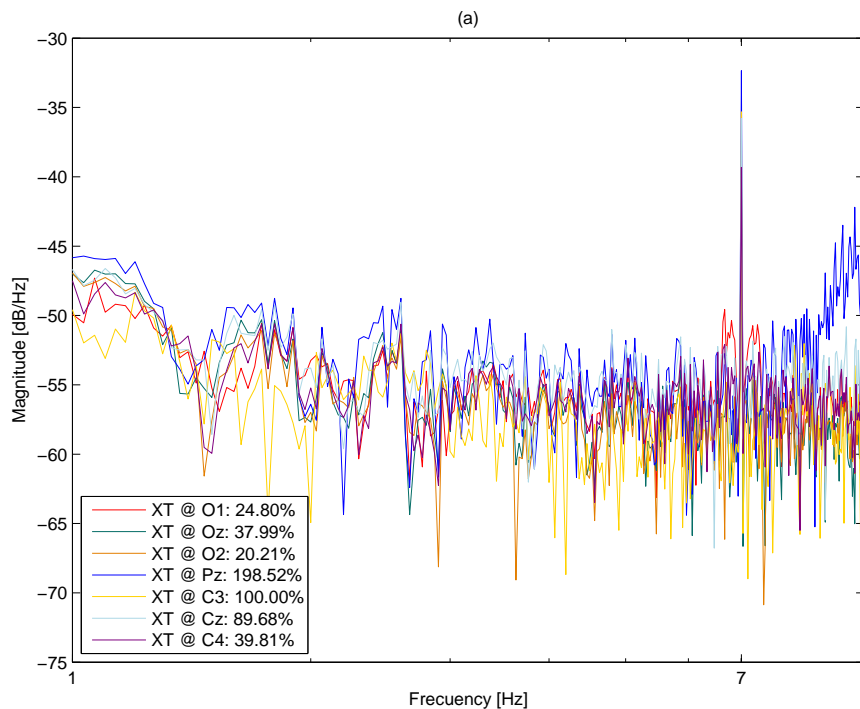
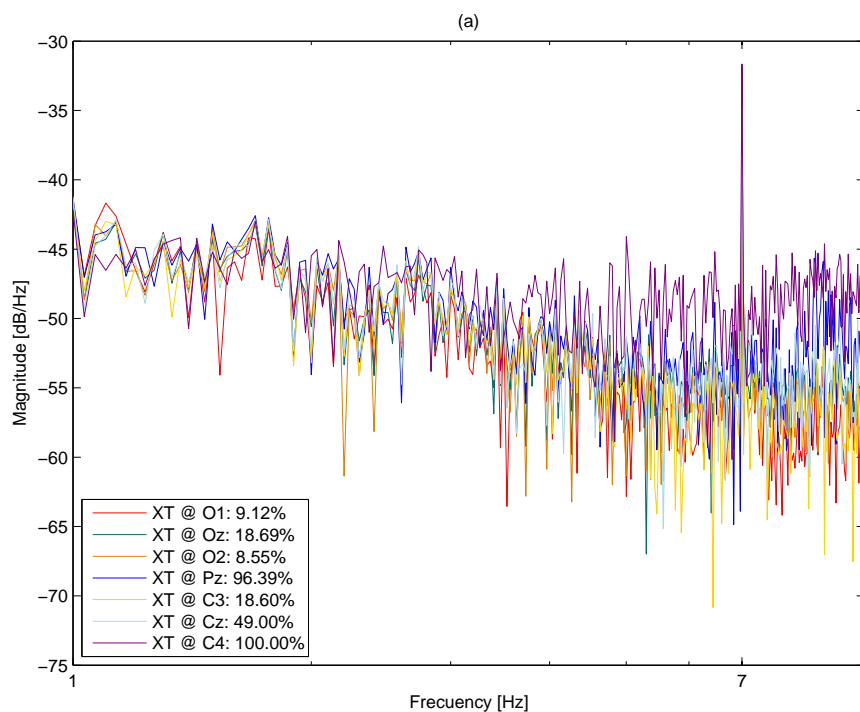
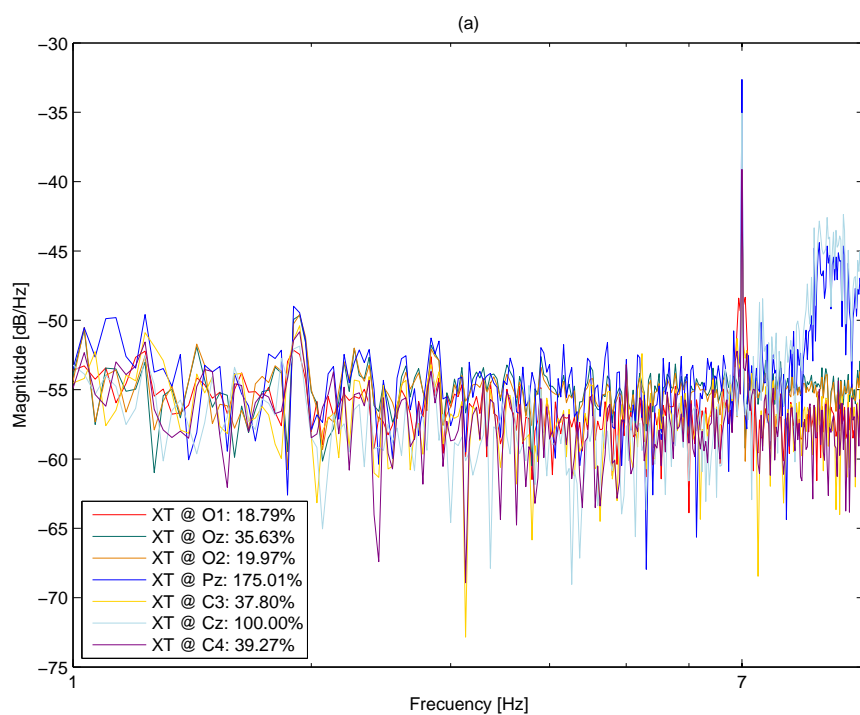


Figure A.27.: Spectrum of each lead with the crosstalk against lead C3 in percentage



## A.7. Time span selection

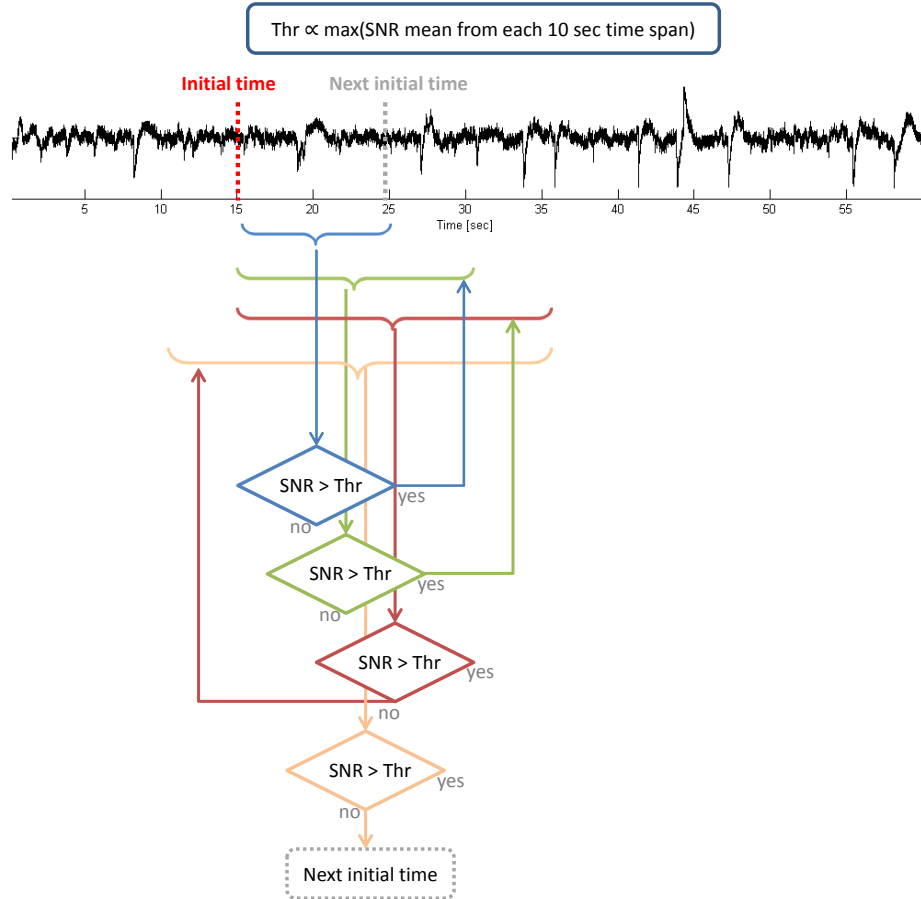


Figure A.30.: A short flow diagram of how the Time Span Selection algorithm works

# Bibliography

- [1] Capical, *GmbH*. Rebenring 33, 38106 Braunschweig, Deutschland, 2010.
- [2] Prof. Dr. rer. nat. M. Schilling, *Institut für Elektrische Messtechnik und Grundlagen der Elektrotechnik*. Technische Universität Braunschweig, 2013-2014.
- [3] M. Piccolino, “Luigi galvani and animal electricity: two centuries after the foundation of electrophysiology,” 1997.
- [4] G. J. Tortora and B. Derrickson, *Principles of Anatomy and Physiology*. John Wiley & Sons, 2013.
- [5] L. Sörnmo and P. Laguna, *Bioelectrical Signal Processing in Cardiac and Neurological Applications*. Academic Press Series in Biomedical Engineering, 2005.
- [6] S. Amiri, A. Rabbi, L. Azinfar, and R. Fazel-Rezai, *Brain-Computer Interface Systems - Recent Progress and Future Prospects*. InTech, June 2013.
- [7] [http://questfortransformation.com/brain\\_waves.html](http://questfortransformation.com/brain_waves.html).
- [8] S. M. Ascencio, “Adquisicion de señales eeg con bioelectrodos no invasivos de alta sensibilidad,” Master’s thesis, Instituto Politecnico Nacional, Escuela Superior de Ingenieria Mecanica y Electrica, Unidad Zacatenco, 2011.
- [9] B. A. Torres, “Wireless system for the measurement of bioelectric signals using capacitive electrodes.” Universitat Politècnica de Catalunya, May 2011.
- [10] Y. M. Chi, T.-P. Jung, and G. Cauwenberghs, “Dry-contact and noncontact biopotential electrodes: Methodological review,” *IEEE Reviews in Biomedical Engineering*, vol. 3, pp. 106–119, 2010.
- [11] J. Devasena, M. V. M. Reddy, S. Kartik, and M. Sasikala, “Development of non-contact capacitive coupled electrodes for bio-potential signal acquisition.” College of Engineering, Guindy, Anna University,.

- [12] R. Matthews, N. J. McDonald, I. Fridman, P. Hervieux, and T. Nielsen, “The invisible electrode: zero prep time, ultra low capacitive sensing,” tech. rep., Quantum Applied Science and Research, 2005.
- [13] M. Müller, “Kapazitätsbestimmung von kapazitiven elektroden,” Master’s thesis, TU Braunschweig, June 2013.
- [14] D. W. Klass, “The continuos challenge of artifacts in the eeg,” *EEG Technologies*, vol. 35, pp. 239–269, 1995.
- [15] S. Noachtar, C. Binnie, J. Ebersole, F. M. Áre, A. Sakamoto, and B. Westmoreland, *Recommendations for the Practice of Clinical Neurophysiology: Guidelines of the International Federation of Clinical Physiology*. Elsevier Science B.V., 1999.
- [16] A. Rémond, “Handbook of electroencephalography and clinical neurophysiology.” Elsevier Scientific Pub. Co., University of California, 1972.
- [17] A. G. Correa, E. Laciár, H. D. Patiño, and M. E. Valentinuzzi, “Artifact removal from eeg signals using adaptive filters in cascade,” in *Journal of Physics: Conference Series 90*, 16th Argentine Bioengineering Congress and the 5th Conference of Clinical Engineering, IOPscience, 2007.
- [18] Y. L. Wang, J. H. Liu, and Y. C. Liu, “Automatic removal of ocular artifacts from electroencephalogram using hilbert-huang transform.” Dept. of Electrical and Information Engineering Zhe Jiang Institute of Communication and Media; Hang Zhou, China.
- [19] M. Bruce Fisch, “Eeg artifacts.”
- [20] P. C. Richardson and A. Lopez, “Electrocardiographic and bioelectric capacitive electrode,” 1970.
- [21] T. Clark, R. Prance, and C. Harland, “Electrodynamic sensors and applications thereof,” June 2003.
- [22] A. Lopez and P. C. Richardson, “Capacitive electrocardiographic and bioelectric electrodes,” *IEEE*, vol. BME-16 Issue:1, p. 2, 1968.
- [23] B. Eilebrecht, T. Wartzek, J. Willkomm, A. Schommartz, M. Walter, and S. Leonhardt, “Motion artifact removal from capacitive ecg measurements by means of adaptive filtering,” in *5th European Conference of the International Federation for Medical and Biological Engineering* (Ákos Jobbág, ed.), vol. 37 of *IFMBE Proceedings*, Springer Berlin Heidelberg, 2012.

- [24] T. Wartzek, T. Lammersen, B. Eilebrecht, M. Walter, and S. Leonhardt, “Triboelectricity in capacitive biopotential measurements,” *IEEE transactions on Biomedical Engineering*, vol. 58, pp. 1268–1278, May 2011.
- [25] E. M. Whitham, K. J. Pope, S. P. Fitzgibbon, T. Lewis, C. R. Clark, S. Loveless, M. Broberg, A. Wallace, D. DeLosAngeles, P. Lillie, A. Hardy, R. Fronsko, A. Pulbrook, and J. O. Willoughby, “Scalp electrical recording during paralysis: Quantitative evidence that eeg frequencies above 20 hz are contaminated by emg,” *Elsevier, International Federation of Clinical Neurophysiology*, vol. 118, pp. 1877–1888, 2007.
- [26] B. Yin, M. Meftah, and T. J. Ikkink, “Compensation of motion artifacts in capacitive measurement of electrophysiological signals,” 2011. US Patent App. 13/059,076.
- [27] S. M. Lee, K. K. Kim, and K. S. Park, “Wavelet approach to artifact noise removal from capacitive coupled electrocardiograph,” in *30th Annual International IEEE EMBS Conference*, 2008.
- [28] L. Qin and B. He, “A wavelet-based time-frequency analysis approach for classification of motor imagery for braincomputer interface applications,” *J. Neural Eng*, vol. 2, pp. 65–72, 2005.
- [29] A. Mognon, J. Jovicich, L. Bruzzone, and M. Buiatti, “Adjust: An automatic eeg artifact detector based on the joint use of spatial and temporal features,” *Psychophysiology*, vol. 48, pp. 229–240, 2011.
- [30] H. Hallez, A. Vergult, and R. Phlypo, “Muscle and eye movement artifact removal prior to eeg source localization,” in *Proceedings of the 28th IEEE EMBS Annual International Conference New York City*, 2006.
- [31] X. Yong, R. K. Ward, and G. E. Birch, “Artifact removal in eeg using morphological component analysis.” Department of Electrical and Computer Engineering, University of British Columbia.
- [32] A. Materka and M. Byczuk, “Using comb filter to enhance ssvep for bci applications,” in *3rd Int. Conf. MEDSIP 2006, Advances in Medical, Signal and Information Processing*, 2006.
- [33] S. P. Fitzgibbon, T. W. Lewis, D. M. W. Powers, E. W. Whitham, J. O. Willoughby, and K. J. Pope, “Surface laplacian of central scalp electrical signals is insensitive to muscle contamination,” *IEEE Transactions on Biomedical Engineering*, vol. 60, pp. 4–9, 2013.

- [34] D. A. Peterson, K. J. N., K. M. J., A. C. W., and T. M. H., "Feature selection and blind source separation in an eeg-based braincomputer interface," *EURASIP J. Appl. Signal Process.*, vol. 19, pp. 3128–40, 2005.
- [35] A. Delorme, T. Sejnowski, and S. Makeig, "Enhanced detection of artifacts in eeg data using higher-order statistics and independent component analysis," *ELSEIVER, NeuroImage*, vol. 34, pp. 1443–1449, 2007.
- [36] Navarro, X., Poree, F., and G. Carrault, "Ecg removal in preterm eeg combining empirical mode decomposition and adaptive filtering," in *IEEE International Conference on Acoustics, Speech and Signal Processing (ICASSP)*, 2012.
- [37] H. Yoon, H. Kim, S. Kwon, and K. Park, "An automated motion artifact removal algorithm in electrocardiogram based on independent component analysis," in *The Fifth International Conference on eHealth, Telemedicine, and Social Medicine*, 2013.
- [38] Y. Wang, Z. Zhang, X. Gao, and S. Gao, "Lead selection for ssvep-based brain-computer interface," in *Proceedings of the 26th Annual International Conference of the IEEE EMBS*, 2004.
- [39] B. W. McMenamin, A. J. Shackman, J. S. Maxwell, D. R. Bachhuber, A. M. Koppenhaver, L. L. Greischar, and R. J. Davidson, "Validation of ica-basedmyogenic artifact correction for scalp and source-localized eeg," *ELSEIVER, NeuroImage*, vol. 49, pp. 2416–2432, 2010.
- [40] M. Akhtar, C. James, and M. W., "Modifying the spatially-constrained ica for efficient removal of artifacts from eeg data," in *Proceedings of 4th International Conference on Bioinformatics and Biomedical Engineering (iCBBE)*, 2010.
- [41] P. Senthil Kumar, R. Arumuganathan, and C. Vimal, "An adaptive method to remove ocular artifacts from eeg signals using wavelet transform," *Journal of Applied Sciences Research*, vol. 5, pp. 741–745, 2009.
- [42] M. Misiti, Y. Misiti, and G. Oppenheim, *Les ondelettes et leurs applications. IC2 Traitement du signal et de l'image*, Hermes Science Publications, 2003.
- [43] A. Jia, W. M, L. F, B. C, and Z. X., "Wavelet-based denoising algorithm for eeg signals—using scale dependent threshold based on median," *MEDLINE*, vol. 26, pp. 1227–1236, 2009.

- [44] G. Geetha and D. Geethalakshmi, "Eeg de-noising using sure thresholding based on wavelet transform," *International Journal of Computer Applications*, vol. 24, pp. 29–33, 2011.
- [45] P. S. Kumar, R. Arumuganathan, K. Sivakumar, and C. Vimal, "Removal of ocular artifacts in the eeg through wavelet transform without using an eog reference channel," *Int. J. Open Problems Compt. Math.*, vol. 1, pp. 188–200, 2008.
- [46] P. A. Babu and D. Prasad, "Removal of ocular artifacts from eeg signals using adaptive threshold pca and wavelet transforms," in *International Conference on Communication Systems and Network Technologies*, 2011.
- [47] N. P. Castellanos and V. A. Makarov, "Recovering eeg brain signals: Artifact suppression with wavelet enhanced independent component analysis," *Journal of Neuroscience Methods*, vol. 158, pp. 300–312, 2006.
- [48] J. Walters-Williams and Y. Li, "A new approach to denoising eeg signals - merger of translation invariant wavelet and ica." University of Southern Queensland and University of Southern Queensland.
- [49] J. Baraniak, J. Hauer, N. Schuhmann, and G. Leugering, "Implementation of adaptive filters for biomedical applications." Institut für Angewandte Mathematik, Friedrich Alexander Universität Erlangen-Nürnberg, Germany.
- [50] F. Chan, W. Qiu, F. lam, and P. Poon, "Evoke potential estimation using modified time-sequence adaptive filter," *Medical & Biological Engineering & Computing*, vol. 36, pp. 407–414, 1998.
- [51] S. C. Douglas, *Introduction to Adaptive Filters*. CRC Press LLC, 1999.
- [52] K. Sweeney, "Motion artifact processing techniques for physiological signals," Master's thesis, NATIONAL UNIVERSITY OF IRELAND MAYNOOTH, 2013.
- [53] S. McLoone, T. Ward, and K. Sweeney, "A simple bio-sugnals quality measure for in-home monitoring." National University of Ireland Maynooth.
- [54] F. Hosseini, D. Schroeder, and W. H. Krautschneider, "Capacitive sensors for detection of the movement artifacts in active capacitive electrocardiography electrodes," in *The 2012 Biomedical Engineering International Conference (BMEiCON-2012)*, 2012.

- [55] C. Wehrmann, M. Oehler, M. Gerloff, and Sch, “Drahtloses kapazitives 8-kanal helmsystem zur eeg-messung,” in *Innovative Verarbeitung bioelektrischer und biomagnetischer Signale*, 2012.
- [56] M. Oehler, “Kapazitive elektroden zur messung bioelektrischer signale,” Master’s thesis, TU Braunschweig, 2009.
- [57] M. Oehler, V. Ling, K. Melhorn, and M. Schilling, “A multichannel portable ecg system with capacitive sensors,” *Physiological Measurement*, vol. 29, pp. 783–793, 2008.
- [58] M. Gerloff, M. Oehler, S. Mitschke, and M. Schilling, “Lightweight capacitive 8 channel-eeg-helmet,” *Biomed Tech Proceedings*, vol. 55, pp. –, 2010.
- [59] *Agilent 33220A 20 MHz Waveform Generator / Arbitrary Waveform Generator*.
- [60] T. Instrument, *ADS1258 16-Channel, 24-Bit Analog-to-Digital Converter*, 2005.
- [61] *pro-SIGNAL; BDM8760F-RX Speaker*.
- [62] P. C. Liu, “A fifteen minutes introduction of wavelet transform and applications.” Paul C. Liu.
- [63] M. Misiti, Y. Misiti, G. Oppenheim, and J.-M. Poggi, *Wavelet Toolbox R2013b, Users Guide*. Matlab.
- [64] R. Ganesh, Naik, and D. K. Kumar, “An overview of independent component analysis and its applications,” *Informatica*, vol. 35, pp. 63–81, 2011.
- [65] M. Jaber, “The ultra high speed lms algorithm implemented on parallel architecture suitable for multidimensional adaptive filtering.”
- [66] D. L. Donoho and I. M. Johnstone, “Adapting to unknown smoothness via wavelet shrinkage,” *Journal of the American Statistical Association*, vol. 90, pp. 1200–1224, 1995.
- [67] A. Cichocki, S. Amari, K. Siwek, T. Tanaka, and A. H. Phan, “Icalab toolboxes.”
- [68] A. Chen, “Kdica algorithm.” UC Village at Albany, CA, January 2004.
- [69] H. Gävert, J. Hurri, J. Särelä, and A. Hyvärinen, “Fastica,” October 2005.
- [70] Y. Wang, Z. Zhang, X. Gao, and S. Gao, “Lead selection for ssvep-based brain-computer interface,” in *Proceedings of the 26th Annual International Conference of the IEEE EMBS*, 2004.

- [71] D. A. and M. S., “Eeglab: an open source toolbox for analysis of single-trial eeg dynamics,” *Journal of Neuroscience Methods*, vol. 134, pp. 9–21, 2004.
- [72] A. C. Tang, M. T. Sutherland, and C. J. McKinney, “Validation of sobi components from high-density eeg,” *Elsevier Neuro Image*, vol. 25, pp. 539–553, 2004.



# Danksagung

Die vorliegende Arbeit entstand im Rahmen meines Stipendium des DAAD in Deutschland. Am Institut für Elektrische Messtechnik und Grundlagen der Elektrotechnik der Technischen Universität Braunschweig hatte ich die Möglichkeit, die vorliegende Masterarbeit zu schreiben. Bei allen, die zum Gelingen dieser Arbeit durch ihre Unterstützung beigetragen haben, möchte ich mich herzlich bedanken. Mein besonderer Dank gilt:

- Herrn Prof. Dr. rer. nat. Meinhard Schilling für die Unterstützung von Anfang an und für die Überlassung dieses interessanten Themas,
- Herrn Christof Wehrmann, M. Sc. für die ausgezeichnete Betreuung während dieser Arbeit,
- Frau Katharina Olze, M. Sc. für all die Hilfe, Mitbetreuung und die Korrekturarbeiten,
- Frau Tanja Coenen für die professionell gestalteten Fotos und meinen Bruder für die 3D Abbildungen,
- Frau Ying Su, die sich als Probandin zur Verfügung gestellt hat und für Ablenkung vom Arbeitsalltag sorgte.

Ein ganz besonderer Dank gilt meiner Freundin für die grenzenlose Unterstützung. Zum anderen danke ich meiner Familie, die mir immer ein verlässlicher Rückhalt waren.

Braunschweig, 4. Juli 2014